Summer 8-31-2003

Measurement of the nonlinear refractive index (n2) and stimulated Raman scattering in optical fibers as a function of germania content, using the photorefractive beam coupling technique

Ferdinand Anayo Oguama
New Jersey Institute of Technology

ABSTRACT

MEASUREMENT OF THE NONLINEAR REFRACTIVE INDEX (n_2) AND STIMULATED RAMAN SCATTERING IN OPTICAL FIBERS AS A FUNCTION OF GERMANIA CONTENT, USING THE PHOTOREFRACTIVE BEAM COUPLING TECHNIQUE

By

Ferdinand A. Oguama

One of the greatest challenges in optical communication is the understanding and control of optical fiber nonlinearities. While these nonlinearites limit the power handling capacity of optical fibers and can cause noise, signal distortion and cross talk in optically amplified transmission systems, they have been equally harnessed for the development of new generations of optical amplifiers and tunable laser sources. The two prominent parameters that characterize the nonlinear properties of an optical fiber are the nonlinear refractive index (n_2) and the Raman gain coefficient (g_R). These parameters are related to the third order nonlinear susceptibility [$\chi^{(3)}$].

In this work, the photorefractive beam coupling technique, also called induced grating autocorrelation (IGA), has been used to measure the nonlinear refractive index (n_2) and the Raman gain coefficient (g_R) of short lengths ($z \sim 20$ m) of optical fibers. In the IGA experiment, a transform limited Gaussian pulse is propagated through a short length of an optical fiber, where it undergoes self-phase modulation (SPM) and other nonlinear distortions, and the output pulse is split into two. The two-excitation pulses are then coupled into a photorefractive crystal, where they interfere and form a photorefractive phase grating. The IGA response is determined by delaying one beam (the probe) and plotting the diffracted intensity of the probe versus the relative delay (τ).

Analysis of the IGA response yields information about the nonlinear phase distortions and other calibration parameters of the fiber. Using the IGA technique the author has measured the nonlinear refractive index in several types of fibers, including pure silica, Er-Al-Ge doped fibers, DCF (dispersion compensating fiber) and the recently developed TrueWave Rs fiber, and investigated the dependence of n_2 on the doping profiles of Er, Al, and Ge in optical fibers.

The standard IGA model for n_2 measurements was derived from the solution of the nonlinear wave equation for pulse propagation in the limit of pure self-phase modulation. This model assumed that GVD (group velocity dispersion) and other nonlinear processes such as SRS (stimulated Raman scattering) are negligible. This model has been successfully used to fit the experimental data and determine the n_2 of the fiber from the time dependent phase shift. However, SRS has been observed to distort the IGA trace, thus leading to a breakdown of the standard IGA model. A new IGA model has been developed in this study from the solution of the coupled-amplitude nonlinear Schrodinger equation, using both analytical and numerical approaches. This new model successfully accounts for the SRS effects on the IGA trace, in the limit of zero GVD, and allows the direct determination of the Raman gain coefficient from the fit of the SRS-distorted IGA trace. The measured nonlinear refractive index and Raman gain coefficients are in good agreement with published results. It was also shown that in the limit of zero GVD and no Raman, the IGA technique reduces to the widely accepted spectral domain SPM technique pioneered by Stolen and Lin, but is readily applicable to shorter lengths of fiber and is sensitive to smaller phase shifts.

MEASUREMENT OF THE NONLINEAR REFRACTIVE INDEX (n_2) AND STIMULATED RAMAN SCATTERING IN OPTICAL FIBERS AS A FUNCTION OF GERMANIA CONTENT, USING THE PHOTOREFRACTIVE BEAM COUPLING TECHNIQUE

by

Ferdinand Anayo Oguama

A Dissertation
Submitted to the Faculty of
New Jersey Institute of Technology and
Rutgers, The State University of New Jersey
in Partial Fulfillment of the Requirements for the Degree of
Doctor of Philosophy in Applied Physics

Federated Physics Department

August 2003

APPROVAL PAGE

MEASUREMENT OF THE NONLINEAR REFRACTIVE INDEX (n_2) AND STIMULATED RAMAN SCATTERING IN OPTICAL FIBERS AS A FUNCTION OF GERMANIA CONTENT, USING THE PHOTOREFRACTIVE BEAM COUPLING TECHNIQUE

Ferdinand Anayo Oguama

August 2003

Dr. Anthony M. Johnson — Date
Distinguished Professor of Physics, NJIT

Dr. John Federici — Date
Professor of Physics, NJIT

Dr. Dan Murnick — Date
Professor of Physics, Rutgers University

Dr. Haim Grebel — Date
Professor of Electrical & Computer Engineering, NJIT.

Dr. Gordon Thomas — Date
Professor of Physics and Biomedical Engineering, NJIT.

Dr. David DiGiovanni — Date
Director, OFS Optics Inc. Murray Hill, NJ

BIOGRAPHICAL SKETCH

Author: Ferdinand A. Oguama.

Degree: Doctor of Philosophy

Date: August 2003

Undergraduate and Graduate Education:

- Doctor of Philosophy in Applied Physics
  New Jersey Institute of Technology/Rutgers University -Newark, NJ, 2003

- Master of Science in Physics
  Nnamdi Azikiwe University, Awka, Nigeria,1990

- Bachelor of Science in Industrial Physics
  Anambra State University of Technology, Enugu, Nigeria, 1986

Major: Applied Physics

Publications and Presentations:

H. Garcia, A. M. Johnson, F. A. Oguama, and Sudhir Trivedi, " A new approach to the measurement of the nonlinear refractive index of short (<25 m) lengths of silica and erbium-doped fibers," *Accepted for publication in Optics Letters.*

F. A. Oguama, A. Tchouassi and A. M. Johnson, "Influence of Stimulated Raman Scattering and High GeO_2 Doping on the Induced Grating Autocorrelation Measurements in Er-Al-Ge Doped Single Mode Fibers", 2003 Annual Conference of the National society of Black Physicists-NSBP, Feb. 12-15, Atlanta, GA, (2003).

F. A. Oguama, A. Tchouassi and A. M. Johnson, "Effect of High Germania Content and Stimulated Raman Scattering on n_2 Measurements in Erbium-Doped Single Mode Fibers", Optical Society of America (OSA) annual meeting, (Orlando Florida) October, (2002).

F. A. Oguama, H. Garcia, A. M. Johnson and S. Trivedi, "Photorefractive Beam Coupling Measurement of the Nonlinear Refractive Index (n_2) of Erbium-Doped Fibers as a Function of Germania and Aluminum Content", in: *Conf. Lasers and Electro-optics – CLEO' 2001 Technical Digest,* Baltimore MD, pp. 303-304 (2001).

F. A. Oguama, H. Garcia, A. M. Johnson and S. Trivedi, "Photorefractive Beam Coupling Measurement of the Nonlinear Refractive Index (n_2) of Erbium-Doped Fibers as a Function of Germania Content", A paper presented at the 84th Annual Meeting/Conference of the Optical Society of America held at Providence, RI, Oct. 22nd-26th, (2000).

F. A. Oguama and H. Shields, Measurement of the Spin Hamiltonian Parameters of Cu^{2+} Ion in Zn^{2+}-Doped $CaCd(CH_3COO)_4.6H_2O$. *Japanese Journal of Applied Physics,* **30**, pp. 2753-2759 (1999).

F. A. Oguama, H. Shields and D. K. De, Effect of Zn^{2+} Doping on the Phase Transition Temperature of Cadmium Calcium Acetate Hexahydrate Single Crystals, in: *Proceedings of the 12th Annual Conference of the National Society of Black Physicists (NSBP/NCBPS)* Lexington, Kentucky, pp. 111-119 (1998).

F. A. Oguama, H. Shields and D. K. De, EPR Studies of Phase Transition in Cadmium Calcium Acetate Hexahydrate as a Function of Different Paramagnetic Impurities: *Phys. Rev. B* **56,** pp. 2611-2615 (1997).

Dedicated to

my grand mother – Mrs. Maria Ibekwe

ACKNOWLEDGEMENT

I would like to express my gratitude to my dissertation advisor, Dr. Anthony M. Johnson. He was instrumental in attracting me to NJIT and in stimulating my interest (which was then leaning towards condensed matter Physics) in optics and photonics research. He provided the insightful suggestions that encouraged my strong and consistent research endeavors that led to the successful findings made in this study. I am also grateful to the members of my dissertation committee: Dr. John Federici, Dr. Dan Murnick, Dr. Haim Grebel, Dr. Gordon Thomas and Dr. David DiGiovanni. Their useful advice and suggestions were of immense help in the completion of this thesis.

My appreciation goes to Dr. Hernando Garcia and Dr. Alain Tchouassi, who also contributed useful ideas that helped me advance forward in the course of this investigation. I would like to give special thanks to Dr. Bill Reed for devoting some of his time and expertise in helping to operate the sensitive apparatus for measuring the mode-field diameter and the effective area of the fibers, at the OFS laboratory, Murray Hill, NJ; and also for providing some of the fibers studied in this work.

Other individuals that deserve recognition for providing some research materials include Dr. Jake Bromage of OFS laboratory, Holmdel, NJ; Dr. Nelson Newbury of the National Institute of Standards and Technology (NIST), Boulder CO; and Dr. Sudhir Trivedi, Brimrose corporation of America, Baltimore, MD.

TABLE OF CONTENTS

TABLE OF CONTENTS
(Continued)

Chapter **Page**

TABLE OF CONTENTS
(Continued)

Chapter **Page**

TABLE OF CONTENTS
(Continued)

Chapter **Page**

LIST OF TABLES

LIST OF FIGURES

LIST OF FIGURES
(Continued)

LIST OF FIGURES
(Continued)

LIST OF FIGURES
(Continued)

Figure **Page**

GLOSSARY OF TERMS

DCF	Dispersion Compensating Fiber
DSF	Dispersion Shifted Fiber
DWDM	Dense Wavelength Division Multiplexing
EDFA	Erbium-Doped Fiber Amplifier
FWHM	Full Width at Half Maximum
FWM	Four Wave Mixing
GVD	Group Velocity Dispersion
IGA	Induced Grating Autocorrelation
LD	Laser Diode
LPG	Long Period Fiber Grating
MFD	Mode Field Diameter
Nd:YAG	Neodymium-Doped Yttrium Aluminum Garnet
NLSE	Non Linear Schrodinger Equation
RFA	Raman Fiber Amplifier
RFL	Raman Fiber Laser
RGP	Raman Gain Parameter
SBS	Stimulated Brillouin Scattering
SHG	Second Harmonic Generation
SHGA	Second Harmonic Generation Autocorrelation
SPM	Self-Phase Modulation
SPMP	Self-Phase Modulation Parameter

GLOSSARY OF TERMS
(Continued)

SPMS	Self-Phase Modulation Strength
SRS	Stimulated Raman Scattering
WDM	Wavelength Division Multiplexing
WOT	Walk-Off Term
XPM	Cross-Phase Modulation

CHAPTER 1

INTRODUCTION

1.1 Background

The ability to communicate worldwide on demand would not have possible without the development of low loss silica fiber as a broadband medium for transporting voice, video, and data traffic. At the time the laser was invented in 1960 [1] following an earlier suggestion [2], it was already recognized that communication using lightwaves offered immense potential but it took over ten years before a practical medium capable of effectively transporting light pulses around the world was developed.

The manufacture of *low loss* optical fibers began in the 1970s [3-5], and continuous improvements on fiber fabrication technology resulted by 1979 in the reduction of fiber loss to only about 0.2 dB/km near 1.55 μm wavelength [6]. The availability of such low loss fibers represented a critical milestone in the global telecommunication and information technology revolution. Added to its low loss is its enormous bandwidth, which makes it possible for large amounts of different information to be transmitted simultaneously through the same fiber in a process referred to as wavelength division multiplexing (WDM).

Another major revolution in the optical communication industry occurred in the early 1990s when erbium doped fiber amplifiers (EDFAs) invented in 1987 [7-9]] became commercially available. Prior to the advent of EDFAs, the standard way of coping with the effect of attenuation and dispersion in long-haul fiber optic communication was to use periodically spaced electronic repeaters. Such repeaters consist of a photodetector to detect the weak incoming light, electronic amplifiers, timing

circuitry to maintain the timing of the signals and a laser along with its driver to launch the signals along the next span. Thus the input optical signal is first detected and converted to electrical signals. The electrical signals are processed (reshaped and retimed) to remove the effect of pulse dispersion and then amplified to drive an optical pulse, hence regenerating the pulse train. The emerging optical signal is then sent again through the next segment of the link.

The use of EDFAs permits the direct amplification of optical signals without the optical-to-electrical-to-optical conversion associated with electronic repeaters. These optical amplifiers are now referred to as optical repeaters. Transmission systems with tens of thousands of kilometers of fibers are now possible using EDFAs for periodic optical amplification (typically every 40 to 80 km) to compensate for fiber loss. A major advantage of EDFAs is they operate independent of data rate, format and wavelength (within the erbium gain spectrum), and this paves the way for dense wavelength division multiplexing (DWDM). The DWDM technology utilizes many independent lasers, each operating at evenly spaced wavelengths and each carrying its own stream of data or information and all propagating down a single optical fiber. For example, in DWDM technology, one could have 100 lasers, each operating at a data rate of 10 Gbits/s resulting in an aggregate data rate of 1 Tbit/s. The introduction of a two-band architecture, which includes amplifier sections for the C-band (1530 nm – 1560 nm) and L-band (1570 nm – 1620 nm), resulted in a further increase of the bandwidth. In addition, these amplifiers provide high output power and low noise figure to support the ever-increasing capacity demand on lightwave systems.

All these attempts to fully utilize the capabilities of silica fibers will ultimately be limited by nonlinear interactions between the information bearing lightwaves and the transmission medium. These optical nonlinearities can cause noise, signal distortion, crosstalk, and excess attenuation of the optical signals, resulting in system degradation [10-12]. Thus, as the world continues to push for ever higher data rates, continued progress in research and understanding of the impairments caused by optical nonlinearities is critical. There exist a collection of nonlinear effects in optical fibers [13-31] each of which manifests itself in a unique way and affects specific lightwave systems in different ways. The majority of the fiber nonlinearities arise from the dependence of the refractive index on light intensity. This intensity induced refractive index change referred to as the nonlinear refractive index (n_2), is responsible for self-phase modulation (SPM) [13,14]; cross phase modulation (XPM) [15]; four wave mixing (FWM) [16,17], and soliton formation [18,19].

Self-phase modulation can lead to a shift in the frequency of the pulse (self-chirping), which influences the pulse shape via its interaction with the fiber dispersion. It is possible for self-chirping and dispersion to cancel each other. If this happens, solitons can form [18-20]. However, when the cancellation is not complete, self-chirping leads to broadening of the optical spectrum and can cause additional pulse distortion. XPM results from the intensity variation in one channel modulating the phase of all the other channels in the fiber. In FWM, two or more optical waves (signals) at different wavelengths mix to produce new optical waves at other wavelengths. This depletes certain waves and by means of frequency conversion, generates interfering signals for other channels in wavelength-multiplexed systems. This leads to both noise and crosstalk, thus degrading

the quality of the transmitted signals. Another class of optical nonlinearities that occur in optical fibers is stimulated (Raman and Brillouin) scattering [21-28]. Stimulated Raman scattering [21-23], an interaction between light and vibrations of silica molecules, causes frequency conversion of light and results in crosstalk, and attenuation of short-wavelength channels in wavelength multiplexed systems. Stimulated Brillouin scattering [24-28] arises from the interaction between light and sound waves in the fiber. This causes frequency conversion and reversal of propagation direction of light and can lead to depletion of signal power and modulation instability [29].

Therefore, accurate measurement and characterization of these fiber nonlinearities are crucial for predicting and improving the performance of optical communication systems.

In as much as it is crucial to control the adverse effects of fiber nonlinearities, it is equally pertinent to note that nonlinear effects in optical fibers are also useful in some aspects [30-49] and this creates additional incentives to the study of fiber nonlinearities. For example the nonlinear phenomenon of SPM has been used in optical pulse compression [30-34] by taking advantage of the SPM-induced chirp and spectral broadening. Soliton based optical communication systems have been developed [35-40]. Optical solitons result from the interplay between SPM and GVD in the anomalous dispersion regime. The development of the Raman fiber amplifier (RFA) [41-43] and Raman fiber lasers (RFL) [43,44] are also other positive rewards stemming from fiber nonlinearities. The RFA has been used as discrete, analog, and digital amplifiers at both 1.3 μm [45] and 1.5 μm [46,47] and as remotely pumped amplifiers in the repeaterless optical communication systems [48,49].

It is in recognition of all these effects that considerable attention has been given to the study of optical fiber nonlinearities. Stolen and Ippen measured the gain coefficients for SRS and SBS in single mode silica fiber as early as 1972 [50,51]. Measurements of the nonlinear index of refraction in silica fibers have also been reported by a number of authors, using different techniques [13, 52-62]. The most widely used of all these techniques is the self-phase modulation method developed by Stolen and Lin [13]. In this technique, a transform limited optical pulse is coupled into a fiber of appreciable length ($z \sim 100$ m to 2 km) where it suffers self-phase modulation as it propagates. The output spectrum is measured as a function of the input power using a scanning Fabry-Perot interferometer. The frequency broadening is proportional to the spectral phase shift, which is in turn proportional to the input power. As the input power is increased, maxima and minima peaks occur in the frequency spectrum when the phase shift is in integer multiple of $\pi/2$. The number of peaks in the spectrum reveals the magnitude of the spectral phase shifts. From the analysis of the phase shifts versus peak power, n_2/A_{eff} can be precisely deduced. However, in this technique and other known approaches, one would typically require several hundred meters of fiber and sometimes several kilometers for experiments utilizing cw lasers [57].

The investigation embodied in this thesis utilizes a new technique – the photorefractive beam coupling technique (also called induced grating autocorrelation-IGA) to measure n_2 and stimulated Raman scattering in short lengths ($Z \leq 20$m) of Er-Al-Ge doped single mode fibers. IGA was originally developed for characterization of ultrashort pulses [63,64]. The use of the photorefractive beam coupling technique for measuring n_2 relies on the fact that the IGA can detect the time dependent phase change

acquired by an optical pulse after propagating through a nonlinear medium, such as optical fiber. It is the SPM induced phase change that is used to characterize the nonlinear medium. Generally, because of the short length of fiber needed to generate SPM in IGA experiments, GVD (group velocity dispersion) can be neglected. The first application of the IGA technique for n_2 measurement in optical fiber was carried out in previously characterized pure silica fibers and Er-doped fibers [66] and a good agreement with earlier published results confirmed the accuracy of the this technique. This technique has also been utilized to measure the magnitude and sign of n_2 in 1 mm thick GaAs, ZnTe and CdTe films and proved to be within 5%s of published values as determined by Z-scan [67]. The main goal of this thesis is three-fold: (1) A systematic study of the n_2/A_{eff} as a function of Er, Al and Ge contents. (2) To establish the ultimate sensitivity of the IGA technique and relate it to other known techniques, and (3) To modify the existing IGA model which is based on the simple theory of SPM, include the Raman contribution to the nonlinearity (in the limits of zero GVD). This modified model was successful in explaining the observed deviation in IGA model and has paved the way for the use of IGA technique for the measurement of the Raman gain coefficient in optical fibers. These outlined objectives have been achieved and the details of the work are reported in this thesis and in conference presentations that the author has delivered [68-71].

1.2 Overview of the Dissertation

The dissertation consists of eight chapters, including this introduction that forms Chapter 1. In Chapter 2, the basic nonlinear effects in optical fibers are discussed, together with the conditions under which they occur. The relation between the nonlinear refractive index and the third order nonlinear susceptibility was derived for linearly polarized optical field. The simple theory of SPM was presented, and the nonlinear wave equation was solved for a self-phase modulated Gaussian pulse in the zero GVD regimes, to show the nonlinear phase shift and frequency broadening associated with SPM are determined. Stimulated Brillouin and Stimulated Raman scattering are briefly explained. Pulse dispersion in optical fibers is discussed, and the role of GVD in the nonlinear interactions in optical fibers at different propagation regimes is explained.

Chapter 3 contains a survey and description of the different measurement techniques that have been used to measure the nonlinear index of refraction (n_2) in optical fibers, including the "famous" spectral domain SPM method pioneered by Stolen and Lin [13]. The levels of performance of these techniques as well as their limitations are discussed, and the need for a new approach, such as the IGA technique was highlighted.

In Chapter 4 the basic theory and principles of the IGA technique is discussed. The concept of photorefractive effect and photorefractive two beam coupling are explained. The simple model of the IGA technique is presented in the limit of pure self-phase modulation for a propagating Gaussian beam, in the regime of negligible GVD (group velocity dispersion) of the fiber. The experimental set-up and procedures to for taking IGA measurements are explained.

In Chapter 5, the author reports the results of several n_2 measurements he has done in different fibers using the IGA technique. Of particular interest in this chapter is the result of the dependence of the nonlinear coefficient (n_2/A_{eff}) on the doping profiles in Er-Al-Ge doped single mode fibers. Results of the measurement of n_2/A_{eff} in DCF (dispersion compensating fiber) and in True-Wave fiber are also presented. These results are compared with published values.

Chapter 6 contains the new modification of IGA model, which takes into account the stimulated Raman scattering as an additional nonlinear process to SPM, for a propagating Gaussian pulse in the zero GVD regime. The initial observation of the break-down of the pure-SPM IGA model in high GeO_2-doped fibers is outlined, which necessitated the modification. As a result of the new model, IGA can be used to measure another crucial parameter in optical fibers, known as the Raman gain coefficient. The results of the Raman gain coefficient measurements in four different fibers including pure silica core fiber, dispersion compensating fiber (DCF), and highly GeO_2 doped fibers are outlined in this chapter. A numerical modeling of IGA, in the presence of pump depletion during SRS is also presented.

In Chapter 7, the author relates the IGA technique to the widely accepted spectral domain n_2 measurement technique. It is shown that, in the pure SPM limit, IGA results converge with the results of the Stolen's method [13,52], through a direct mathematical relation. The measured sensitivity of IGA is also discussed in this chapter and it is shown that IGA could detect phase shifts as small as 0.14π.

Chapter 8 contains the conclusion and the recommendations for further research in this field.

CHAPTER 2

NONLINEAR EFFECTS AND PULSE DISPERSION IN OPTICAL FIBERS

2.1 Nonlinear Susceptibility and Index of Refraction

The nonlinear effects in optical fibers originate from the polarizability of the molecules under applied optical field. The polarizability of a molecule is affected on two time scales during pulse propagation in optical fiber. The first is an essentially instantaneous time scale associated with the electronic response and leads to an intensity-dependent refractive index (Kerr nonlinearity). This effect arises from an optically induced distortion of electronic charge distribution within the medium. Typical response time of electronic nonlinearity is approximately 1 fs. [72]. The second time scale is associated with molecular vibrations with response time in order of 50-100 fs [73], which is regarded as a non-instantaneous time scale. The later is responsible for SRS in fibers.

When light passes through a dielectric medium such as an optical fiber, there is induced electric polarization arising from the influence of the applied field on the electric dipoles:

$$\mathbf{P} = \varepsilon_o \chi \mathbf{E} \tag{2.1}$$

Where ε_o is the vacuum permittivity, E is the electric field of the optical pulse, and χ is the susceptibility. If the laser beam is of high intensity, the response of the medium becomes nonlinear and the induced polarization **P** can be expressed as a perturbation expansion in successive higher orders of the optical electric field:

$$P = \varepsilon_o \left[\chi^{(1)}.E + \chi^{(2)} : EE + \chi^{(3)} : EEE + ... \right]$$

$$\approx \varepsilon_o \chi^{1)} E + \varepsilon_o \chi^{(2)} E^2 + \varepsilon_o \chi^{(3)} E^3 + ... \qquad (2.2)$$

where $\chi^{(n)}$ (n = 1,2,...) is the nth order dielectric susceptibility. In general, the third order susceptibility is a fourth-rank tensor (i.e. $\chi^{(3)} \equiv \chi^{(3)}_{ijkl}$). To simplify the problem, one normally assumes a linearly polarized optical field, which ensures that only one component $\chi^{(3)}_{xxxx}$ contributes to the refractive index, and the problem can be treated using scalar approach. This assumption is justified in the present circumstance as well, considering the short length of single mode fibers utilized in this work. In practice, the tensorial nature of $\chi^{(3)}$ can affect the polarization properties of the optical field through nonlinear birefringence [77,78]. The linear susceptibility $\chi^{(1)}$ represents the dominant contribution to **P**. Its effect is included through the linear refractive index (n) and the attenuation constant α. The second order susceptibility $\chi^{(2)}$ is responsible for such nonlinear effects as second harmonic generation (SHG), sum-frequency generation, parametric fluorescence and optical rectification [74]. It is nonzero only for media that lack inversion symmetry. As a result, since SiO_2 is a symmetric molecule, $\chi^{(2)}$ vanishes for silica fibers. Thus optical fibers do not normally exhibit second-order nonlinear effects. However, electric-quadrupole and magnetic dipole moments can sometimes generate weak second-order nonlinear effects. Defects or color centers inside the fiber can also give rise to SHG, under certain conditions [75,76]. The lowest order nonlinear effects in optical fibers therefore originate from the third order susceptibility $\chi^{(3)}$ which

gives rise to nonlinear refraction. Nonlinear refraction refers to the intensity dependence of the refractive index resulting from the contribution of $\chi^{(3)}$.

The relationship between $\chi^{(3)}$ and the nonlinear refractive index (n_2) will be derived in the following analysis:

Assume a plane optical wave with electric field of the form:

$$E(z,t) = E_o e^{i(wt-kz)} \tag{2.3}$$

with the real part given simply by:

$$E = E_o \cos(\omega t - kz) \tag{2.4}.$$

Equation (2.2) can now be re-written as:

$$P = \varepsilon_o \chi^{1)} E_o \cos(\omega t - kz) + \varepsilon_o \chi^{(3)} E_o^3 \cos^3(\omega t - kz) + ... \tag{2.5}.$$

Using the trigonometric identity [79] $\cos^3\theta = \frac{1}{4}(\cos 3\theta + 3\cos\theta)$, equation (2.5) can be written as

$$P = \varepsilon_o \left(\chi^{1)} + \frac{3}{4}\chi^{(3)} E_o^2 \right) E_o \cos(\omega t - kz) \tag{2.6}$$

The intensity of an optical field is related to the electric field by the expression [20] :

$$I = \frac{1}{2} c \varepsilon_0 n_0 E_0^2 \tag{2.7}$$

where n_0 is the low field refractive index of the medium. Equation (2.7) can thus be written as:

$$P = \varepsilon_o \left(\chi^{(1)} + \frac{3}{2c\varepsilon_0 n_0} \chi^{(3)} I \right) E_o \cos(\omega t - kz) \tag{2.8}$$

The general relation between polarization and refractive index is given by [80]:

$$P = \varepsilon_o \left(n^2 - 1\right) E_o \cos(\omega t - kz) \tag{2.9}$$

Comparing Equations. (2.8) and (2.9), one can write

$$n^2 = 1 + \chi^{(1)} + \frac{3}{2c\varepsilon_0 n_0} \chi^{(3)} I . \tag{2.10}$$

Since the last term in Equation (2.10) is usually very small even for very intense light, one can approximate by Taylor series expansion

$$n \approx n_0 + \frac{3}{4c\varepsilon_0 n_0^2} \chi^{(3)} I . \tag{2.11}$$

Equation (2.11) can be written as:

$$n \approx n_0 + n_2 I = n_0 + \Delta n \tag{2.12}$$

where

$$n_0^2 = 1 + \chi \tag{2.13}$$

and

$$n_2 = \frac{3}{4c\varepsilon_0 n_0^2} \chi^{(3)} \tag{2.14}$$

In the above Equation, n_2 is the nonlinear refractive index, n_0 is the linear refractive index, ε_0 is vacuum permittivity ($\varepsilon_0 = 8.85 \times 10^{-12}$ F/m), c is the velocity of light in vacuum ($c = 2.998 \times 10^8$ m/s) and n_0 is the low field refractive index.

To have a feeling of typical values, note that for silica fibers $n_0 \approx 1.46$ and $n_2 \approx 2.5 \times 10^{-20}$ m^2/W, [2.5×10^{-16} cm/W]. Thus for a laser beam with peak power of 30W propagating through a single mode fiber with effective core area (A_{eff}) of 50 μm^2. The resultant intensity ($I \approx P/A_{eff}$) is 6.0×10^{11} W/m^2, [6.0×10^7 W/cm^2] and the change in refractive index due to nonlinear effects is $\Delta n = n_2 I = 1.5 \times 10^{-8}$. This change in refractive index seems very small, but due to very long interaction lengths in optical fiber communication (typically 10,000 km in long haul systems), the accumulated effects become significant and can result to severe penalty. In fact, it is this small nonlinear term that is responsible for SPM, XPM, FWM and for the formation of solitons in optical fibers.

2.2 Self-Phase Modulation

Self-phase modulation (SPM) is a phenomenon in which a laser beam propagating in a medium interacts with the medium and imposes a phase modulation on itself. The physical origin of SPM lies in the fact that the strong field of a laser beam is capable of inducing an appreciable intensity-dependent refractive index change in the medium. The medium then reacts back and inflicts a phase change on the incoming wave, resulting in self-phase modulation. This phase modulation is associated with frequency broadening of the optical pulse. The first observation of SPM was made in the context of transient self-focusing of an optical pulse propagating in a solution of a CS_2-filled cell [81]. Alfano and Shapiro observed SPM in solids and glasses by using picosecond pulses [82]. The first observation of SPM in optical fibers was made by Ippen *et al* [83] in a fiber whose core was filled with CS_2. This work led to a systematic study of SPM in optical fiber by Stolen and Lin [3].

To describe the process of SPM of light in optical fibers, the author starts with the nonlinear wave equation for the electric field:

$$\left(\frac{\partial^2}{\partial z^2}-\frac{n_0^2}{c^2}\frac{\partial^2}{\partial t^2}\right)E=\frac{4\pi}{c^2}\frac{\partial^2}{\partial t^2}P^{(3)} \tag{2.15}$$

where $\mathbf{P}^{(3)}$ is the third order polarizability and can given by:

$$\mathrm{P}^{(3)}=\chi^{(3)}|E|^2E \tag{2.16}$$

One can assume a plane wave of the form:

$$E=\Xi(z,t)\exp(ik_0z-i\omega_0t) \tag{2.17}$$

In the simple theory of SPM [84-86], it is normal to use the slowly varying amplitude approximation by neglecting the $\partial^2\Xi/\partial t^2$ term in the equation. Also assume an instantaneous response of $\chi^{(3)}$. The assumption of instantaneous response amounts to a neglect of the contribution of molecular vibrations (Raman effect) to $\chi^{(3)}$. Thus, from Equations (2.15), (2.16) and (2.17) together with the assumptions, one obtains,

$$\left(\frac{\partial}{\partial z}-\frac{n_0}{c}\frac{\partial}{\partial t}\right)\Xi=-\frac{4\pi\omega_0^2}{i2k_0c^2}\chi^{(3)}|\Xi|^2\Xi \tag{2.18}$$

If one sets $z' \equiv z + ct/n_0$ and $\Xi = |\Xi|\exp(i\phi)$, Equation (2.18) will yield two sets of equations for the electric field amplitude and the phase:

$$\frac{\partial|\Xi|}{\partial z}=0 \tag{2.19a}$$

$$\frac{\partial\phi}{\partial z'}=\frac{2\pi\omega_0^2}{c^2k_0}\chi^{(3)}|\Xi|^2 \tag{2.19b}$$

These equations have the following solution:

$$|\Xi|=|\Xi(t)| \tag{2.20a}$$

$$\phi(z,t) = \phi_0 + \frac{2\pi\omega_0^2}{c^2 k_0}\chi^{(3)}|\Xi(t)|^2 z \qquad (2.20b)$$

Equation (2.20a) implies that the laser pulse propagates in the fiber without distortion of the pulse shape. Equation (2.20b) on the other hand shows that as the optical pulse propagate along the fiber from 0 to z, it acquires an induced phase change $\Delta\phi$, given by:

$$\Delta\phi = \phi(z,t) - \phi_0 = \frac{2\pi\omega_0^2}{c^2 k_0}\chi^{(3)}|\Xi(t)|^2 z \qquad (2.21)$$

The SPM induced spectral broadening can be deduced from the time derivative of the phase.

$$\Delta\omega(t) = -\frac{\partial(\Delta\phi)}{\partial t} = \frac{2\pi\omega_0^2}{c^2 k_0}\chi^{(3)}\frac{\partial|\Xi|^2}{\partial t} z \qquad (2.22)$$

The spectrum of the SPM broadened pulse can be calculated from the Fourier transform of the electric field:

$$|E(\omega)|^2 = \left|\frac{1}{2\pi}\int_{-\infty}^{\infty}\Xi(t)\exp[i\Delta\phi(t) - i(\omega-\omega_0)t]\right|^2 \qquad (2.23)$$

where Ξ is the field amplitude which is assumed to be normalized such that $|\Xi(0,0)| = 1$ and $|\Xi(z,t)|^2$ represents the optical power. Such a spectrum calculated from Equation (2.23) is called the power spectrum.

2.3 Cross-Phase Modulation

Cross-phase modulation (XPM) refers to the nonlinear phase change of an optical pulse induced by another pulse, co-propagating with it at a different wavelength. The XPM-induced coupling among optical waves can give rise to spectral broadening, nonlinear birefringence and modulation instability. A detailed discussion of XPM and its effects on pulse propagation can be found in the following references [20, 87-90]. An important characteristic of XPM is that for equally intense optical fields (copropagating), the contribution of XPM to the nonlinear phase shift is twice compared with that of SPM. However, the XPM interaction between counter propagating optical pulses is generally weak and contributes little to the nonlinear phase shifts. This is because the group velocity mismatch is so large that the two pulses have little time to interact with each other.

2.4 Four-Wave Mixing

This is a process in which three optical wave interact to generate another wave at different frequency.

$$\omega_1 + \omega_2 + \omega_3 = \omega_4 \tag{2.24}$$

The intensity of the generated wave is proportional to the product of the intensities of the incident waves. FWM is a $\chi^{(3)}$ process and originates from the response of the bound electrons of a material to an applied optical field. One important property of four-wave mixing is that it requires phase matching. The phase matching condition required for the process shown in Equation (2.24) to occur is that $\Delta k = 0$, where:

$$\Delta k = k_4 - k_1 - k_2 - k_3 . \quad (2.25)$$

The four wave mixing process can also be defined as an interaction between four photons – a photon of frequency ω_3 combines with a photon of frequency ω_4 to produce a photon of frequency ω_1 and another of frequency ω_2.

This can be written simply as:

$$\omega_3 + \omega_4 = \omega_1 + \omega_2 \quad (2.26)$$

with the phase matching condition:

$$\Delta k = k_3 + k_4 - k_1 - k_3 = 0 \quad (2.27)$$

A special case is obtained when $\omega_1 = \omega_2 = \omega_3 = \omega_4$. The process is then called degenerate four wave mixing [91]. FWM processes in optical fibers have been studied extensively [16-17,20, 92-94].

2.5 Stimulated Raman Scattering

Raman scattering describes the interaction of light with molecular vibrations. Incident light scattered by molecules experience a downshift in optical frequency. The change in optical frequency is equal to molecular vibrational frequency (called the Stokes frequency). This process is called Raman effect. In silica fibers, this frequency shift is about 13.2 THz (1 THz = 10^{12} Hz). If two optical waves separated by the Stokes frequency co-propagate in a Raman active medium, such as an optical fiber, the lower frequency (probe) wave will experience optical gain generated by, and at the expense of,

the higher frequency (pump) wave. This process is called stimulated Raman scattering (SRS). The growth of the Stokes wave in optical fibers can be describe by the following expression [12]:

$$P_s(L) = P_s(0)\exp\left(g_R \frac{L_{eff} P_p(0)}{bA_{eff}}\right) \tag{2.28}$$

where $P_s(0)$ is the initial power of the Stokes wave, $P_s(L)$ is the final (output) power of the Stokes wave after traveling a length (L) in the fiber. $P_p(0)$ is the initial injected power of the pump wave, L_{eff} is the effective length. The effective length is introduced to account for the exponential decay with length of the pump power due to fiber loss. It is given by:

$$L_{eff} = \int_0^L \exp(-\alpha l)dl = \frac{1-\exp(-\alpha L)}{\alpha} \tag{2.29}$$

where α is the loss coefficient for the fiber (for $\alpha << 1$, $L_{eff} = L$). A_{eff} is the effective area of the fiber [18]. The factor *b* accounts for the relative polarizations of pump and probe waves and the polarization properties of the fiber. In a polarization maintaining fiber, with identical pump and probe polarization states, b = 1. In a conventional fiber that does not maintain polarization, b = 2. The quantity g_R is called the Raman gain coefficient. The g_R for silica fiber was measured by Stolen *et al,* in the early experiments on SRS in single mode fibers [50,95]. In general, g_R scales inversely with wavelength. The value of g_R for silica fibers is about 1.5×10^{-11} cm/W [50] in the visible and at 1064 nm, $g_R = 0.92 \times 10^{-11}$ cm/W [96]. It also depends on the composition of the fiber core and can vary significantly with the use of different dopants [97,98].

In general, the Raman gain coefficient is related to the imaginary part of the third order susceptibility [$\chi_I^{(3)}$] through the following expression [91]:

$$g_R = \frac{12\pi\eta_0 P}{n_0^2 \varepsilon_0 \lambda_0 A} \chi_I^{(3)} \tag{2.30}$$

where η_0 is the impedance of free space $\{\eta_0 = (\mu_0/\varepsilon_0)^{1/2}\}$, P is the optical power, λ_0 is the laser wavelength and A is cross-sectional area (for optical fibers, $A \equiv A_{eff}$).

The Raman threshold is defined as the input pump power at which the Stokes power becomes equal to the pump power at the fiber output [99]. This implies that:

$$P_s(L) = P_p(L) \equiv P_p(0)\exp(-\alpha_p L) \tag{2.31}$$

where α_p is the fiber loss coefficient at the pump wavelength and the rest of the symbols have their usual meanings as earlier defined. Smith [99] has shown that the threshold power (P_{th}) for this condition to occur can be given in terms of the Raman gain coefficient and the fiber length as follow:

$$P_{th} = 16\left(\frac{bA_{eff}}{g_R L_{eff}}\right) \tag{2.32}$$

where L_{eff} is the effective fiber length defined by Equation (2.29) and A_{eff} is the effective core area of the fiber. The factor b accounts for polarization (b = 2 if polarization is completely scrambled and b = 1 if polarization is maintained). Thus for a typical silica fiber with A_{eff} = 50 μm^2 and L_{eff} = 20 m and b = 1, the SRS threshold power is about 600W. For long fibers (say L_{eff} = 2 km), the threshold power can be as low as 3 W for a

25 μm^2 core fiber. An important feature of the Raman gain in silica is that g_R extends over a large frequency range (~ 40 THz), with a broad peak near 13.2 THz [20,50,100]. Figure 2.1 shows typical Raman gain spectrum for fused silica.

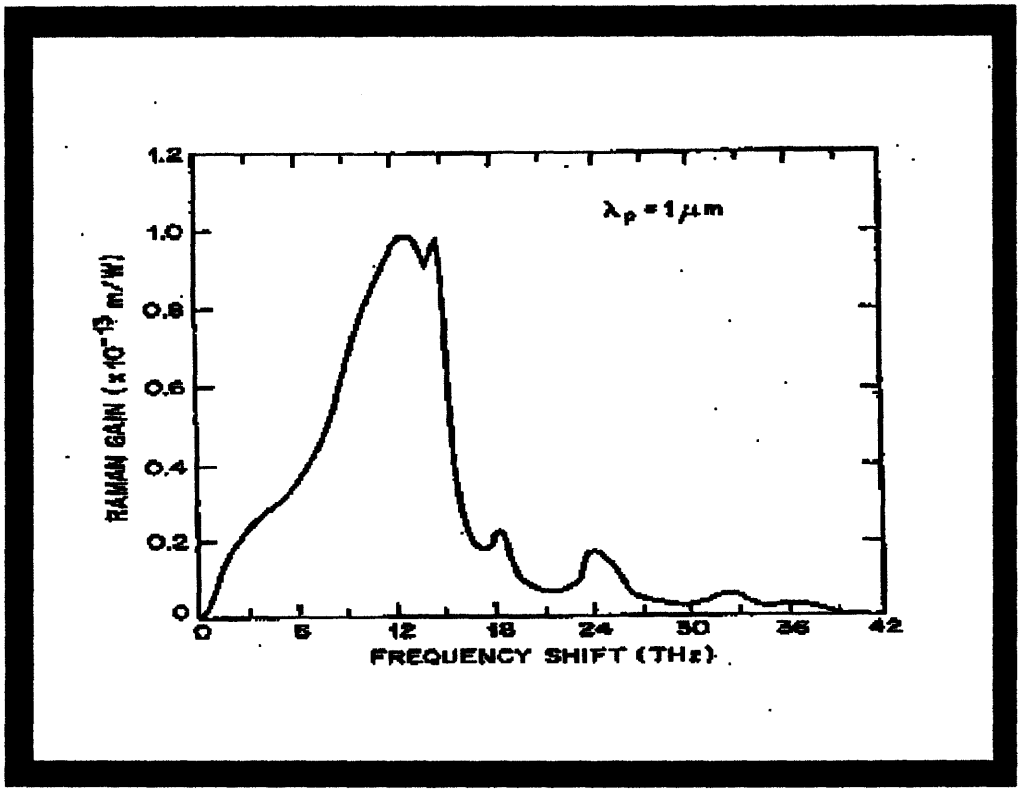

Figure 2.1 Raman gain spectrum for fused silica at a pump wavelength of 1.0 μm [100].

A few words needs to be mentioned about the formation of a higher frequency photon during SRS. The optical wave associated with the high frequency photons is called anti-Stokes and is generated when a phonon combines with the pump photon to generate a high frequency photon at frequency $\omega_a = \omega_p + \Delta\omega$ for a Stokes wave of frequency $\omega_s = \omega_p - \Delta\omega$, where ω_p is the pump frequency and $\Delta\omega$ is the Raman frequency shift. The anti-Stokes waves are typically much weaker than the Stokes

intensity. Since $2\omega_p = \omega_s + \omega_p$ the formation of anti-Stokes during SRS leads to four-wave mixing – a process where two photons annihilate themselves to produce Stokes and anti-Stokes photons, provided that the total momentum is conserved. The momentum conservation requirement is associated with the phase matching condition ($\Delta k = 2k_p - k_a - k_s = 0$) that must be fulfilled for four-wave mixing to take place. This phase matching condition is not easily satisfied in single mode fibers for $\Delta\omega$ ~ !0 THz [20]. Thus, the anti-Stokes wave is rarely observed during SRS in single mode fibers.

2.6 Stimulated Brillouin Scattering

Stimulated Brillouin scattering (SBS) is similar to SRS except that SBS involves the interaction of light with sound (acoustic) waves rather than molecular vibrations. Part of the incident (pump) light is converted into Stokes light of lower frequency with a concomitant excitation of an acoustical phonon. The Stokes shift in SBS (~ 10 GHz) is smaller by three orders of magnitude compared with that occurring in SRS. In addition, the SBS generated Stokes wave propagates in the backward direction. The peak SBS gain coefficient (g_B) in silica fibers (g_B ~ 4.0 x 10^{-9} cm/W [51]) is over two orders of magnitude larger than the gain coefficient for SRS, but the bandwidth of the Brillouin gain spectrum is very narrow, typically 20 MHz [101]. The threshold power for SBS is given by [99]

$$P_B^{th} = 21\left[\frac{bA_{eff}}{g_B L_{eff}}\right] \qquad (2.33).$$

Although SBS can occur in optical fibers at input power levels much lower than those needed for stimulated Raman Scattering, SBS only occurs for a continuous wave (cw) pump or when the pumping is in the form of relatively wide pulses (with pulsewidth in the range of nanoseconds and higher). For short pulses in the picosecond range SBS is negligible. As a result, the author would not consider SBS in his measurements and analysis in this work.

2.7 Optical Solitons in Fibers

Optical soliton refers to optical wave that preserves its pulse shape and velocity as it travels over long distances. Solitons can form in optical fiber if there is an exact balance between the effects of non-linearity and the dispersion in the fiber material. The condition can be fulfilled in the anomaous dispersion regime, with $\beta_2 < 0$, where β_2 is the GVD parameter. Therefore, for single mode fibers the operating wavelengths for solitons are usually about 1.3 μm or longer. The work discussed in this thesis has been carried out below the soliton regime. For more detailed discussion on soliton propagation, readers should consult the following references [20, 56-59]

2.8 Two-Photon Absorption

This is a process in which an atom makes a transition from its ground state to an excited state by simultaneous absorption of two laser photons. Thus in this process when two low-energy photons strike a molecule at almost the same time and get absorbed, they have approximately the same effect as one photon of half the wavelength (twice the frequency). This process is related to the optical absorption property of the materials and

is generally observed at high intensities. At high optical intensity, the absorption coefficient (α) of a nonlinear material becomes intensity dependent and can be written as:

$$\alpha = \alpha_0 + \alpha_2 I, \tag{2.34a}$$

where I is the optical intensity α_0 is the linear (low field) absorption coefficient and α_2 is the two-photon absorption coefficient. The two-photon absorption is related to the imaginary part of the third order nonlinear susceptibility in the following manner [20]:

$$\alpha_2 = \frac{3\omega_0}{4nc}\chi_I^{(3)} \tag{2.34b}$$

where ω_0 is the central angular frequency of the laser, n is the linear refractive index of the material and c is the speed of light. In optical fibers, two-photon absorption can lead to intensity dependent loss and sometimes cause color center formations that degrade the quality of an optical fiber. It has been reported that two-photon absorption also leads to modulation instability [102]. It should be noted however that two-photon absorption can only occur in silica fibers for laser wave lengths of about 320 nm or less, because the sum of the energy of two photons at this wavelengths is typically greater than the band gap of fused silica (~8.3 eV). Typical value of α_2 measured in silica fiber at 260 nm is 3.0×10^{-5} [103]. Because of the long wavelength (1064 nm) of the laser used in this work, two-

photon absorption is not expected to occur and as such it will not be taken into account in analyzing the data obtained in the present work.

2.9 Pulse Dispersion and GVD in Optical Fibers

Pulse dispersion refers to broadening in time of an optical pulse as it propagates through the fiber. There are three types of pulse dispersion in optical fibers namely: intermodal dispersion, material dispersion and waveguide dispersion. Intermodal dispersion arises due to different group velocities of different modes in the waveguide. This form of dispersion is dominant in multimode fibers and negligible in single mode fibers. Both material dispersion and waveguide dispersion are called intramodal dispersion and arise due to the different transverse times taken by different wavelength components of the source.

In single mode fibers, material dispersion and waveguide dispersion are the dominant dispersion mechanisms. Material dispersion results from the dependence of the fiber material on wavelength. On the other hand, waveguide dispersion is purely a geometric effect resulting from the waveguide structure. Both material and waveguide dispersions depend on the spectral width of the source and form what is known as chromatic dispersion in single mode fibers. Chromatic dispersion plays an important role in the propagation of short laser pulses because different spectral components associated with the pulse travel at different speeds given by $c/n(\omega)$. Mathematically, the effect of fiber dispersion can be accounted for by expanding the mode-propagation constant β in a Taylor series (since the propagating pulse is assumed to have a relatively narrow frequency spectrum) about the frequency (ω_0) at which the pulse spectrum is centered:

$$\beta(\omega) = n(\omega)\frac{\omega}{c} \approx \beta_0 + \beta_1(\omega - \omega_0) + \frac{1}{2!}\beta_2(\omega - \omega_0)^2 + \frac{1}{3!}\beta_3(\omega - \omega_0)^3 + \ldots\ldots \quad (2.35)$$

where

$$\beta_m = \left(\frac{d^m \beta}{d\omega^m}\right)_{\omega=\omega_0} \qquad (\text{m} = 0, 1, 2, \ldots\ldots) \quad (2.36)$$

The parameters β_1 and β_2 are related to the linear refractive index n and its derivative in the following manner:

$$\beta_1 .. = \frac{1}{v_g} = \frac{n_g}{c} = \frac{1}{c}\left(n + \omega\frac{dn}{d\omega}\right) \quad (2.37)$$

$$\beta_2 .. = \frac{1}{c}\left(2\frac{dn}{d\omega} + \omega\frac{d^2 n}{d\omega^2}\right), \quad (2.38)$$

where n_g is the group index and v_g is the group velocity and β_1 is the group velocity parameter. In principle, the envelope of an optical pulse moves at the group velocity (v_g) while the β_2 represents the dispersion of the group velocity. For this reason, this phenomenon is called the group velocity dispersion (GVD) and β_2 is referred to as GVD parameter and represents the lowest order dispersion term. The term β_3 appearing in the

Taylor expansion is called the third order dispersion parameter and is usually generally negligible except in the vicinity of zero dispersion wavelength of the fiber, where β_2 vanish. For ultrashort pulses in the femtoseconds regime, it may be necessary to include the effect of β_3 even if $\beta_2 \neq 0$, because the expansion of $\Delta\omega/\omega$ is no longer small enough to neglect it. Typical value of β_3 is 0.1 ps^3/km [20]. The quantity β_2 is measured in ps^2/km. Typically β_2 is of the order 50 ps^2/km in the visible region, while at 1550 nm it is about –20 ps^2/km. In the literature, the dispersion D (also called dispersion coefficient) is sometimes used in place of β_2, and the two are related by:

$$D = -\frac{2\pi c}{\lambda^2}\beta_2 \tag{2.39}$$

The dispersion coefficient D is defined as the time delay per unit length of the propagating distance per unit spectral width of the source. The commonly used unit for D is (ps/km.nm). Figure 2.2 shows a typical dispersion curve for conventional single mode fibers [104] with contributions from material and waveguide dispersion to the total dispersion in the fiber.

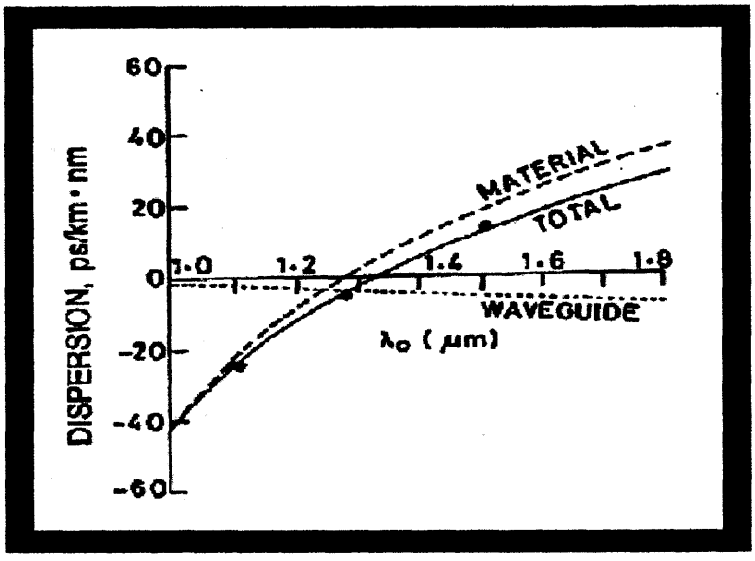

Figure 2.2 Variation of material, waveguide and total dispersion (D) with wavelength [104].

The material dispersion curve passes through zero around 1.27 μm and changes sign, while the waveguide dispersion is continually negative. The combined effect of the two results to a total dispersion curve that passes through zero around 1.3 μm. This is the so-called zero dispersion wavelength, denoted by λ_D. It should be noted however that dispersion does not completely go to zero at $\lambda = \lambda_D$, because in the vicinity of zero dispersion wavelength higher order dispersion terms (such as the cubic term) become important and the pulse will still undergo dispersion although by a much smaller amount. The slope of the total dispersion in Figure (2.2) is called the dispersion slope, and is related to the cubic dispersion term (β_3). Figure (2.3) shows the variation of GVD parameter β_2 with wavelength for fused silica [20].

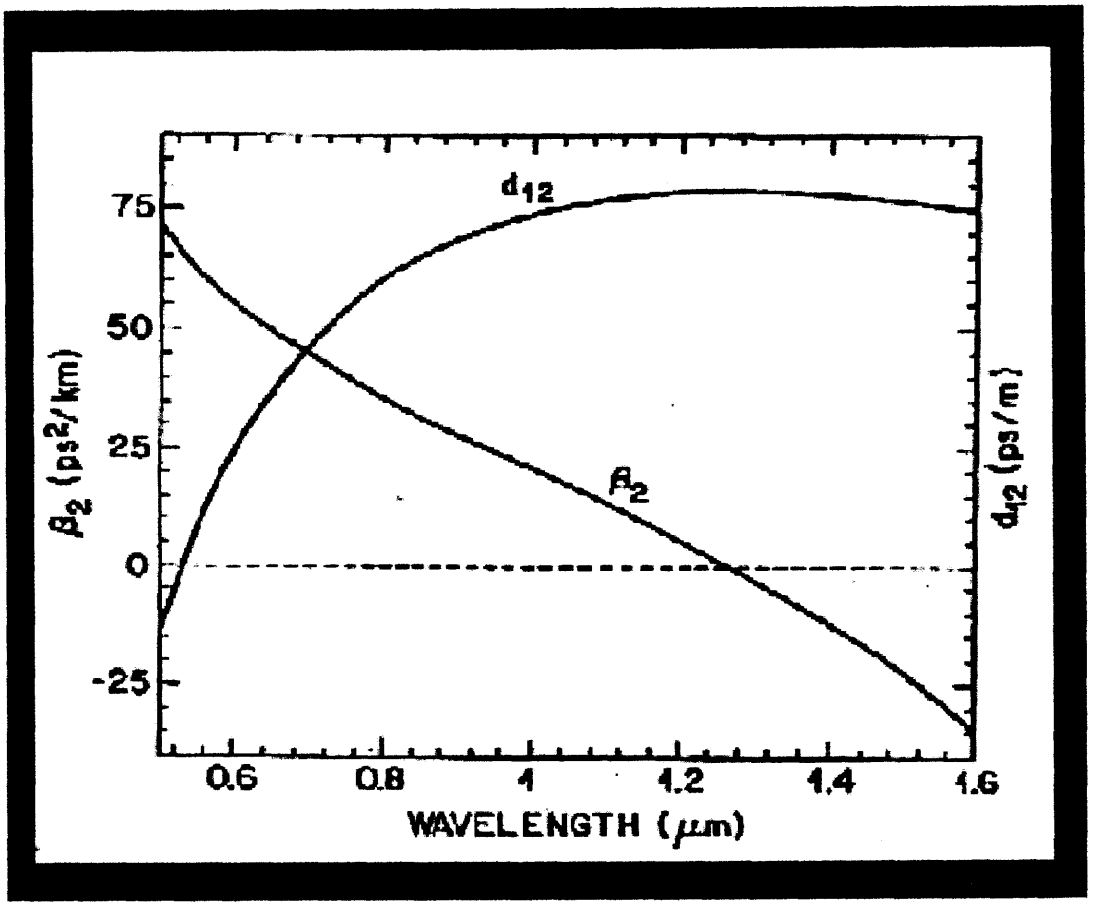

Figure 2.3 Variation of β_2 and d_{12} (walk-off parameter) with wavelength for fused Silica [20].

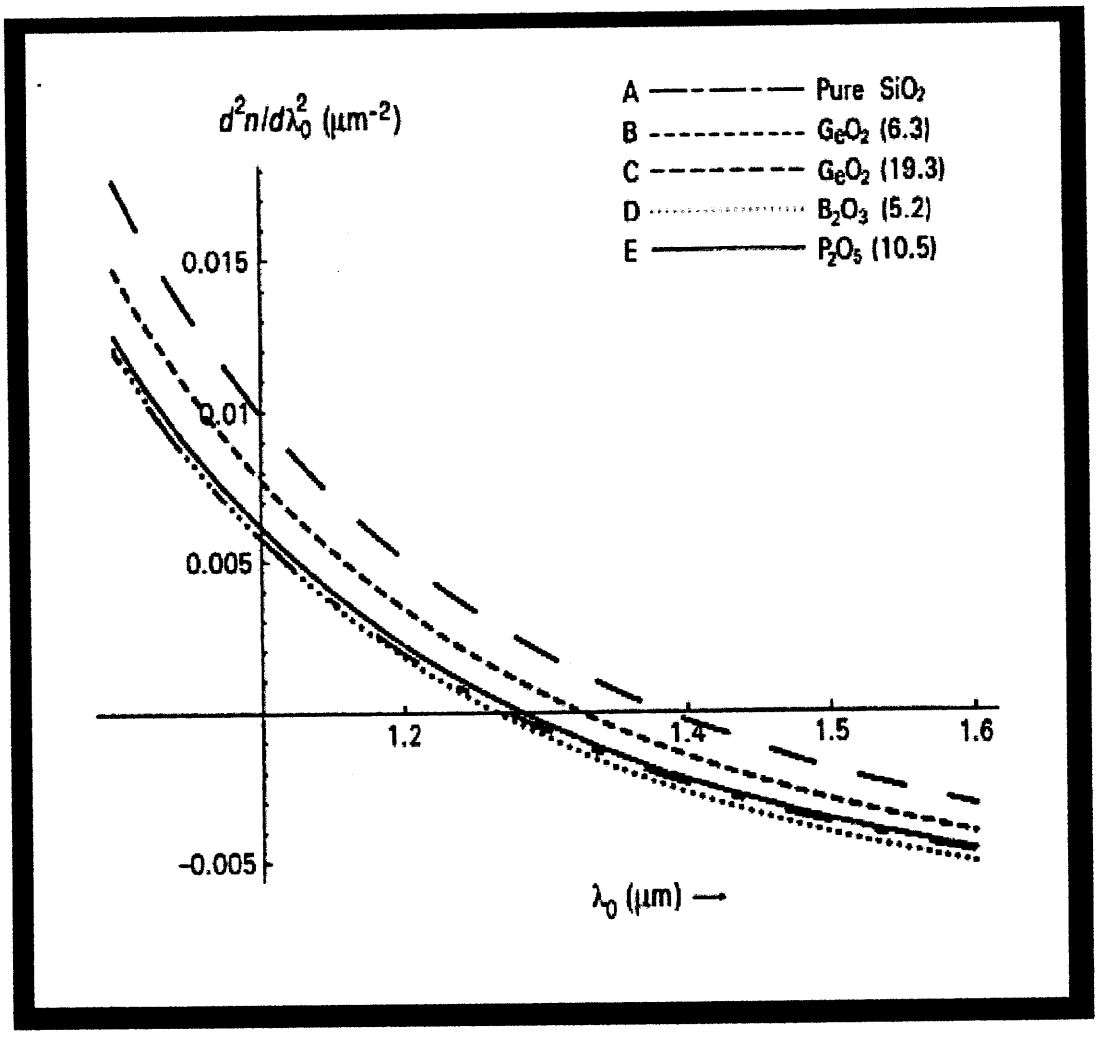

Figure 2.4 Variation of $d^2n/d\lambda^2$ with λ for pure silica and doped fibers. Dopant concentration is in parenthesis [105].

It needs to be mentioned that the dispersion behavior of some telecommunication fibers may deviate from the that shown in Figures (2.2) and (2.3) because the fiber core is sometimes doped with GeO_2, P_2O_5, or other dopants which changes the refractive index of the fiber and modifies the dispersion curve. Figure 2.4 shows the variation of $d^2n/d\lambda^2$ with λ for doped silica fibers. This shows that $d^2n/d\lambda^2$ depends significantly on dopant concentration and varies also with wavelength.

The dispersion coefficient due to material dispersion (D_m) can be written:

$$D_m = \frac{\Delta\tau}{L\Delta\lambda} = -\frac{1}{\lambda c}\left(\lambda \frac{d^2n}{d\lambda^2}\right)\times 10^9 [ps/(km-nm)], \qquad (2.41)$$

where $\Delta\tau$ is the time delay in the arrival of the fastest and the slowest wavelength component in a material with refractive index $n(\lambda)$. $\Delta\lambda$ is the spectral width of the source and L is the propagation distance. For single mode fibers, the total dispersion is given by a similar expression, except that the refractive index n is replaced with the effective index of the mode (n_e) thus:

$$D_T = -\frac{1}{\lambda c}\left(\lambda \frac{d^2n_e}{d\lambda^2}\right)\times 10^9 [ps/(km-nm)], \qquad (2.42)$$

where λ is measure in μm and c is in km/s (i.e. c = 3.0 x 10^5km/s). This expression contains contributions from both material and waveguide dispersion. The parameter n_e is called the effective index of the mode ($n_e = \beta/k_0$), where β is the propagation constant of

the mode and $k_0 = 2\pi/\lambda$. In the case of waveguide dispersion alone, the parameter D_w can be written in terms of the normalized frequency (V) thus:

$$D_w = -\frac{n_{cl}\Delta}{3\lambda}\left[V\frac{d^2(bV)}{dV^2}\right]\times 10^7[ps/(km-nm)] \qquad (2.43)$$

where n_{cl} is the cladding index, Δ is the relative refractive index between the core and the cladding, b is the normalized propagation constant. The normalized frequency (V) is given by $V = (2\pi a/\lambda.)(n_c^2-n_{cl}^2)^{1/2}$ where n_c is the refractive index of the fiber core and a is the core radius. Thus waveguide dispersion can be changed considerably by varying the operating V-value and the value of Δ. By changing the magnitude of the waveguide dispersion, one can locate zero dispersion at a desired wavelength. This feature is used in the telecommunication industry to shift the zero dispersion wavelengths in the vicinity of 1.55 μm where the fiber loss is minimum. Such fibers are called dispersion-shifted fibers (DSF). If the GVD is shifted beyond 1.6 μm, then the fiber is called dispersion compensating fiber (DCF). It is also possible to design a fiber with relatively low dispersion over the wavelength region 1.3-1.6 μm. Such fibers are called dispersion-flattened fibers. Figure (2.5) shows a combined plot of dispersion curves for standard silica fiber, dispersion shifted fiber and dispersion flattened fiber p on the same scale.

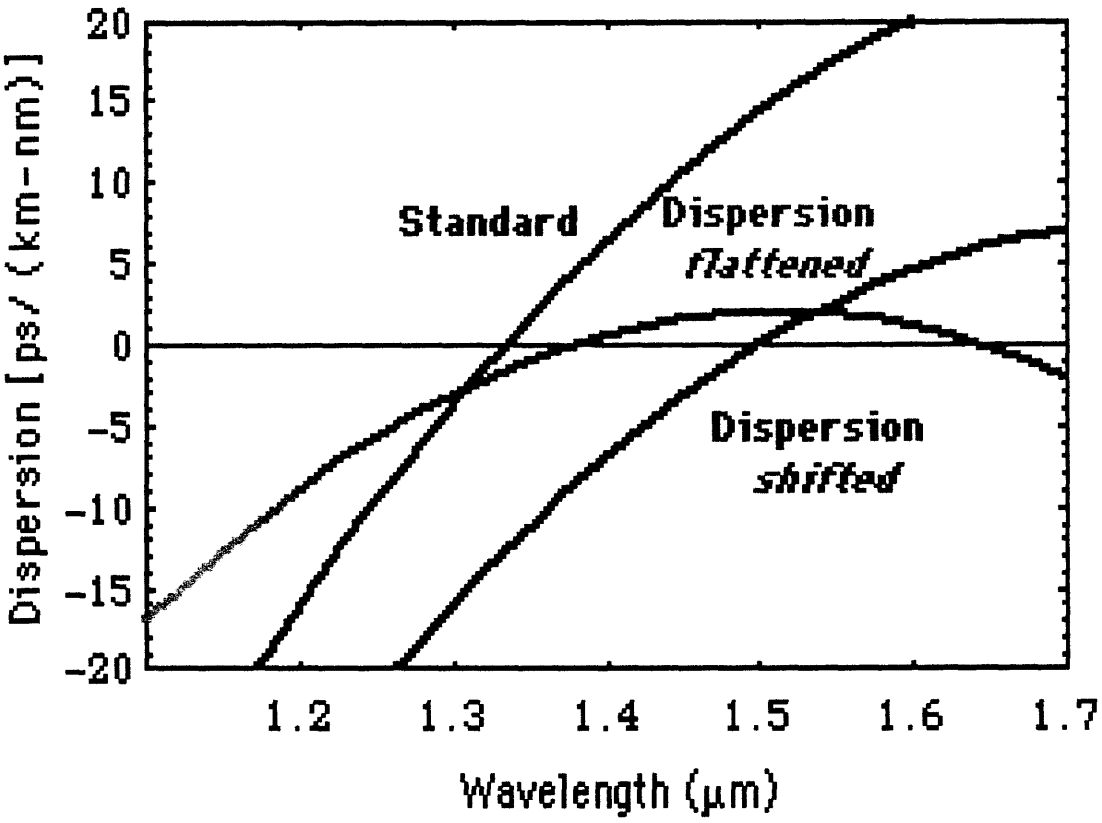

Figure 2.5 Dispersion curves for three types of fibers (standard silica fiber, dispersion shifted fiber and dispersion flattened fiber).

2.10 The Role of GVD in Nonlinear Interactions in Optical Fibers

Pulse dispersion plays an important role in nonlinear interaction in optical fibers because nonlinear effects can manifest qualitatively different behavior depending on the sign of GVD. For wavelengths less than the zero-dispersion wavelength ($\lambda > \lambda_D$), GVD is positive ($\beta_2 > 0$) and the fiber is said to exhibit normal dispersion. In the normal dispersion regime, the red shifted (low frequency or long wave length) component of an optical pulse travel faster that the blue shifted (short wavelength) component. In the wavelength region beyond the zero-dispersion wavelength, GVD is negative ($\beta_2 < 0$) and the fiber exhibits anomalous dispersion. In this regime, the blue shifted component of the pulse now travels faster than the red-shifted component. It is in this regime that optical fibers can support solitons through a balance between dispersion and self-phase modulation. Because of GVD effects, two different pulses at different wavelengths would travel at different speeds in the fiber.

The nonlinear interactions between the two pulses would cease to occur when the faster moving pulse has completely "walked" through the slower moving pulse. The separation between them is governed by the walk-off parameter d defined by $d = (1/v_{g1} - 1/v_{g2})$. Here, v_{g1} and v_{g2} represent the group velocities of the two pulses. One can define a walk-off length L_w as the distance within which the faster moving pulse walks through the slower moving pulse. The walk-off length can be given in terms of the walk-off parameter thus:

$$L_W = \frac{\tau_p}{|d|} \tag{2. 43}$$

where τ_p is the pulsewidth.

In order to properly analyze experimental results involving pulse propagation in optical fibers, it is necessary to classify the experimental fiber length (L) in terms of two length scales, (depending on the laser pulsewidth and peak power used), namely: the nonlinear length (L_{NL}) and the dispersion length (L_D). The nonlinear length represents the length scale over which the effect of nonlinearity (both SPM and XPM) becomes important. In terms of the pump peak power (P_0) this length can be is given by:

$$L_{NL} = (\gamma P_0)^{-1} \tag{2.44}$$

where γ is the nonlinear coefficient ($\gamma = n_2\omega_0/cA_{eff}$), A_{eff} is effective core area of the fiber and c is the speed of light. Similarly, the dispersion length, L_D represents the length scale over which the effect of GVD becomes important. In terms of the laser pulsewidth and the GVD parameter (β_2), this length can be given by:

$$L_D = \left(\frac{|\beta_2|}{\tau_p^2}\right)^{-1} \tag{2.45}$$

Generally, when the experimental fiber length (L) is such that $L \ll L_D$, but $L \sim L_{NL}$, GVD can be neglected and the pulse propagation is governed by nonlinear effects. If on the other hand, (through the choice of pulsewidth, laser power and experimental length) L is comparable to both L_{NL} and L_D the GVD will no longer be negligible and must be included in the analysis of experimental results. As a check, the author would like to run through some numbers and establish valid experimental and theoretical conditions for the work. Typically $\gamma \sim 3$ $W^{-1}km^{-1}$ for standard silica fibers and $\beta_2 \approx 24$ ps^2/km at 1.064 μm. Thus, for 50 ps pulses with a peak power of 36 W, L_{NL} is approximately 10 meters while

L_D is about 100 km. In practice however, dispersion may set in at a length shorter than this (100km), since there are other factors than β_2 that contribute to dispersion in fibers (see Section 2.8). However, the above estimate gives a justification as to why GVD in neglected in analyzing the results presented in this thesis. Most of the fibers used are in the range of 10 - 20 m, except in few cases where 100 m was required for SRS measurements. Even at that, this length is still far below the dispersion length for silica fibers.

CHAPTER 3

OTHER TECHNIQUES FOR MEASURING n_2 IN OPTICAL FIBERS AND THE NEED FOR A NEW APPROACH

3.1 Introduction

It has been realized over the years that most of the nonlinear effects in optical fiber are associated with the nonlinear refractive index (n_2) and that these nonlinear effects can have a relevant impact on the performance of optical telecommunication systems [10-12]. As a result, n_2 is a crucial parameter whose value in the fiber must be known precisely in order to perform calculations for predicting system performance. A variety of techniques [13, 15, 54-59, 107-113] have been developed since the pioneering work of Stolen and Lin in 1978 [13]. Some of these include spectral domain self-phase modulation method by use of pulsed lasers [13, 53-54, 56, 62, 107], cross phase modulation [15, 55, 108-109], four wave mixing [110] and modulation instability [111]. A technique based on LPG (long period fiber grating) pairs, utilizing enhanced absorption of rare earth ions has also been developed [61]. In this chapter the author wishes to discuss briefly some of these techniques and point out their utility and limitations.

3.2 The Spectral Domain SPM Technique

This is the most widely used method for n_2 measurement in fibers [13, 53, 62, 66, 107]. The method utilizes pulsed lasers and typical pulsewidths reported ranges from 50–120 picoseconds. In this technique, the laser pulses are launched into the test fiber whose length is typically 100-250 meters or more [13,107] and sometimes kilometers [62]. Spectral broadening occurs due to SPM because of the phase delay at the pulse maximum

relative to the wings. The output is passed through a scanning Fabry-Perot interferometer, which resolves the spectrum. The spectrum assumes readily identifiable shapes characterized by maxima and minima peaks at maximum phase shifts given by:

$$\Delta\phi_m = \frac{\pi}{2}(2N-1) \tag{3.1}$$

One measures the power after adjusting the input power to produce these identifiable shapes. As the input power is increased, the number of peaks increases. The number of peaks is proportional to the spectral phase shift which is in turn proportional to $n_2/A_{eff.}$ (where A_{eff} is the effective core area of the fiber).

$$\Delta\phi_m = \frac{2\pi L n_2 P_m}{\lambda A_{eff}} \tag{3.2}$$

The fiber length L and the vacuum wavelength (λ) are usually known, so that the slope of a plot of $\Delta\phi_m$ versus P_m produces the nonlinear coefficient in the form of $n_2/A_{eff.}$ If A_{eff} is known, n_2 can be deduced . The experimental setup is shown in Figure 3.1.

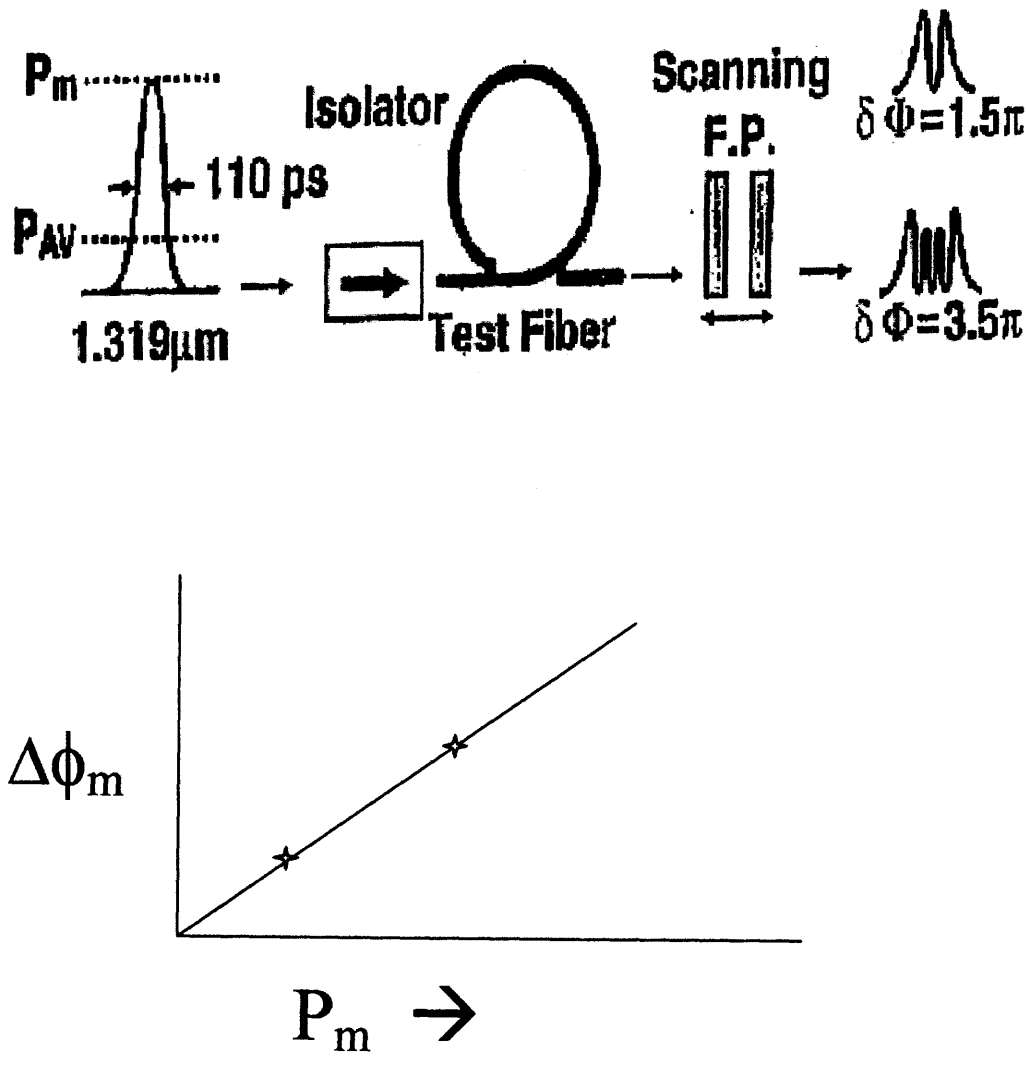

Figure 3.1 Experimental setup and analysis procedure for the spectral domain SPM technique [107].

This technique is relatively simple (because one can deduce the phase shift simply by counting the number of nodes in the spectrum) and yields accurate results. The pioneering work on this performed in 1978 at 514.5 nm gave the well-known value of n_2 = 1.14 x 10^{-13} esu (3.26 x 10^{-16} cm^2/W). This technique has been used extensively for measuring n_2 in optical fibers [13, 53, 62, 66, 107].

However, this technique requires long fibers in order to generate some orders of $\pi/2$ phase shifts. It may therefore not be suitable for use in measuring n_2 in standard EDFAs (Erbium-Doped Fiber Amplifiers) which are typically between 15 to 25 meters. In addition, because the technique relies on counting of the number of nodes that appear at integer orders of $\pi/2$ phase shift, the minimum detectable phase shift is limited to $\pi/2$.

3.3 Cross-Phase Modulation Technique

The cross-phase modulation (XPM) technique has been used to measure n_2 as early as 1987 [54] using interferometric method. In a 1995 experiment Kato et *al* [15] used a pump and probe configuration utilizing two independent cw laser sources from laser diodes (LDs) at the same wavelength (1550 nm) as the pump and probe signals. The probe signal was made relatively weaker than the pump, so that the phase shift in the test fiber was caused principally by the pump, through XPM. The two were coupled into the fiber where they interact as shown in Figure 3.2.

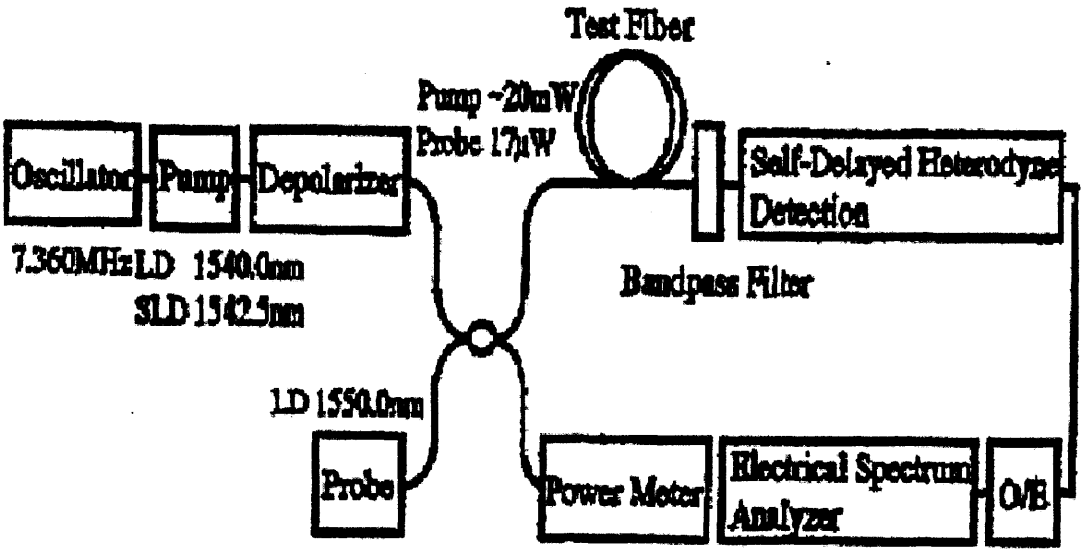

Figure 3.2 Measurement system of the nonlinear refractive index by the XPM method [15].

When the pump light was modulated in its intensity at low frequencies (7.36 MHz) with the electrical oscillator, the probe signal developed FM sidebands because of the XPM induced phase modulation. To ensure that the relative polarization between the pump and the probe varied randomly, the pump light was depolarized before entering the fiber. Typical fiber length used ranged from 5-15 km. The n_2 values obtained here ranged from 2.48 x 10^{-16} cm^2/W for silica core fibers to 3.95 x 10^{-16} cm^2/W for DCF (dispersion compensating fibers). Measured n_2 values in these experiments are in many cases higher than that obtained using SPM-based techniques. This is due to the fact that there is electrostrictive contribution to n_2 that occurs for pulsewidths greater than 1 ns or modulation frequency less than 1 GHz. The electrostrictive process results from the density change of an optical material due to the stress caused by intense electromagnetic

waves. This change in density alters the index of refraction of the material. The speed of response is however very slow, since the growth of the density change is governed by acoustic propagation. The XPM technique has also been used to study the frequency dependence of the electrostrictive contribution to n_2 by changing the pump modulation frequency from 10 MHz to values over 1 GHz [109,112].

Apart from the electrostrictive contribution that is known to occur for measurements with this technique, another drawback is that it requires very long fibers and two laser sources and therefore appears to be an expensive venture.

3.4 Four-wave Mixing Technique

In the four-wave mixing technique one uses two cw laser sources [110]. When two pump waves of frequencies v_1 and v_2 are launched into a single mode fiber, the nonlinear Kerr effect is responsible through FWM process for the creation of new beating frequencies at $(2v_2 - v_1)$ and $(2v_1 - v_2)$ which give rise to sidebands on the output spectrum, whose amplitude and frequency depend on n_2. In an experiment performed by Prigent and Hamaide in 1993 [110] using this technique, two cw laser sources operating near 1550 nm with a wave length separation of 0.8 nm were used. The output of the two lasers was amplified using fiber amplifier and then injected into 12.5 kilometers of the test fiber. Figure (3.3) shows a sketch of the experimental setup. The powers in the FWM sidebands were fitted numerically and used to estimate the n_2 value. A value of $n_2 = 2.25 \times 10^{-16}$ cm^2/W was reported in that measurement [110].

This technique requires very long fibers (~12 km) and in addition, the use of two lasers.

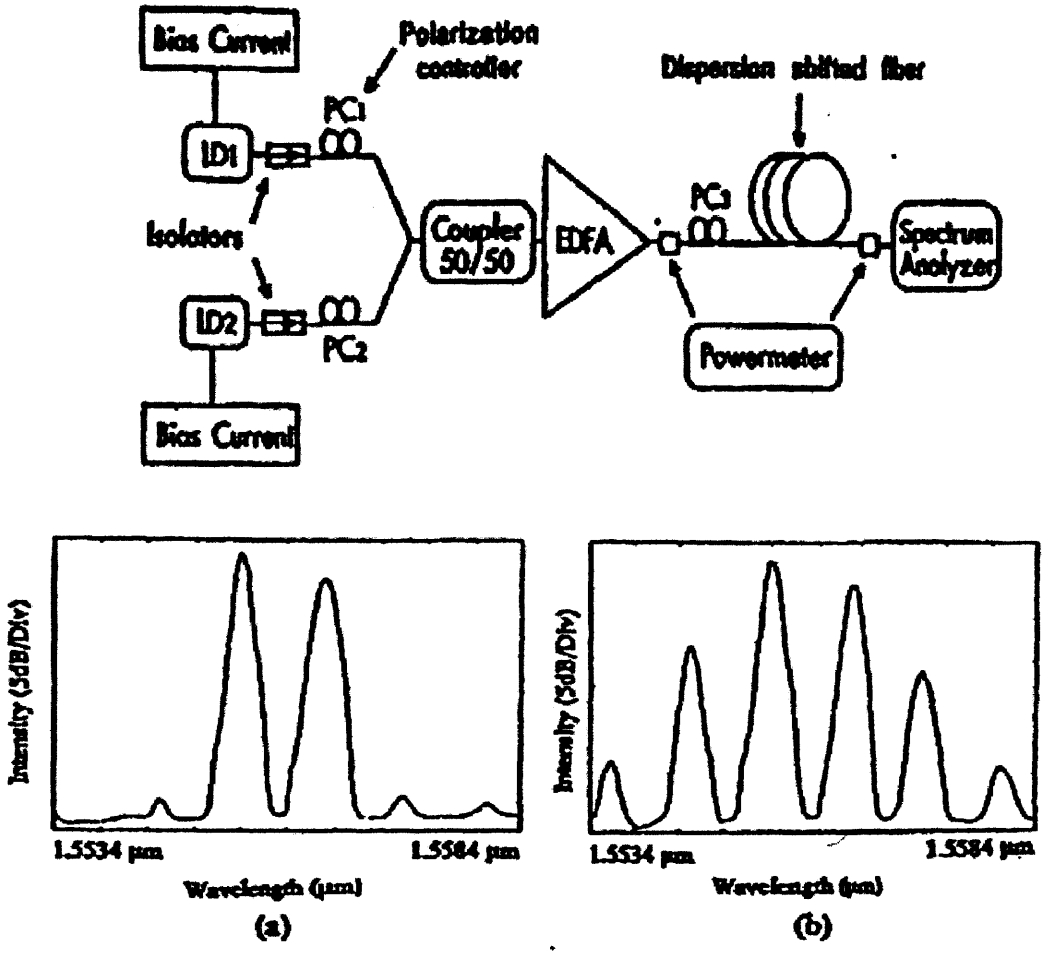

Figure 3.3 Experimental setup and typical spectra for the four-wave mixing n_2 technique (a) represents the spectrum of the fiber input and (b) represents the spectrum of the fiber output [110].

3.5 Modulation Instability Method

The technique based on modulation instability is similar to FWM technique except that only a single pump beam is needed at the fiber input. The method relies on the measurement of the modulation instability peak gain as a function of pump power. Modulation instability originates from the interplay between Kerr effect and anomalous dispersion, and gives rise to two spectral gain bands symmetrically located with respect to the pump frequency. The frequency shift and the amplitude of the sidebands depend on n_2 and can be used to deduce it.

In a recent experiment, Artiglia and co-workers [111] utilized a DFB (distributed feedback) laser operating at 1553 nm, which was modulated externally to produce 25 ns pulses at a repetition rate of 4 MHz. The pulses were amplified using two cascaded fiber amplifiers and then coupled into the test fiber. The test fiber consisted of a 10.1 km DSF (dispersion shifted fiber). The experimental setup is shown in Figure 3.4. The spectrum of output of the fiber was measured by means of an optical spectrum analyzer. The spectral gain due to modulation instability was obtained by normalizing the spectrum of the light exiting the fiber to that of the input light, which consists of the amplified laser signal superimposed onto the ASE (amplified spontaneous emission) of the optical amplifiers. The amplitude of the modulation instability sidebands was used to determine n_2 for the fiber. They reported a value of $n_2 = 2.64 \times 10^{-16}$ cm^2/W [111]. This value must include electrostrictive contribution because of the wide pump pulses used in the experiment, which explains why it appears larger than typical values obtained from the SPM technique.

In this technique however, the major drawback of long fiber resurfaces, and the electrostrictive contribution that tends to exaggerate the n_2 values. One cannot also apply this technique for measuring n_2 in typical EDFAs, for the same reason of fiber length requirement.

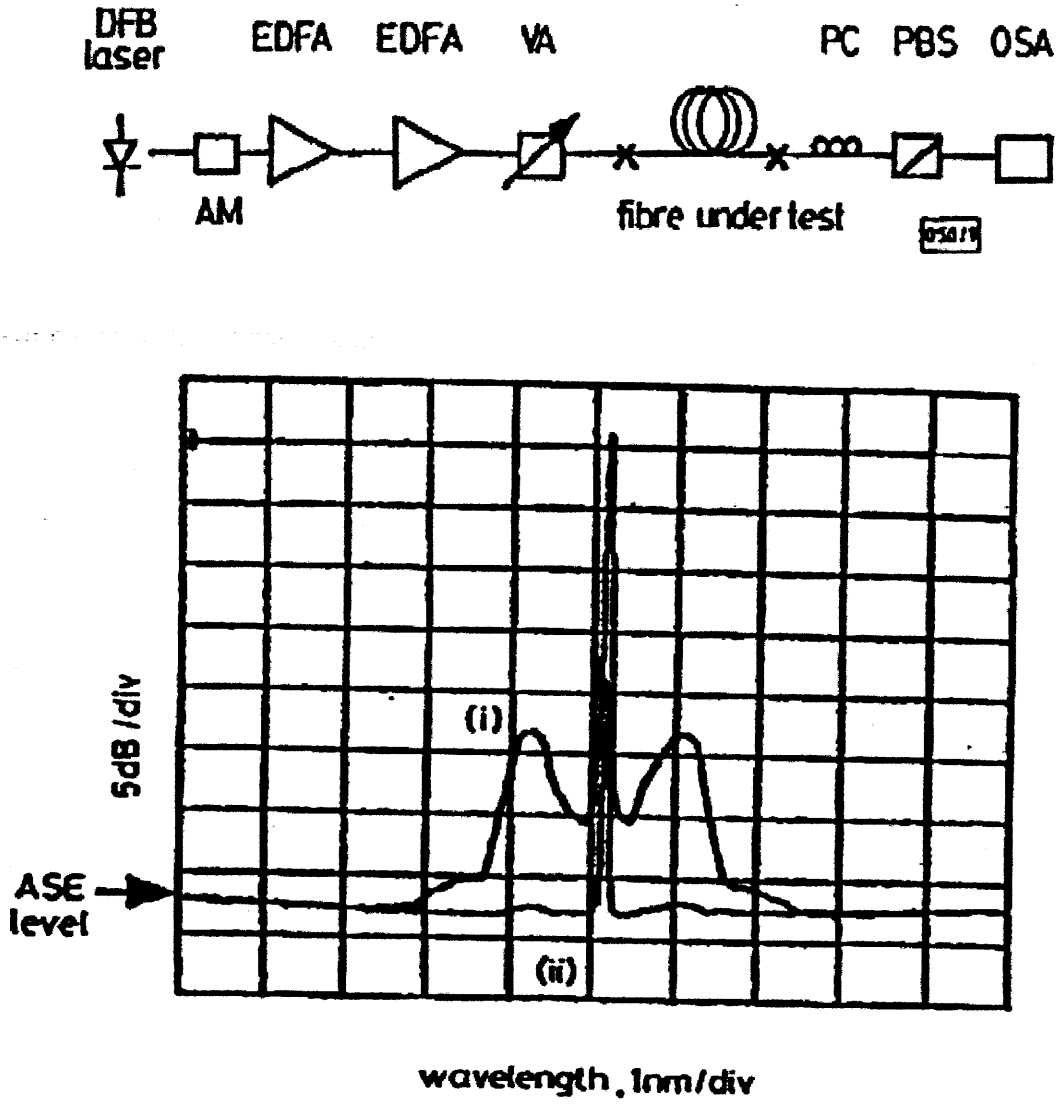

Figure 3.4 Experimental setup and typical output spectrum for the modulation instability technique for n_2 measurement in fibers [111].

3.6 Long Period Fiber Grating Pair (LPG) Method for n_2 Measurement

Recently, Kim et al [61] reported the use of LPG (long period fiber grating) pairs to measure resonant nonlinearity in short lengths of Yb^{3+}/Al^{3+} co-doped nonlinear optical fibers. This technique is based on the changes on the absorption properties of ytterbium ions on laser pumping. A long period fiber grating (LPG) pair is used as a sensor. In the experimental arrangement shown in Figure 3.5, the test fiber with lengh L_1 is spliced between the two LPGs with lengths L_2. The light sources consist of a signal beam from a 1550 nm broadband source together with a 980 LD (laser diode) pump laser.

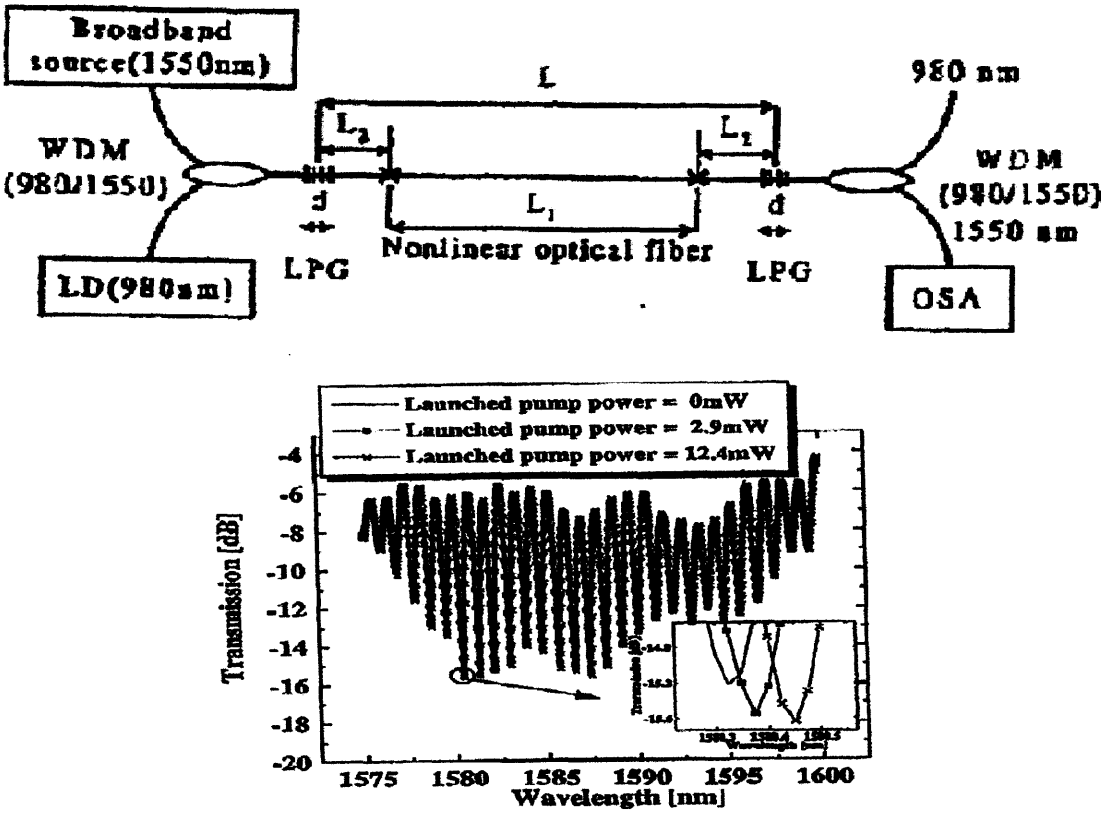

Figure 3. 5 Experimental arrangement and typical emission spectra in the measurement of n_2 in Yb^{3+}/Al^{3+} doped fibers using LPG [61].

In this technique, the change in refractive index of the fiber core is related to the shift in wavelength that arises from the interference between the core mode and the cladding mode of the fiber through the LPG pair [61, 114-115]. When a laser beam (1550 nm) pumped by a LD at 980 nm is lunched into the core of the high-concentration ytterbium doped fiber, a change in effective refractive index takes place with the pump power, and this results in a shift of the interference fringes. Because the intensity of the pump beam decreases exponentially with increasing absorption through the fiber, the amounts of the effective refractive index is different along the fiber. The total phase shift induced by the effective index change of the core along the fiber can be deduced from the shift of the interference fringe pattern, and from the phase shift n_2 can be calculated. The reported value of n_2 in this measurement was approximately 5.6×10^{-11} cm^2/W [61]. This is over four orders of magnitude higher than the n_2 reported with the other techniques described above. This is because the nonlinearity measured here is mainly due to carrier-enhanced nonlinearity, which differs from the well-known small Kerr coefficient. This technique works well in very short lengths of fiber (typically 45 centimeters), which is a good advantage.

Unfortunately however, the use of this technique is only limited to measuring the nonlinear index of refraction due to the absorption-enhanced nonlinearities resulting from Kramers-Kronig effect [60] in highly rare earth doped fibers. This type of nonlinearity although large, is inherently very slow, of the order of milliseconds in comparison to the known fast Kerr nonlinearity. The technique is therefore not suitable for measuring n_2 due to the Kerr nonlinearity in standard telecommunication fibers.

3.7 The Need for a New Technique for Measuring n_2 in Fibers

A reliable determination of n_2 in optical fibers is a difficult task. Several methods have been discussed above, with their corresponding merits and demerits. It is however fair to say that there is no experimental technique that is at the same time simple, fast, accurate and applicable to a variety of situations. With the spectral SPM technique using pulsed lasers [13, 56, 62, 107], one avoids electrostrictive contribution but it still needs a long fiber. The long fiber requirement is also a general problem to the other techniques except in the case of the LPG method, which however fails to meet the general applicability as seen in Section 3.6.

A major problem with n_2 measurements in long fibers is the fact that parameters such as effective area and dispersion are not constant along the entire length of the fiber. Generally, the accuracy of n_2 measurement depends strongly on how accurately one can determine the effective area of the fibers and the laser power. A variation in effective area along the length of the fiber during measurements would lead to additional uncertainties in the measured n_2 values. The effect of dispersion introduces pulse broadening which reduces the peak power along the fiber in a non-uniform way. Even for measurements at 1550 nm, which is near the zero dispersion wavelength of DSF (dispersion shifted fibers), dispersive broadening is still a problem, because of the incredibly long length (~20 km) of fibers required [62] in such circumstance, to obtain the necessary phase shifts with the relatively low power lasers available. In a recent report [62], Stolen et *al* have shown that in order to improve the accuracy of n_2 in measurements in long fibers, one would need to fit the experimental spectrum with a computer program that simulates the variation of the power, pulse shape, and fiber properties along the length of the fiber. This is necessary to

properly account for the fiber loss and the pulse spreading. This is certainly a tedious exercise.

Another problem in measuring n_2 in long fibers is the effect of polarization. The nonlinear refractive index depends on the state of polarization of the field. In isotropic glass fibers, the nonlinear refractive index is maximum for linear polarization and drops to 2/3 of maximum for the circular polarization state [59]. In long non-polarization maintaining fibers, the polarization state wanders over all values from linear to circular and it is practically impossible to map the evolution. These polarization changes have been shown to produce significant variations in n_2 values with the result that an approximate factor [59, 116-117] of 8/9 of the value for linear polarization is needed to correct the values of n_2 obtained in such measurement.

An accurate method for measuring n_2 in short lengths of fibers is therefore highly desirable to overcome these problems associated with n_2 measurements in long fibers. In addition, with the increasing use of erbium doped fiber amplifiers (EDFAs) in long-haul optical communication and in DWDM (Dense-Wave Division Multiplexed) systems, it is crucial that a technique capable of measuring n_2 in commercial available EDFAs be developed, in order to accurately predict the performance of the systems. The standard length of EDFAs is between 15 to 25 meters.

Therefore, in this thesis, a new method [66-68] for measuring n_2 (due to Kerr nonlinearity) in short lengths of fibers has been used. This technique is based on photorefractive two-beam coupling also known as induced grating autocorrelation (IGA). The use of the photorefractive beam coupling technique for measuring n_2 relies on the fact that the IGA can detect the time dependent phase change acquired by an optical pulse

after propagating through a nonlinear medium, such as optical fiber. It is the SPM induced phase change that is used to characterize the nonlinear medium. Generally, because of the short length of fiber needed (typically 10–20 m) to generate SPM in IGA experiments, GVD (group velocity dispersion) is negligible and the effect of polarization scrambling is highly minimized. In the next chapter, the author will describe the basic principles, modeling and the experimental setup of the IGA technique.

CHAPTER 4

THE PHOTOREFRACTIVE BEAM-COUPLING TECHNIQUE [INDUCED GRATING AUTOCORRELATION (IGA)]

4.1 Introduction

In Chapter 3, the need for a new technique capable of measuring n_2 accurately in short lengths of fibers was made obvious. It is in recognition of this that the photorefractive two-beam coupling technique (also called induced grating autocorrelation) was developed [65,67,68] for measuring n_2 in short lengths of fibers ($z \sim 10$ to 20 meters), with pulses as short as 50 to 75 picoseconds. In this chapter the author would discuss the basics of the photorefractive beam coupling technique, the mathematical formulation and modeling as well as the experimental realization. A general overview on how the self-phase modulation strength is determined from the fit of the experimental data to the IGA model based on pure SPM will be given together with the final steps for calculating n_2 from the data.

4.2 The Photorefractive Effect

The concept of photorefractive effect is well established [119-130]. It can simply be defined as the change in refractive index of an optical material that results from the optically induced redistribution of charges (electrons and holes). The processes involved are explained below. When two mutually coherent beams intersect inside a photorefractive crystal, as shown in Figure 4.1, a light intensity pattern is created due to the beams' interference. Free charge carriers are generated within the bright region by

photo-excitation from impurity energy levels to an energy band at a rate proportional to the optical intensity. These carriers then diffuse away by concentration gradient or drift from the position of high intensity where they are generated to the dark region, leaving behind fixed charges of the opposite sign. These free carriers are then trapped by ionized impurities within the dark region, depositing their charge as they recombine. The result is the creation of an inhomogeneous space-charge distribution that can remain in place for a period of time after the light is removed. The charge distribution creates an internal electric field pattern that modulates the local refractive index of the material by virtue of electro-optic effect. The change in refractive index corresponds to a phase grating. The entire process is illustrated in Figures (4.2) and (4.3). The refractive index change (Δn) is related to the space-charge electric field (E_{sc}) by the following expression:

$$\Delta n = \frac{1}{2} n^3 r_{eff} E_{sc} \tag{4.1}$$

where n is the background refractive index and r_{eff} is the effective electro-optic coefficient.

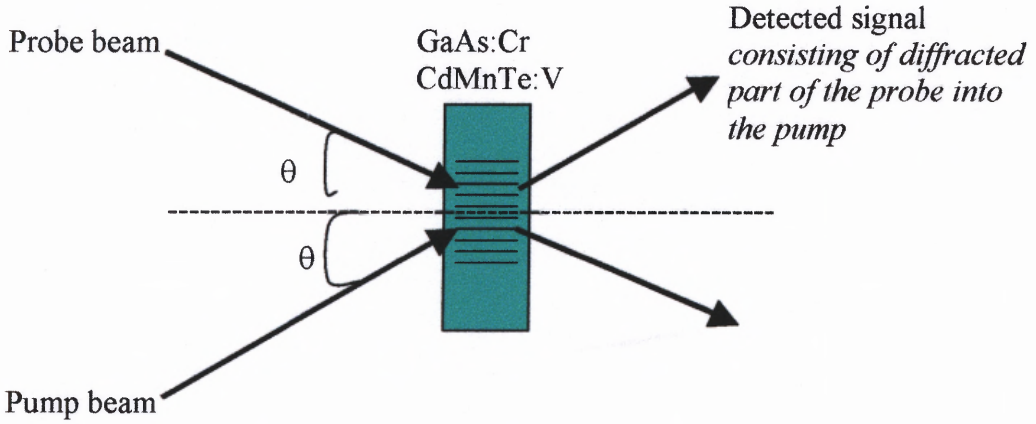

Figure 4.1 Two-beam coupling in photorefractive crystal.

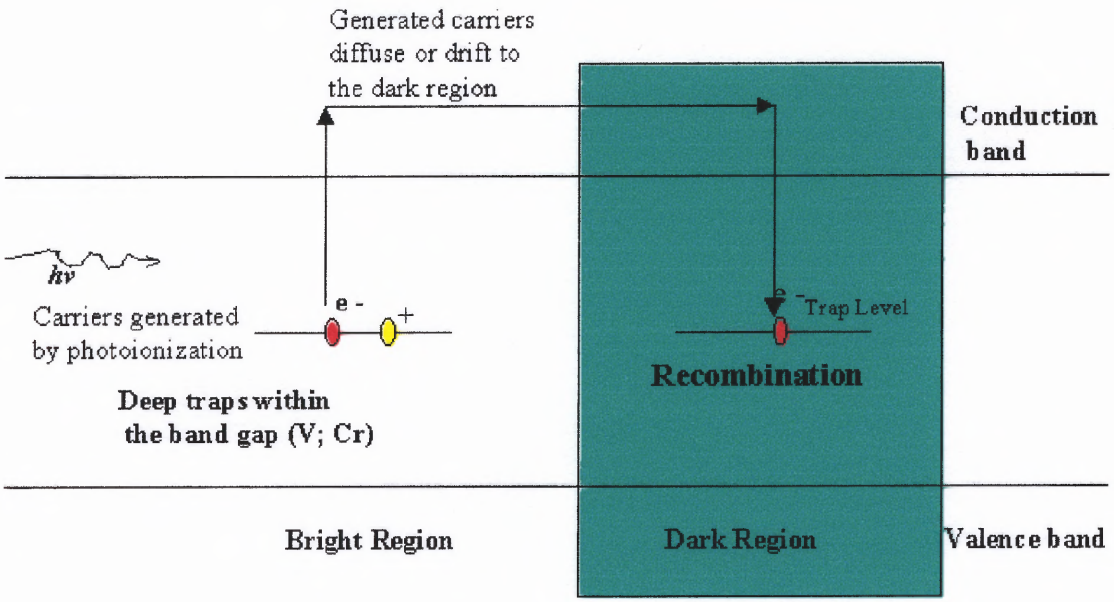

Figure 4.2 Photoexcitation of free carriers in electro-optic material. The free carriers diffuse in concentration gradient thereby creating space-charge fields.

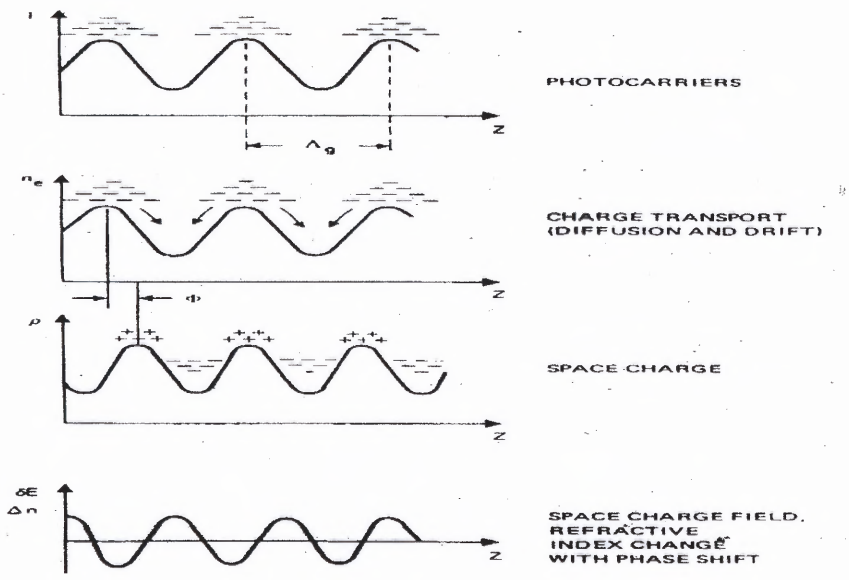

Figure 4.3 Creation of space charge field and photorefractive gratings in photorefractive material. The space charge field is 90° out of phase with the space charge.

In the two-beam coupling configuration (two wave mixing), the photorefractive grating resulting from the refractive index modulation causes energy transfer (by diffraction) from one of the beams (the probe) to the other (the pump) beam. Kukhtarev and co-workers [127] have worked out the mathematical details for two-wave mixing. In the absence of an external field, the amount of energy transfer is determined by the gain coefficient (Γ):

$$\Gamma = \frac{2\pi n^3 r_{eff} E_{sc}}{\lambda_0 \cos\theta} \tag{4.2}$$

where θ is the Bragg angle inside the crystal, λ_0 is the vacuum wavelength of light. For negligible depletion of the signal beam, the transmitted signal intensity, $I_{s(T)}$ is given by:

$$I_{s(T)} = I_{s(0)} \exp(\Gamma L) \tag{4.3}$$

where L is the thickness of the photorefractive crystal and $I_{s(0)}$ is the incident signal intensity. The response time of an elemental grating (for either writing or erasure) is determined by the rate at which space-charge field is created or decays. This is proportional to the dielectric relaxation time $\tau_d = \varepsilon/4\pi\sigma$ of the material, where ε is the dielectric constant and σ is the conductivity. The grating period (spacing) Λ is a function of the wavelength of the laser used and the incident angle ϑ of the beams, thus:

$$\Lambda = \frac{\lambda}{2\sin\vartheta} \tag{4.4}$$

The importance of refractive effect in this work lies with the fact that the photorefractive gratings (Δn) contain the information about the phase of the writing pulses. This allows one to use photorefractive crystal as a phase-detection tool for self-

phase modulated pulses through the induced grating autocorrelation, provided that the decay time of the gratings in the medium is long compared with the pulse length of the laser to be measured and with any delays used in the interaction. In this experiment, the author uses semiconductor CdMnTe:V and GaAs:Cr as the photorefractive medium because semiconductor photorefractive materials have the advantage of significantly faster response time, longer recombination time and better sensitivity in both visible and near infrared wavelength regions compared to conventional oxide based materials (such as $BaTiO_3$) [128-130]. At 1064nm, both CdMnTe:V and GaAs:Cr provide excellent measurement capability.

4.3 IGA Modeling Based on Pure SPM in the Absence of GVD and SRS

The basic idea behind IGA is the splitting of a pulse and the interference in a photorefractive medium of the resulting two excitation pulses. The resulting interference fringes may then induce a modulation of the medium's refractive index (i.e. a grating). The modulation is then probed by one of the excitation pulses and the diffracted light is detected. Different geometries of IGA configuration exist [64], but only the two-beam geometry is relevant to this technique. In this section, IGA will be modeled with the assumption that the effective nonlinear interaction during the pulse propagation in the fiber is the self-phase modulation that leads to nonlinear phase shift of the propagating pulse. Through the choice of fiber length and input power, GVD and SRS are neglected.

In the two-beam coupling geometry (Figure 4.1), one of the excitation pulses also acts as the probe. A small portion of the probe field gets diffracted into the pump beam and co-propagates with it. It is this diffracted beam that is measured in IGA experiments.

The detected IGA signal ($W_{det.}$) is proportional to the squared magnitude of the electric field autocorrelation function given by:

$$W_{det.} \propto |K(\tau)|^2 = \left| \int_{-\infty}^{+\infty} E(t') E^*(t' + \tau) dt' \right|^2 \tag{4.5}$$

where τ is the time delay between the pulses.

In this model, a Gaussian pulse is assumed, with electric field *E(t)* of the form:

$$E(t) = E_0 \exp[-2\ln 2(\frac{t}{\tau_p})^2 - i(\omega_0 t + \phi)] \tag{4.6}$$

where E_0 is the field amplitude, τ_p is the pulse width and ϕ is the phase. The propagation of the pulse in the fiber can be accurately described by the nonlinear wave equation for the electric field given in Equation (2.15). The solution of the nonlinear wave equation (see Section 2.2 for details) showed that in absence GVD, the pulse propagates though the medium without distortion. This is the underlining principle of the simple theory of SPM [84-85]. Shen and Yang have used this theory [84] to show that when a Gaussian pulse propagates through a nonlinear medium of length z, and undergoes SPM (without GVD), the intensity of the pulse retains its Gaussian form and acquires a time-dependent phase-shift $\Delta\phi(t)$ which is also Gaussian in nature. The phase shift can be written as [see Equation (2.21), Section 2.2]:

$$\Delta\phi(t) = \frac{2\pi\omega_o^2}{c^2 k_o} \chi^{(3)} |E(t)|^2 z \tag{4.7}$$

Substitute Equation (4.6) into (4.7) one obtains:

$$\Delta\phi(t) = \frac{2\pi\omega_o^2}{c^2 k_o} E_0^2 \chi^{(3)} z\{\exp[-4\ln 2(\frac{t}{\tau_p})^2]\}. \tag{4.8}$$

This equation can be reduced to the following expression:

$$\Delta\phi(t) = \omega_0 \tau_p Q \exp[-4\ln 2(\frac{t}{\tau_p})^2], \tag{4.9}$$

where

$$Q = \frac{2\pi\omega_0 \chi^{(3)} E_0^2 z}{k_0 c^2 \tau_p}, \ (Q<<1). \tag{4.10}$$

In the above equations, Q is the spectral broadening parameter, ω_0 is the central (angular) frequency of the laser, z is the propagation length in the fiber and $\chi^{(3)}$ is the third order susceptibility. The quantity $\omega_0\tau_p Q$ is termed the self-phase modulation strength (SPMS) – this defines the magnitude or strength of the self-phase modulation experienced by the propagating pulse in the nonlinear medium and provides a direct measurement of the temporal phase shift imparted on the pulse. From Equations (4.6 & 4.9), the electric field of the self-phase modulated Gaussian pulse can be written as:

$$E(t) = E_0 \exp[-2\ln 2(\frac{t}{\tau_p})^2 - i\{\omega_0 t + \omega_0 \tau_p Q \exp\{-4\ln 2(\frac{t}{\tau})^2\}\}] \tag{4.11}$$

This can be substituted into Equation (4.5) to obtain the explicit expression for the detected IGA signal ($W_{det.}$):

$$W_{\text{det}} \propto |K(x)|^2 = 4\left(\frac{\ln 2}{\pi}\right)\left|\int_{-\infty}^{+\infty} du \exp[-2\ln 2u^2 - i\omega_0 \tau_p Q e^{-4\ln 2u^2}]\right.$$
$$\left.\times \exp[-2\ln 2(u+x)^2 + i\omega_0 \tau_p Q e^{-4\ln(u+x)^2}]\right|^2 \tag{4.12}$$

where the author has introduced a normalized time $u = t/\tau_p$ and normalized delay $x = \tau/\tau_p$ and has normalized the correlation function $K(x)$ such that $K(0) = 1$. A numerical evaluation of the complicated integral shown in Equation (4.12) generates a theoretical time-domain IGA trace. Simulated traces for different values of $\omega_0\tau_p Q$ are shown in Figures (4.4), (4.5) and (4.6).

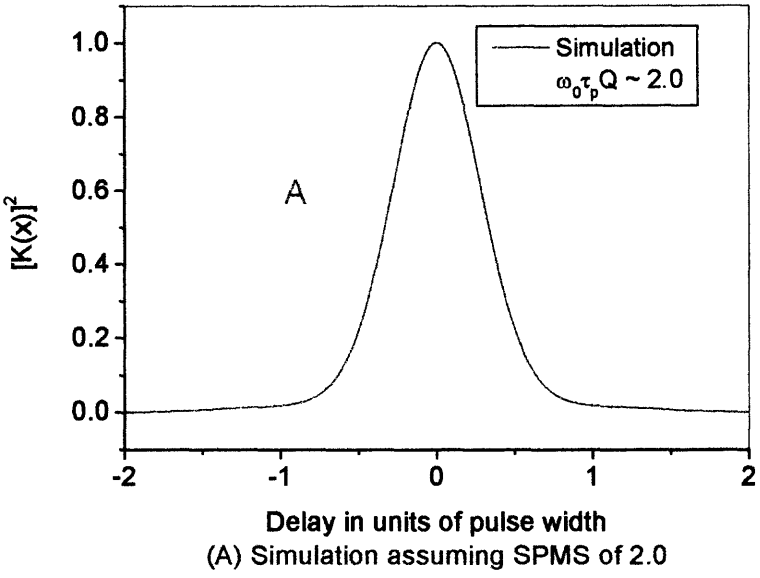

(A) Simulation assuming SPMS of 2.0

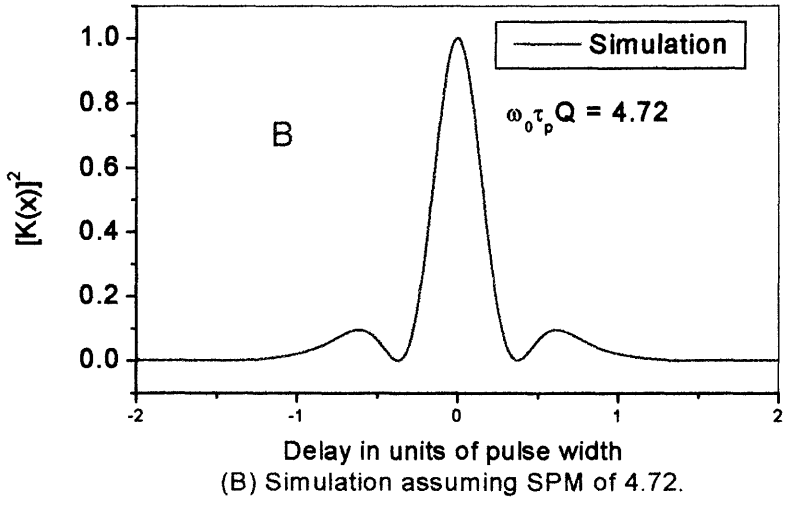

(B) Simulation assuming SPM of 4.72.

Figure 4.4 Simulated IGA traces based on Equation (4.12) for low self-phase modulated Gaussian pulse.

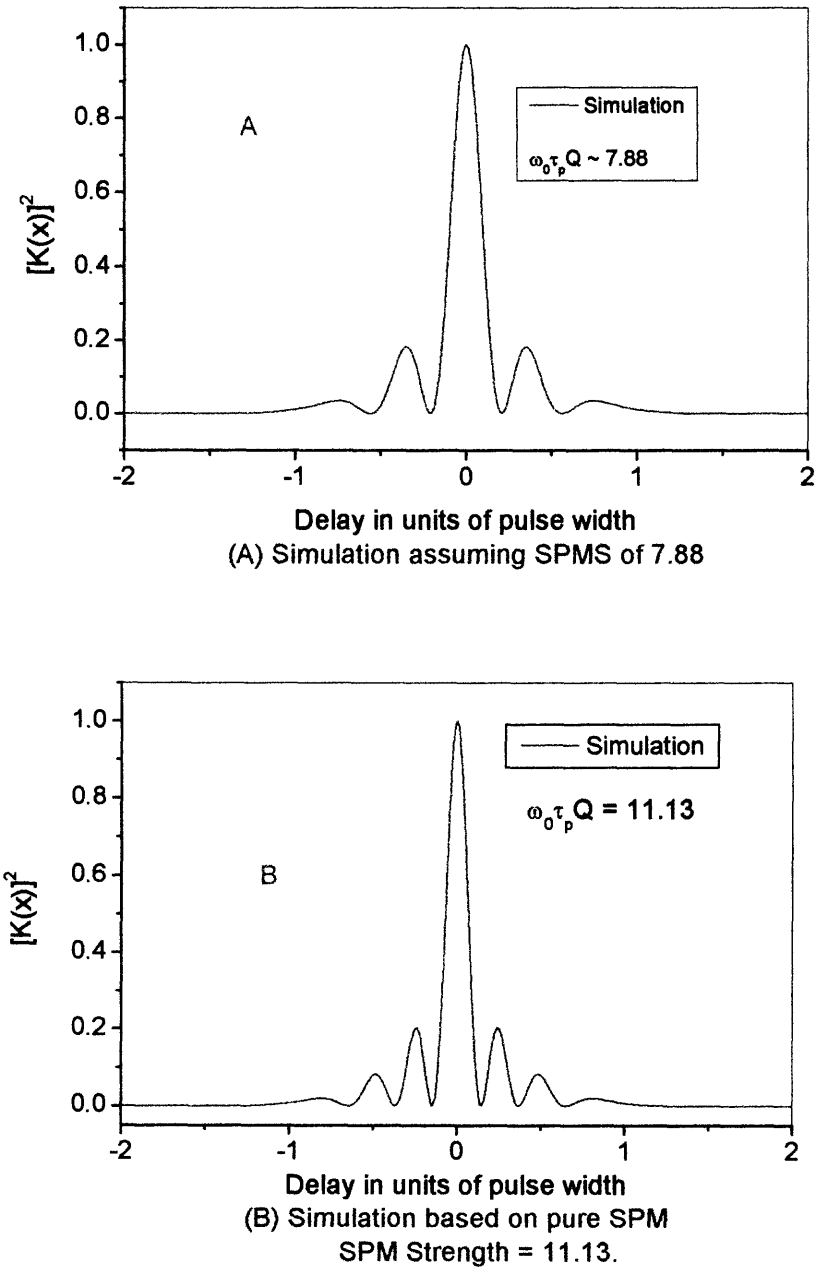

Figure 4.5 Simulated IGA traces for a Gaussian pulse that has been moderately self-phase modulated at two different values of SPMS.

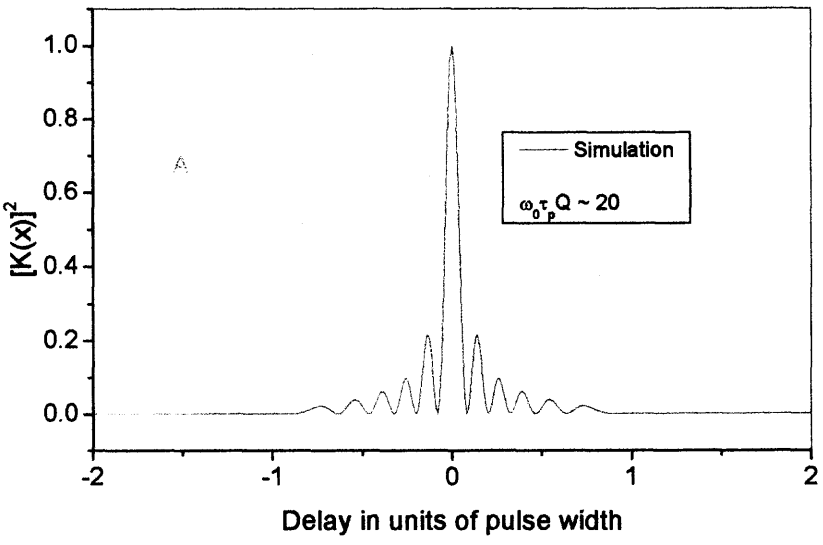

(A) Simulation assuming SPMS of 20

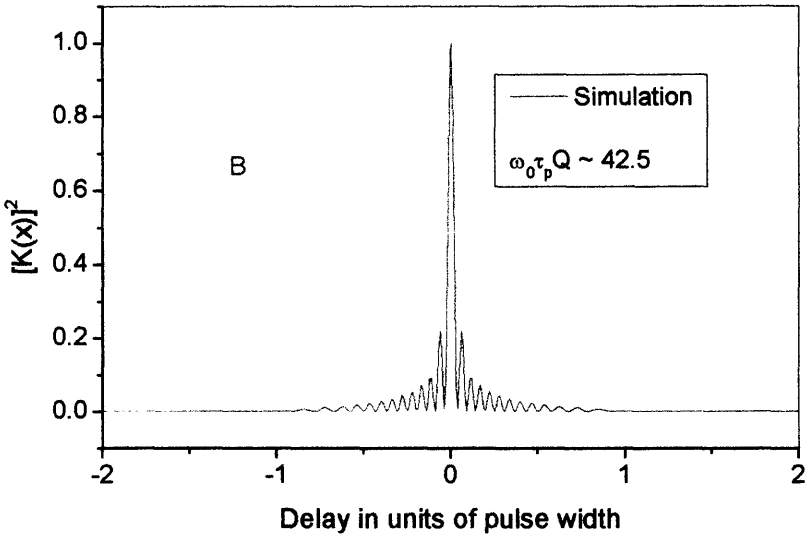

(B) Simulation assuming SPMS of 42.5

Figure 4.6 Simulated IGA traces for a highly self-phase modulated Gaussian pulse at two different values of SPMS.

It can be seen that the IGA trace exhibits oscillation on the wings. At very low value of $\omega_0\tau_p Q$ (SPMS), no oscillation occurs, but only a slight narrowing of the pulse.

As the value of the SPMS is increased to 4.72, two-well established sidelobes are formed, symmetrically located on either sides of the central peak. With increasing value of $\omega_0 \tau_p Q$ the number of oscillations (sidelobes) increases accompanied with increased narrowing of the central peak.

These oscillations can be explained as follow: The self-phase modulation induces a time dependent phase shift on the pulse, whose magnitude is determined by self-phase modulation strength ($\omega_0 \tau_p Q$) as described above. Delaying one signal by an appropriate amount can force the relative phase delay either to add-up or to cancel, which gives rise to the peaks and valleys (zeros) in the trace. The number of specific delays for which exact cancellation (zero) is observed depends on the magnitude of the SPMS. The width of the central peak of the IGA trace is a measure of the bandwidth of the IGA writing pulse – as the bandwidth increases (i.e., by SPM) the narrower the central peak of the IGA trace. Thus the narrowing and oscillations are clear signatures of self-phase modulation on IGA traces.

It should be noted that these oscillations do not exist in the presence of significant GVD. This is because GVD imposes non-uniform chirp (frequency shift) on the self-phase modulated pulse. Thus, nonzero delays result in a frequency difference between pulses. This frequency difference leads to a moving (interference) fringe pattern, which washes out the gratings. As a result, no oscillation can form on the wings of the resulting IGA trace. Hence GVD would cause narrowing of IGA traces without the oscillations. Care must therefore be taken when performing IGA experiments to operate within short lengths of fibers where GVD is negligible.

4.4 Experimental Details and Measurement Procedure for the IGA Technique

4.4.1 Laser Source and Pulse Characterization

4.4.1.1 The Laser Source. The laser source consists of a Quantronix made cw (continuous wave)-modelocked Nd:YAG laser model 116. The laser operates at a wavelength of 1064 nm with a modelocked frequency of 100.486 MHz, which produces pulses every 10-nsec. The Nd:YAG model 116 is a solid state laser. The active lasing material consists of Neodymium-doped yttrium aluminum garnet (YAG) crystal, with chemical formula $Y_3Al_5O_{12}$. Enclosed in the laser pot with the crystal rod, and parallel to it is a high-pressure Krypton lamp that runs on 30 A power supply. Both the crystal rod and the lamp are surrounded by a cylindrical gold reflector which ensures that most of the energy radiated by the lamp is focused on the rod to provide the optical pumping. Optical pumping refers to the excitation of electrons to a higher energy level from which they rapidly relax into the upper level of the lasing transition. In Nd:YAG laser operating at 1064 nm, the upper level has a relatively long life-time (250 ns). Most of the energy in this laser is converted into heat, which is removed through water-cooling.

The mode-locking process is achieved with model 352 Quantronix mode-locker. This is an acousto-optic mode-locker acting as a fast optical gate. The mode-locking technique ensures that laser resonator modes will have coherent phase relationship. The proper modulation frequency for the laser to generate pulses that grow to a stable value is given by [131].

$$f_0 = \frac{1}{2T} = \frac{\Delta f}{2} = \frac{c}{4L} \tag{4.13}$$

where f_o is the modulation frequency, L is the total length of the resonator, c is the speed of light and T is the transit time. The width of the output pulse depends on the number of resonator modes that are phase coherent (mode-locked) or equivalently, the bandwidth of the oscillation. For a Gaussian pulse, the pulsewidth-bandwidth product is given by:

$$\Delta\nu_p\tau_p = 0.5 \tag{4.14}$$

4.4.1.2 Pulse Characterization. IGA experiments require a well-characterized input pulse. This implies that the pulsewidth and the peak power must be precisely known. If the pulsewidth of laser source is known together with the repetition rate, then the peak power can always be determine for any given average power. Thus the pulsewidth of the laser is usually measured before and after a set of IGA measurement. A set of IGA measurements (in this case) consists of about four to five different IGA traces taken successive at different powers. For the pulsewidth measurement, the author uses the well-known [132] noncollinear, background-free, second harmonic generation autocorrelation (SHGA). The experimental set-up is shown in Figure (4.7).

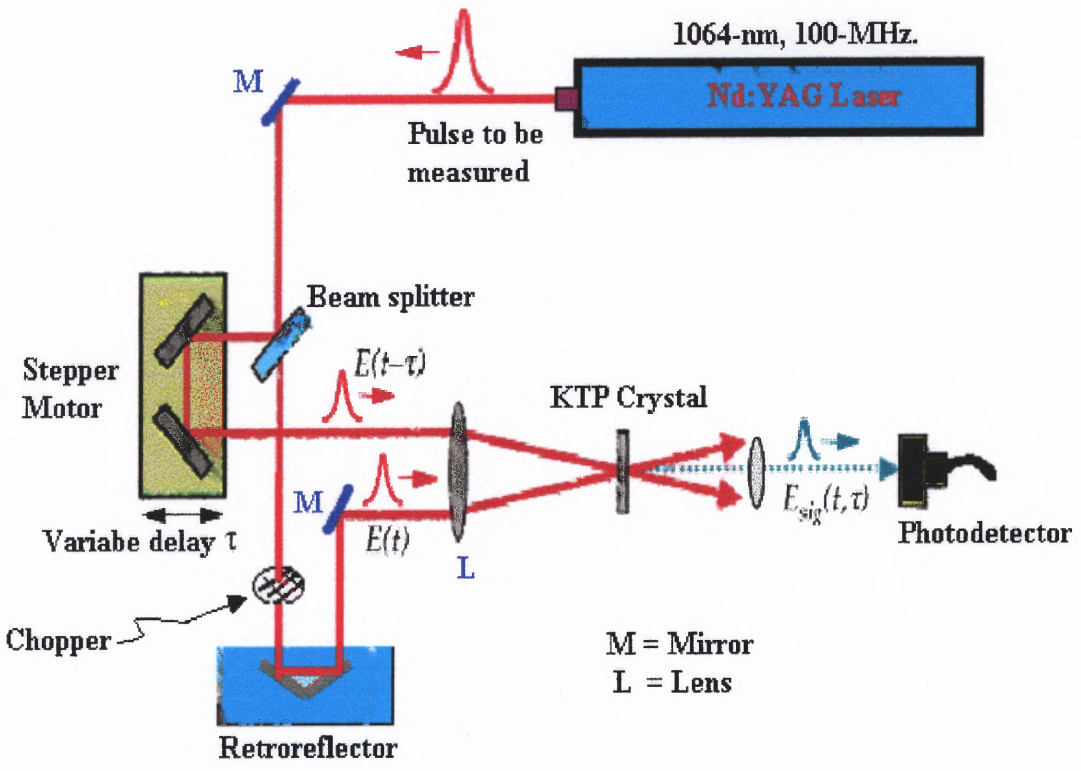

Figure 4.7 Experimental setup for the noncollinear background-free SHG autocorrelation.

In the arrangement shown above, the output of the Nd:YAG laser (at 1064-nm, 100 MHz) is split into two with one beam chopped at a frequency of 2 KHz, to provide a detection reference to a lock-in amplifier. One arm is delayed with respect to the other. The delay time (τ) is varied by mechanically changing the path length transversed by one of the beams using a computer controlled retroreflector/stepper-motor combination. The two beams are spatially overlapped in an instantaneously responding nonlinear-optical medium, such as a second-harmonic-generation (SHG) crystal (in this case KTP crystal). The SHG crystal produces the detected "signal light" at twice the frequency (half the wavelength) of the input light. With 1064 nm, the autocorrelation signal has wavelength

of 532 nm. In this case, the detection system consists of Thorlabs amplified (Model PDA50) photodetector connected to a lock-in amplifier with the reference frequency provided by the chopper. The autocorrelation signal is automatically collected and plotted by the computer using a Labview program with IEEE-488 bus.

The detected SHG signal is proportional to the product of the intensities of the two pulses:

$$S_{SHG}(t,\tau) \propto I(t)I(t+\tau) \tag{4.15}$$

In practice, because detectors are typically too slow to resolve the beam in time, what is actually measured is the integrated (correlation) function $G^2(\tau)$ defined by:

$$G^2(\tau) = \int_{-\infty}^{\infty} E(t)E^*(t-\tau)E^*(t)E(t-\tau)dt \tag{4.14}$$

which is sometimes written as:

$$G^2(\tau) = \int_{-\infty}^{\infty} I(t)I(t-\tau)dt \tag{4.16}$$

where $E(t)$ and $E(t\text{-}\tau)$ are the electric fields of the two pulses, I(t) and I(t-τ) are their intensities and τ is the delay. Equation (4.16) is the so-called second harmonic intensity autocorrelation function.

The pulsewidth (τ_p) of the laser is determined from the FWHM (full width at half-maximum) of the SHG intensity autocorrelation trace (τ_{AUTO}) using the relation:

$$\tau_p = \frac{\tau_{AUTO}}{\sqrt{2}} \tag{4.17}$$

The measured pulsewidth ranges from 50 psec. to 75 psec. The experimental autocorrelation trace is fitted to a Gaussian of the form shown in Equation (4.6):

A typical SHG autocorrelation trace used to determine the pulsewidth is shown in Figure (4.8). The smooth red curve is a Gaussian curve that fits the data shown by blue square dots. The fit is excellent, even in the far wings of the pulse.

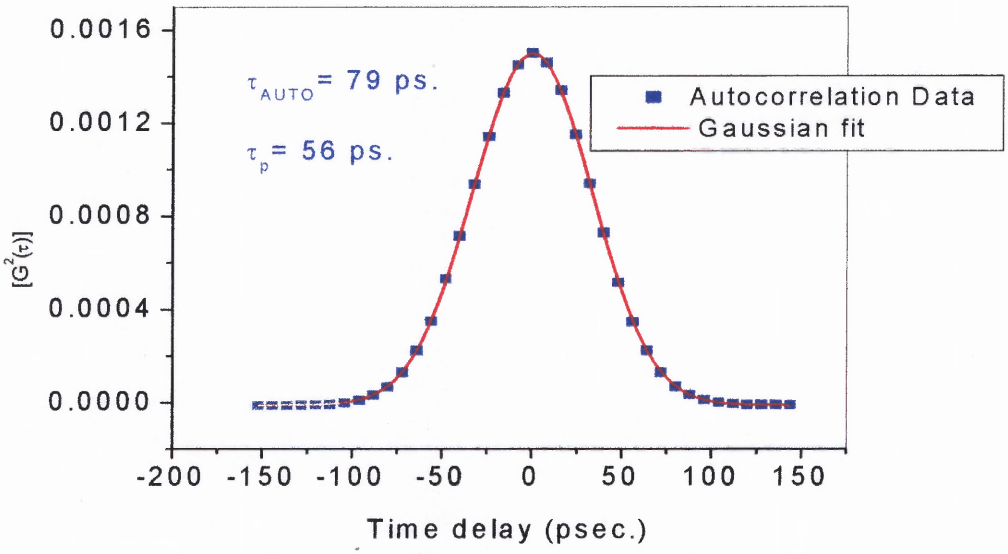

Figure 4.8 Experimental SHG autocorrelation trace fitted to a Gaussian.

4.4.1.3 Analysis of Goodness of Fit for the Autocorrelation Trace. In order to establish further evidence that the pulse used in this work is truly Gaussian, the author has carried out a statistical analysis on the goodness of fit. One of the best-known procedures to evaluate how good experimental data fits a theoretical model is to calculate the residual of the fit defined by:

$$\mathbf{r}_j\,(j = 1....N) = \mathbf{y}_j(\text{exp})\text{-}\mathbf{y}_j(\text{fit}) \qquad (4.18)$$

and evaluate its standard deviation. The smaller the standard deviation of the residual, the closer the data to the model. The residual of the fit in Figure 4.8 has been calculated and the scatter plot shows its distribution about the mean (Figure 4.9). The residual distribution shows that the experimental trace fits excellently to the theoretical Gaussian, including at the wings. The standard deviation (σ) of the residual was calculated using the well-known relation:

$$\sigma = \sqrt{\frac{1}{N}\sum_{j=1}^{N}(r_j - \bar{r})^2} \tag{4.19}$$

where N is the weighting factor, r_j is the jth residual and $\bar{r}$ is the mean. The standard deviation has been calculated to be $\sigma \approx 4.0 \times 10^{-6}$ (for a perfect fit, $\sigma \rightarrow 0$). .This justifies the assumption made in the theoretical derivation of the IGA model that the pulses have a Gaussian nature.

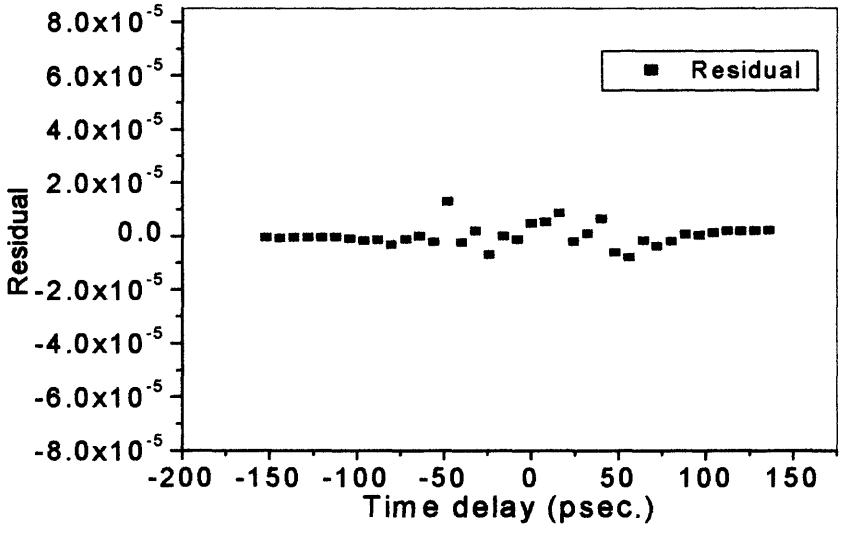

Figure 4.9 Scatter plot of the residual of the Gaussian fit to the autocorrelation trace.

4.4.2 Experimental Setup for IGA Measurement

The experimental set-up for the photorefractive beam coupling technique is shown in Figure 4.10. A train of pulses (with pulsewidth in the range of 50-70 picoseconds) are generated by a cw mode-locked Nd:YAG laser operating at 1064 nm wavelength and 100 MHz repetition rate (described in section 4.4.1.1). These pulses are launched into the test fiber by free-space coupling using a 10X microscope objective focusing lens, mounted on the Newport's model 562 XYZ stage. The test fiber is typically 10-20 meters long. As the pulses propagated through the fiber (a nonlinear medium) they undergo self-phase modulation. The output pulses from the fiber are split in a modified Michelson interferometer, with one arm of a fixed optical delay and the other delayed by a stepper motor-retroreflector combination. The two beams are focused into a photorefractive Cadmium Manganese Telluride crystal doped with Vanadium (CdMnTe:V) or GaAs:Cr by 15-cm focal length convex lenses at an intersection angle of $2\theta = 64\ ^{\circ}$. The beam geometry follows the standard pump-probe configuration in two wave mixing. One beam designated as the probe beam is mechanically chopped at a frequency of about 2 KHz and the transfer of modulation from the probe to the pump is detected in the path of the pump beam with Thorlabs amplified InGaAs high-speed photodetector (model PDA50) connected to a lock-in amplifier (EGG 1510).

The IGA response is determined by measurement of the lock-in amplifier output as a function of delay between the pump and probe beams. The data is collected automatically using a IEEE488 bus and LABView software package. Typical experimentally measured IGA traces are shown in Figure (4.11).

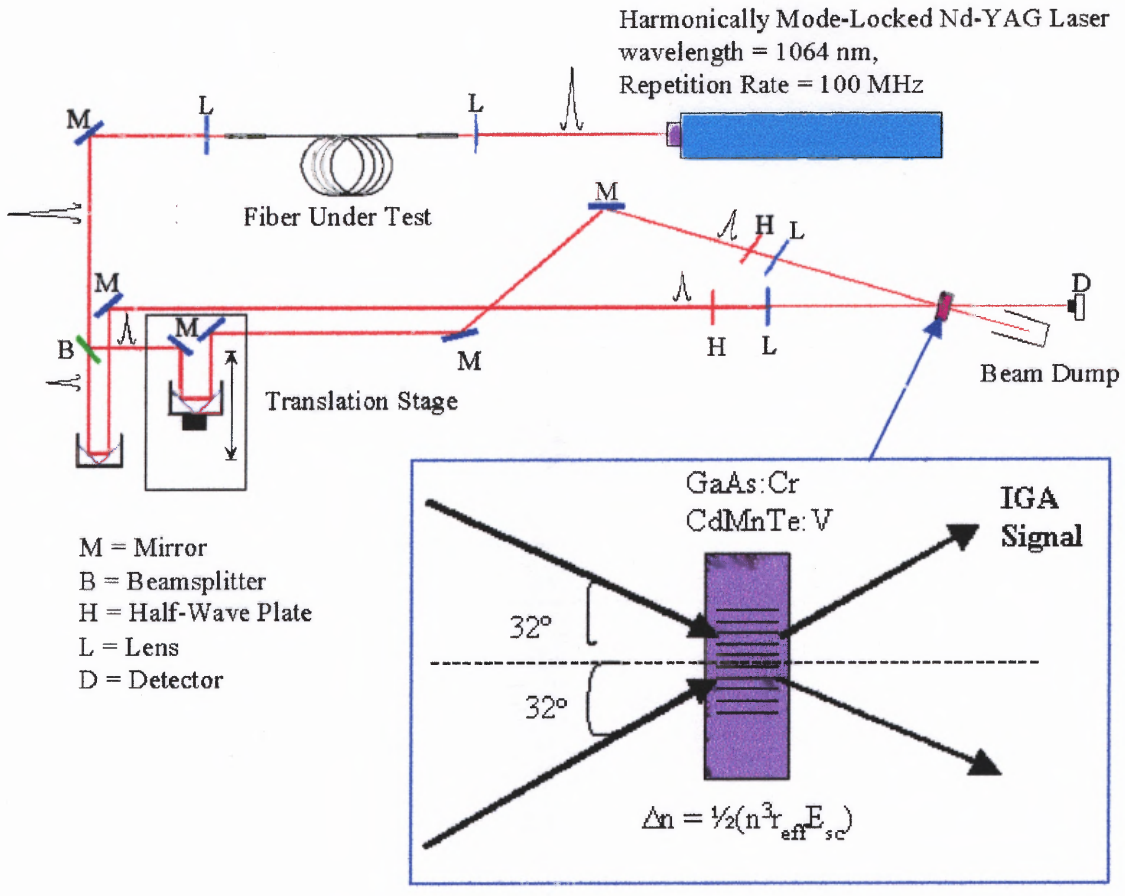

Figure 4.10 Experimental set-up and beam geometry for the photorefractive beam coupling technique.

As can be seen from the recorded traces, as the input power in the fiber is increased there is increased narrowing of the central peak and increased number of sidelobes. This is expected since increasing the input power implies more SPM and hence increasing $\omega_0\tau_pQ$. The dependence of the narrowing and oscillations on the magnitude of $\omega_0\tau_pQ$ has been explained in Section 4.3. The value of $\omega_0\tau_pQ$ is determined for each trace by fitting the experimental data to the IGA model. This will be discussed in the next section.

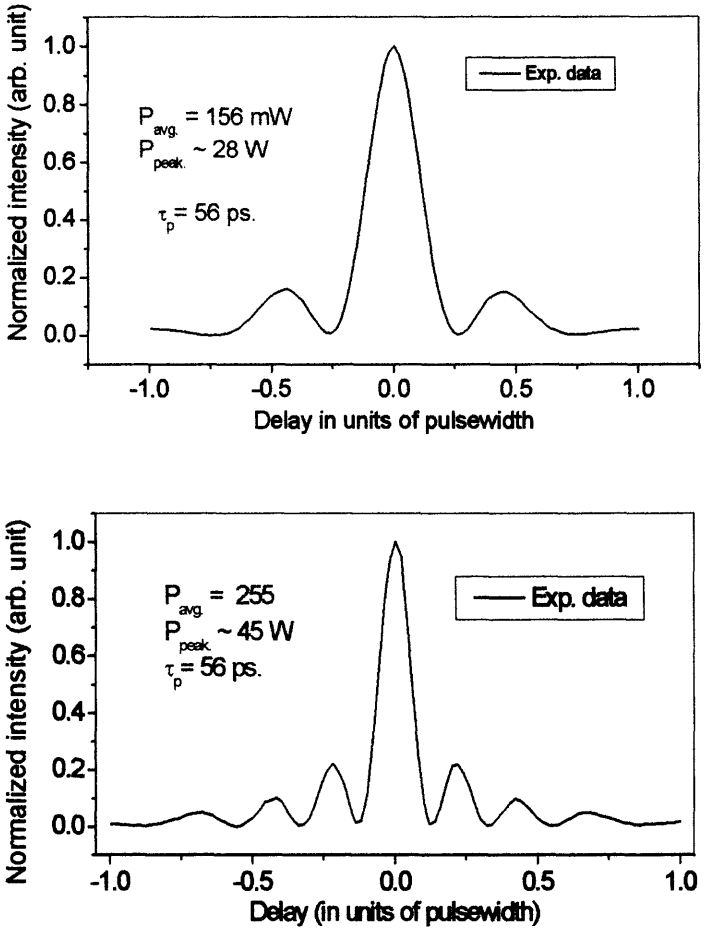

Figure 4.11 Experimental IGA traces at different power levels in 20 m erbium doped fiber.

4.4.3 Analysis of IGA Data and n_2 Determination

In order to extract the nonlinear refractive index from IGA measurements, the experimental data must be fitted to the theoretical model developed in section 4.3. What is actually measured in IGA is modeled after Equation (4.5) whose full expression is given in Equation (4.12). By numerically evaluating this integral and fitting the resultant trace to the experimental data, one obtains the exact value of the self-phase modulation strength ($\omega_0\tau_p Q$) for the given input power. As an illustration, Figure (4.12) shows the two experimental traces fitted to the model with the resulting $\omega_0\tau_p Q$ values.

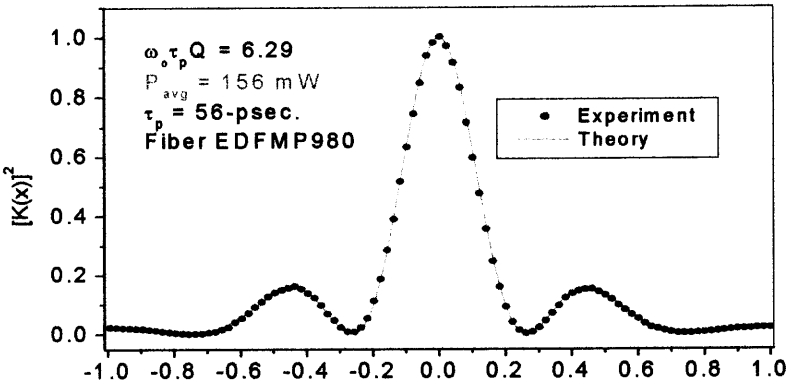

(a) Experimental fit with theory for IGA trace at 156 mW

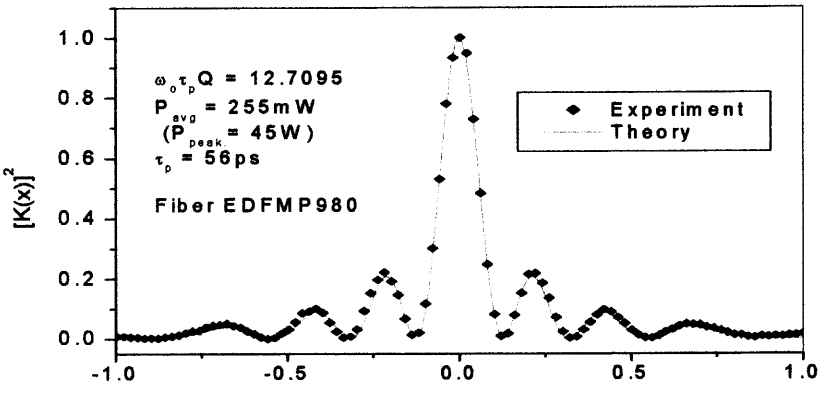

(b) Experimental fit with theory for IGA trace at 255mW

Figure 4.12 Typical experimental IGA traces at different power levels fitted to Equation 4.12 to obtain $\omega_0\tau_p Q$. The fit is excellent.

The process of calculating the nonlinear index (n_2) from the data involves the use of a direct relationship between the average power, n_2 and $\omega_0\tau_p Q$. This relationship will be derive in the following analysis.

The self phase modulation strength can be expressed as [56,57]:

$$\omega_0 \tau_p Q = \frac{n_2 \omega_0 L E_0^2}{c} \tag{4.20}$$

where E_0 is the peak electric field amplitude, n_2 is the nonlinear refractive index, L is the length of the fiber, ω_0 is the angular frequency [$\omega_0 = (2\pi c)/\lambda_0$], and c is the speed of light. The peak electric field amplitude E_0 can be deduced from power measurements and the effective cross-sectional area (A_{eff}) for the mode propagation in the fiber. The relationship is given (in cgs units) by [10]:

$$E_0^2 = \frac{8\pi P_{peak}}{ncA_{eff}} x10^7 \tag{4.21}$$

If I_{peak} denotes the peak intensity [peak power per unit area] averaged over the optical period, then for a Gaussian pulse one can write:

$$I_{peak} = 2\left(\sqrt{\frac{\ln 2}{\pi}}\right)\frac{P_{avg.} t_R}{A_{eff}\tau_p} \tag{4.22}$$

where $P_{avg.}$ is the average power, t_R is the laser repetition rate, τ_p is the laser pulsewidth and the rest have their usual meanings as earlier defined. One can replace (P_{peak}/A_{eff}) in Equation (4.21) by I_{peak} as given in Equation (4.22) and substitute the entire expression into Equation (4.20) to obtain the following result

$$\frac{n_2}{A_{eff}} = \frac{n\tau_p c\lambda}{t_R L}\left[32\pi^2\sqrt{\frac{\ln 2}{\pi}}x10^7\right]^{-1}\left(\frac{\omega_o \tau_p Q}{P_{avg.}}\right) \tag{4.23}$$

This equation can be written in a more compact form thus:

$$\frac{n_2}{A_{eff}} = \Omega\left(\frac{\omega_o \tau_p Q}{P_{avg.}}\right), \tag{4.24}$$

where

$$\Omega = \frac{n\tau_p c\lambda}{t_R L}\left[32\pi^2\sqrt{\frac{\ln 2}{\pi}}x10^7\right]^{-1} \tag{4.25}$$

The parameters appearing in Equation (4.25) are usually known, so that Equation (4.24) can be used to calculate n_2/A_{eff} or n_2 (if A_{eff} is known). In this technique, it is a good practice (for improving the accuracy of measurement) to measure a series of IGA traces at different powers and plot the resulting $\omega_0\tau_p Q$ versus the average powers as determined from power meter readings after correcting for losses in the focusing optics. The slope of the linear plot can then be used in Equation (4.24) to calculate n_2/A_{eff}. This reduces the uncertainties due to the power and pulsewidth measurements.

It should be noted that the n_2 calculated from the above equation is in units of esu (electrostatic units). It is common to quote n_2 in units of cm^2/W, where $n_2[cm^2/W] = (n_2[esu])/348.7$.

CHAPTER 5

MEASUREMENT OF THE NONLINEAR REFRACTIVE INDEX OF Er-Al-Ge DOPED SINGLE MODE FIBERS AS A FUNCTION OF THE DOPING PROFILES, USING THE IGA TECHNIQUE

5.1 Introduction

5.1.1 Why Measuring the Nonlinear Refractive Index in Er-Al-Ge Doped Fibers?

The recent increase in the use of Erbium-Doped Fibers for optical amplification in long haul optical transmission systems has given rise to an overwhelming interest in the study of the optical properties of such fibers [133-137]. Erbium doped fibers are used in modules known as erbium-doped fiber amplifiers (EDFAs) which have rapidly replaced electronic repeaters in transoceanic cable networks [133-134]. The use of EDFAs permits direct amplification of optical signals without the optical-to-electrical-to-optical conversions associated with electronic repeaters.

Optical amplifiers amplify incident light through stimulated emission, the same mechanism used by lasers. Its main ingredient is the optical gain realized when the amplifier is pumped (optically) to achieve population inversion. The two commonly pumping wavelengths for EDFAs are 980 nm and 1480 nm. These erbium ions absorb light at 980 or 1480 nm and store this energy to amplify signals at wavelengths near 1550 nm. Figure (5.1) shows typical absorption and gain profiles for an erbium-doped silica fibers [138]. The key success to erbium is the fact that the amplification band coincides with the minimum loss wavelength of optical fibers [139]. Figure (5.2) shows the variation of fiber loss with wavelength.

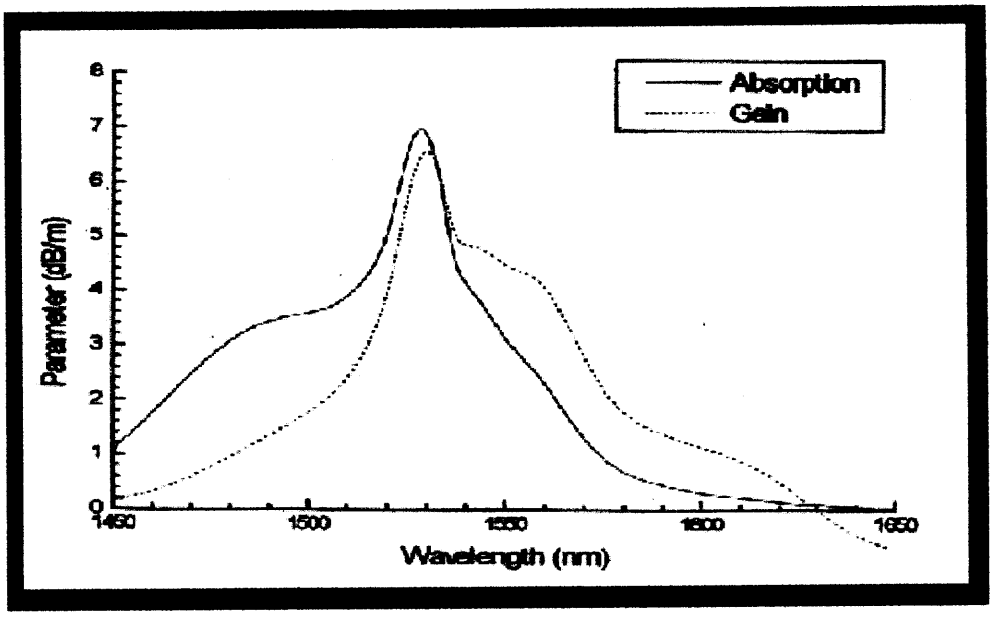

Figure 5.1 Typical absorption and gain curves for an erbium-doped fiber [138].

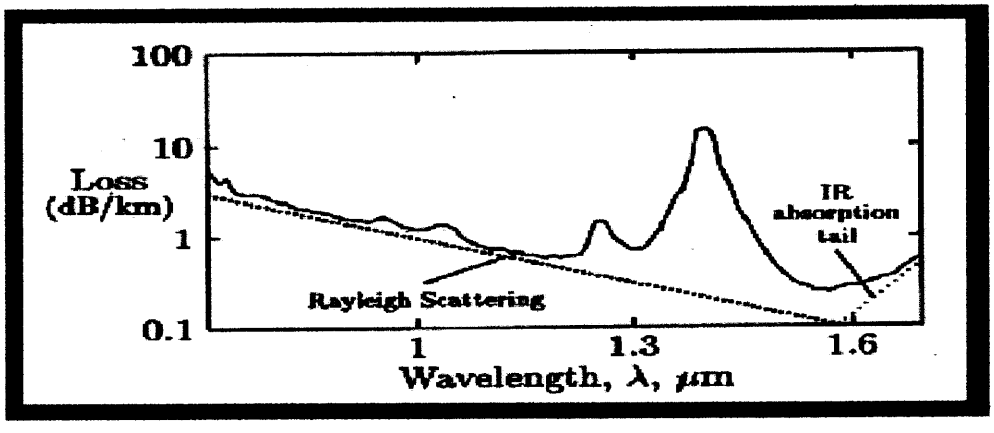

Figure 5.2 Typical variation of total attenuation with wavelength in silica based optical fibers. It also shows the attenuation curve due to Rayleigh scattering and the Infrared (IR) absorption in silica [6].

There are two main mechanisms for losses in optical fibers – radiative losses and absorption losses. The radiative losses are due primarily to Rayleigh scattering, which is caused by small scale (small compared to the wavelength of the light wave) inhomogeneties in the fiber. As a result, a guided mode can sometimes get coupled to a radiation mode. Rayleigh scattering is proportional to λ^{-4} and thus falls rapidly with increase in wavelength. At 1.064 μm, the value is approximately 1dB/.km and at 1.55 μm it is about 0.15 dB/km, which represents the ultimate loss limit of optical fibers. On the other hand, the absorption loss arises from the interaction of the propagating wave with the major components of glass that constitute the fiber, such as the infrared absorption band of SiO_2 and also due to the presence of the OH^- ions in the fiber.

Another success of erbium as an amplifying dopant is that the energy level structure of Er^{3+} ions in silica host is such that all transitions are nonradiative except the last transition between the $^4I_{13/2}$ and $^4I_{15/2}$, which is almost 100% radiative. The lifetime of the $^4I_{13/2}$ is also very long (~ 10 ms) [134]. This long lifetime permits the inversion of the population between the $^4I_{13/2}$ and $^4I_{15/2}$ with a relatively weak and practical pump source. A simplified energy level diagram of Er^{3+} is shown in Figure 5.3. A three level model can be used for the 980 nm pumps, while a two-level model usually suffices for the 1480 nm pumping [133,134].

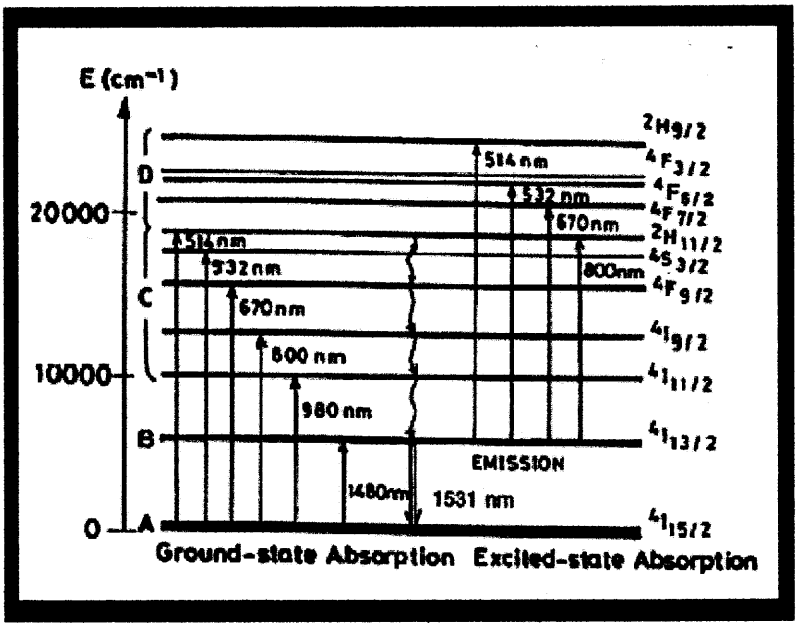

Figure 5.3 Energy level diagram of erbium ions in a silica matrix. Population inversion between $^4I_{13/2}$ and $^4I_{15/2}$ levels leads to amplification in the 1.55 μm band [139].

In spite of the numerous research work done on the optical properties of erbium doped fibers and EDFAs [133-144], the nonlinear index of refraction remains the least studied parameter in this class of fibers. Yet this single parameter (n_2) controls the majority of the nonlinear optical effects that have relevant impacts on optically amplified signals. The nonlinear index has been studied extensively in other types of (non-erbium doped) silica fibers using different measurement techniques [13, 15, 54-59, 107-113] but only few reports are available [136-137, 145] on n_2 measurements in erbium-doped fibers. The situation is further worsened by the fact that some of the few available reports dwelled on the measurement of absorption-enhanced nonlinearity [137, 145] rather than the Kerr nonlinearity. The absorption enhanced nonlinearity in erbium-doped fibers are based on the principle that the refractive index of a material depends on the

electronic population distribution between energy levels and this dependence is enhanced near an electronic absorption transition [146-148]. By applying an optical pump, the population distribution can be modified, which results in a change in refractive index. This is similar to the mechanism responsible for optical nonlinearity present in semiconductors [149]. This type of nonlinearity has been investigated in erbium-doped fibers primarily for switching applications [137, 146-148]. On the other hand, the only known report that considered Kerr nonlinearity in erbium-doped fibers merely estimated [136] n_2 value based on known result for pure silica fibers.

In order to accurately predict and improve the performance of optical transmission systems, it is important for system designers to know the numerical values of n_2 (due to Kerr effect) for all types of fibers used especially the optical amplifiers. Therefore, an accurate measurement of n_2 in erbium-doped fibers has become ever more crucial. As a contribution towards this (part of which is contained in this thesis), the author in collaboration with other workers has recently reported [66] an accurate measurement of n_2 (due to Kerr nonlinearity) in erbium-doped fibers and found that the value of n_2 is higher in erbium-doped fiber than in pure silica fiber. A systematic study of how n_2 would vary with erbium concentration still remains open. This open question would also be answered in this chapter. In addition, present-day telecommunication fibers (including erbium-doped fibers and EDFAs) are doped with varying amounts of aluminum, germanium or phosphorus to modify the structural and transmission properties of the fibers. These dopants (for example GeO_2 and P_2O_5) are particularly used to increase the linear refractive index of the fiber core above that of the cladding to provide

a better guiding structure. Mostly, Al_2O_3 is used to enhance the solubility of rare-earth dopants and to suppress excited state absorption in EDFAs [134,150].

In a recent report, Boskovic et 'al and Kato et' al have independently measured n_2 in germania and fluoride co-doped silica fibers and showed that while fluoride reduced n_2, germania did increase n_2 of the fibers. In this chapter, the author has used the IGA technique to measure n_2 of several Er-Al-Ge doped single mode fibers and investigated the dependence of n_2/A_{eff} on the doping profiles of the three dopants. This appears to be the first known systematic study of n_2 as a function of the dopant contents in erbium-doped fibers. The result would provide system designers with a better understanding of the nonlinear properties of erbium-doped fibers, needed for a more accurate design and evaluation of EDFAs.

5.1.2 TrueWave Rs and Dispersion Compensating Fiber (DCF)

The TrueWave Rs fiber is one of the special new-generation transmission fibers developed by Lucent Technologies in 1998 [156]. An important characteristic of this fiber is that the dispersion slope (the rate of change of dispersion with wavelength) is very small, hence the name "reduced slope". Because of this reduced slope, it is used for extending high-powered long distance networks for operation in both the third and forth communication windows. This fiber is also called Non-zero dispersion fiber (NZDF) and it has zero dispersion around 1450 nm.

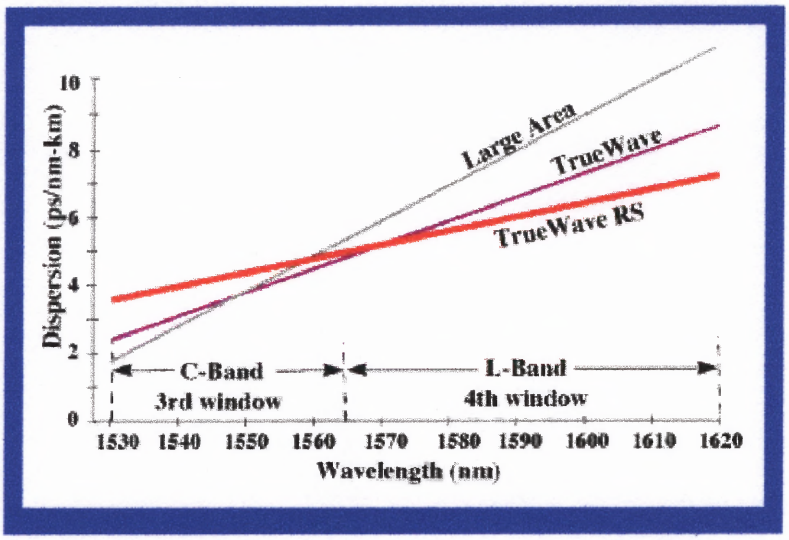

Figure 5.4 Dispersion slope of NZDF fiber compared to other standard fibers [156].

Figure 5.4 shows the dispersion slope of the TrueWave Rs fiber in comparison to other standard telecommunication fibers. Because of the overwhelming choice of this fiber over other standard transmission fibers, it is very important that its nonlinearity be characterized. The Raman gain efficiency in this fiber has recently been measured by Bromage [157]. Research on other nonlinear optical properties of this fiber (especially n_2 measurement) is relatively unexplored. Thus, this measurement will serve to provide the much-needed data on the nonlinear index coefficient of this fiber.

Also of equal importance is the measurement of n_2 in DCF (dispersion compensating fiber). The DCFs are fibers specially designed to compensate for dispersion in the transmission fiber lines. For example, a DCF can be designed to have large "normal dispersion" D ~ -100 ps/km-nm in the region in which standard transmission fibers have anomalous dispersion (D ~ 16 ps/km-nm). A small length of DCF can then be inserted along the line to compensate for dispersion incurred by the

optical pulse in propagating through about 8-10 km of transmission distance. Generally DCF has relatively small core diameter, and this increases the intensity of the information bearing lightwave in the DCF core, which increases nonlinear interactions. Therefore, the understanding the nonlinear properties of DCF has always been a crucial issue. This investigation is expected to provide useful data that will help in this understanding.

5.2 Experimental Details

5.2.1 Fiber Properties – Effective Area and Mode-field Diameter Measurements

Nine different fiber types were investigated. These include a polarization maintaining (PM) silica core fiber with no dopants, True-Wave fiber, DCF, and six other Erbium doped fibers with varying amounts of GeO_2 and Al_2O_3 content. This measurement will investigate how the nonlinear coefficient changes as a function of the dopants' contents in these fibers. Fiber properties are listed in (Table 5.1).

The effective area and mode field diameter (MFD) of the fibers were determined through the transmitted near-filed scanning technique. The measurement was done using EXFO high-resolution optical fiber analyzer, model NR-9200 at 1314 nm and 1552 nm. The fiber effective area is defined from the near-field intensity distribution by [151-152]:

$$A_{eff} = \frac{2\pi\left(\int_0^\infty |E_a(r)|^2 r dr\right)^2}{\int_0^\infty |E_a(r)|^4 r dr} = \frac{2\pi\left[\int_0^\infty I(r) r dr\right]^2}{\int_0^\infty I(r)^2 r dr} \tag{5.1}$$

where $E_a(r)$ is the amplitude and $I(r)$ is the near-field intensity distribution of the fundamental mode, r being the radial distance from the center of the mode profile.

The modified diameter is defined in the near field by [151, 153]

$$MFD_{NF} = \left[\frac{\left(\int_0^{\infty} |E_a(r)|^2 r dr \right)}{\int_0^{\infty} |E_a'(r)|^2 r dr} \right]^{\frac{1}{2}} \tag{5.2}$$

In conventional step-index fibers, the mode-field diameter is well approximated by a Gaussian function of radius w at 1/e amplitude points. In this case, the effective area may be given by

$$A_{eff} = \pi w^2 \tag{5.3}$$

where $2w(\lambda)$ is the so-called "Peterman-II mode-field diameter" of the fiber at wavelength λ. For fibers that do not share the step-index geometry, such as dispersion shifted fibers and dispersion flattened fibers, the mode-field cannot be approximated by a Gaussian function, and Equation (5.3) no longer holds. It has been proposed [154] that the effective area of various types of standard fibers can be calculated using Equation (5.3) but including a correction factor k_{Nam}, that depends on wavelength and type of fiber. This has led to the so called "Namihira relation", given by:

$$A_{eff} = k_{Nam} \pi w^2(\lambda) \tag{5.4}$$

The refractive index profile was measured through the refractive near field (RNF) [155] scanning at 673 nm. The measured refractive index profiles for six of the fibers are shown in Figures (5.5) through (5.7). The core-cladding refractive index difference (Δn) is obtained from the plotted index profile and can also be estimated from the germania concentration in the fiber (see appendix B).

$$\Delta n = n_{core} - n_{clad} \tag{5.5}$$

The delta parameter (Δ), defined as the relative refractive index difference between the core index and the cladding index is given as:

$$\Delta = \frac{n_{core}^2 - n_{cl}^2}{2n_{core}^2} \approx \frac{n_{core} - n_{cl}}{n_{core}} \approx \frac{\Delta n}{n_{core}}, \tag{5.4}$$

where n_{core} is the refractive index of the fiber core and n_{cl} is the cladding refractive index.

Table 5.1 Properties of Er-A-Ge Doped Fibers Studied in Chapter 5; MFD at 1064 nm were Extrapolated from Measured Values at 1314 nm, 1552 nm & 1450 nm (See Appendix D)

S/N	**Er** cm^{-3} x 10^{19}	**Al** %M	**Ge** %M	**Δn** x 10^{-2}	**MFD** (μm) 1.064 μm	**MFD** (μm) 1.314 μm	**MFD** (μm) 1.552 μm	**A_{eff}** (μm^2) 1.064 μm	**A_{eff}** (μm^2) 1.314 μm	**A_{eff}** (μm^2) 1.552 μm
1. Silica JAY 84	-	-	-	0.5	8.21	9.12	10.48	50.0	60.76	78.77
2 EDF-MP980	0.80			1.48	4.32	4.8	6.17	14.70	18.40	28.20
3. E071698	0.48	26	0	2.01	3.93	4.37	5.85	12.13	14.96	25.92
4. E082595	0.24	2	4	1.01	5.70	6.33	8.03	25.52	29.5	46.76
5 E052898	0.24	12	5	1.74	4.22	4.69	5.88	14.00	16.16	25.75
6 E012397	0.15	12	13	2.45	3.33	3.67	4.58	8.71	10.52	16.02
7 E060195	0.88	12	13	2.42	3.45	3.83	4.80	9.35	11.39	18.22
8 DCF A_{eff} = 15 μm^2 @ 1.450μm					3.74	4.15	4.8	10.44	13.53	17.2
9 True Wave A_{eff} = 55 μm^2 @ 1.450μm					7.2	8.01	9.12	40.72	50.39	62.1

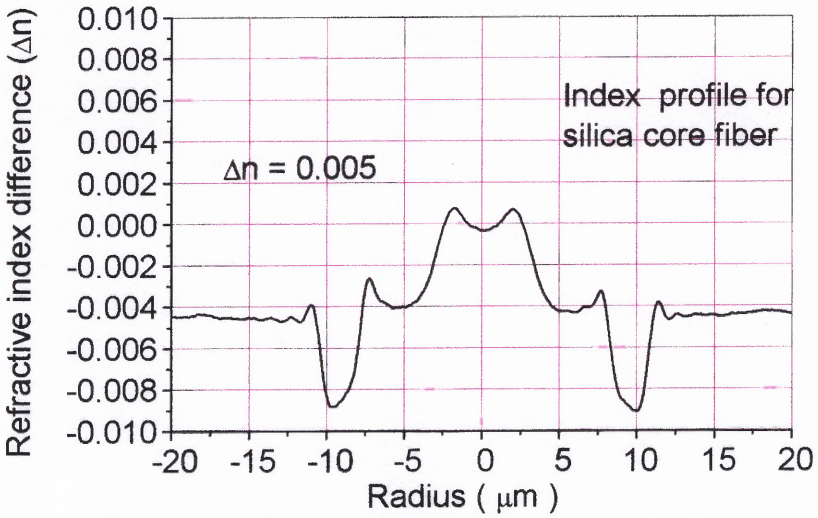

(a) Refractive index profile for the silica core fiber.

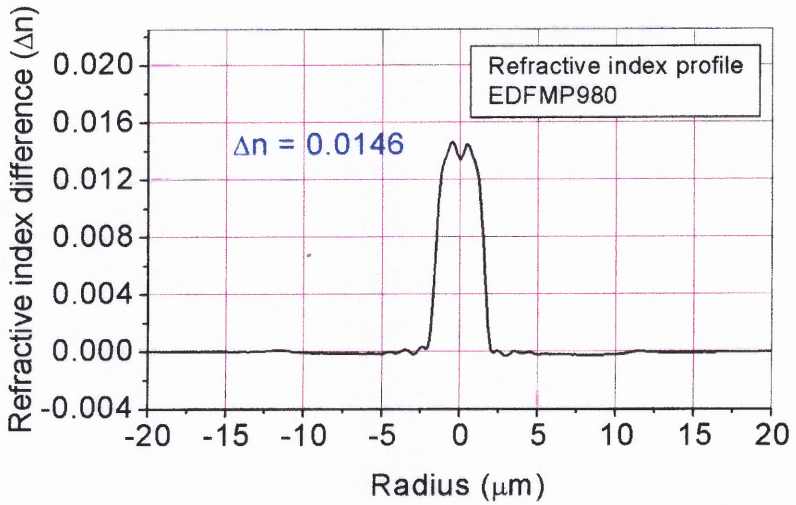

(b) Refractive index profile for Er^{3+} doped fiber
[erbium concentration = 8.0×10^{18} cm^{-3}]

Figure 5.5 Measured refractive index profiles for (a) pure silica fiber and (b) erbium- doped fiber. Notice that the cladding of the pure silica fiber has depressed-index profile.

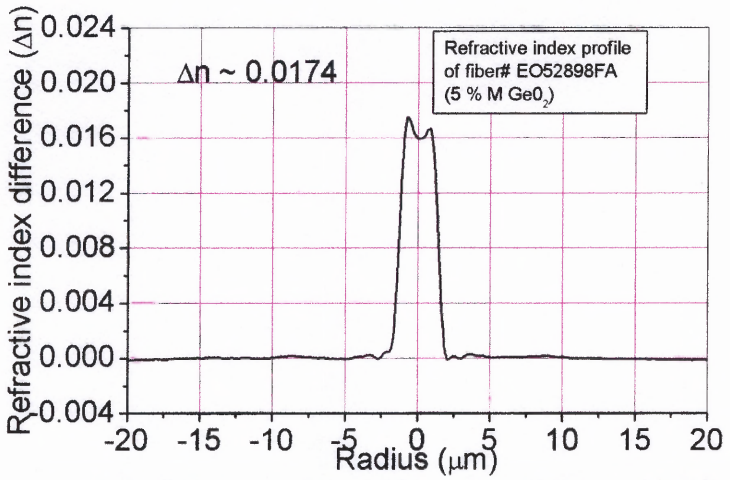

(a) Refractive index profile of Er-Al-Ge doped fiber with 5 %M Ge and 12 %M of Al

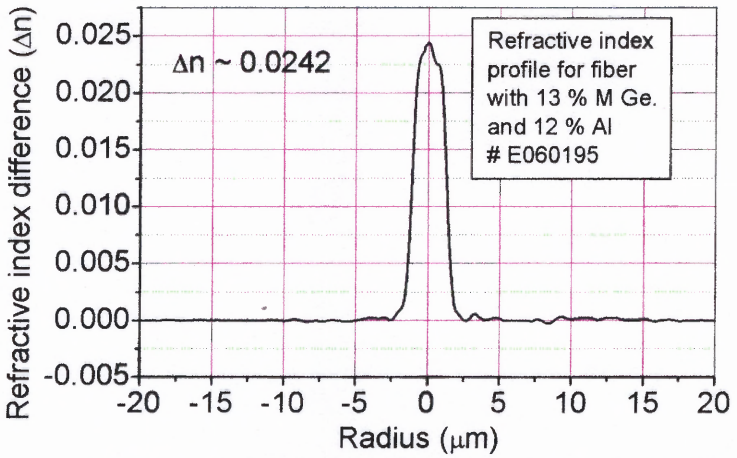

(b) Refractive index profile for Er-Al-Ge doped fiber with 13%M Ge and 12 %M Al.

Figure 5.6 Measured refractive index profiles for two Er-Al-Ge doped fibers with different dopant contents.

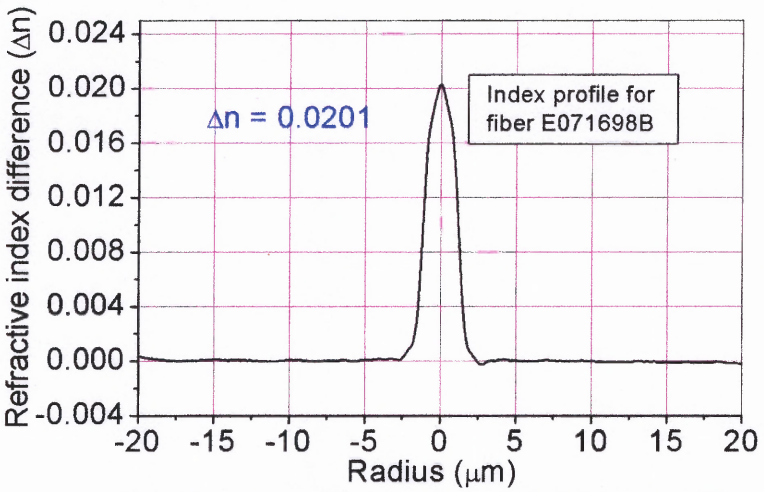

(a) Refractive index profile for Er-Al doped fiber with 0 %M Ge and 26 %M Al.

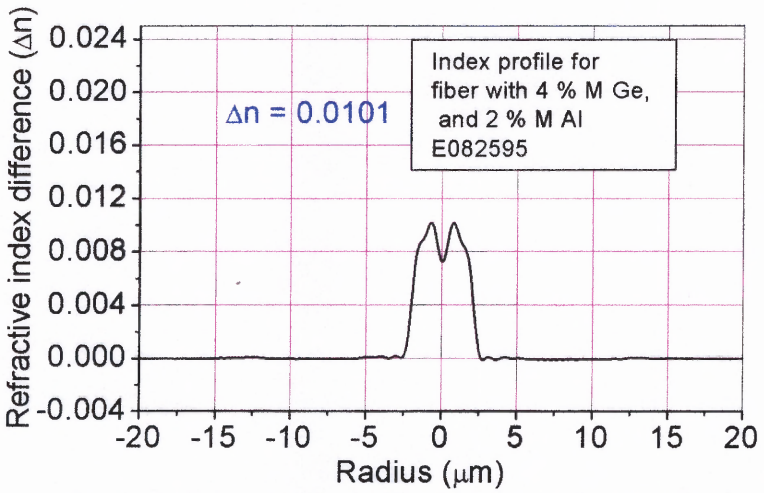

(b) Refractive index profile for Er-Al-Ge doped fiber with 4 %M Ge and 2 %M Al.

Figure 5.7 Measured refractive index profiles for two fiber with different doping profiles.

5.2.2 Measurement of n_2 using IGA

The IGA measurements were taken on the fibers listed in Table 5.1. The experimental set up was arranged in the usual form described in Chapter 4 (Figure 4.10). The experiments were carried out on the fibers one at a time. The laser pulses (with pulsewidths 49-56 picoseconds) were coupled into the test fiber using 10X microscope objective. The average power coupled into the fiber ranged from 20 mW to 800 mW, depending on the fiber effective area and the level of SPM desired. . In each case, these pulses undergo self-phase modulation as they propagate through the fiber. The IGA traces of the out pulses from the fiber were recorded at different power inputs by following the procedure described in Chapter 4, Section 4.4.2. In measuring the power, attention was paid to the losses encountered within the focusing optics and these were corrected for. Losses within the fibers were negligible because with L ~ 20 m, L_{eff} ~ 19.9 m. Therefore, $L_{eff} \approx L$ for $L \leq 20$ m, where L is the experimental fiber length and L_{eff} is the effective length.

5.3 Results and Analysis

The IGA traces obtained from the above measurements were fitted to the pure SPM model (Equation 4.12) as described in Chapter 4. In order to obtain the nonlinear coefficient (n_2/A_{eff}) for each fiber, several traces are fitted, and the resulting SPM strength is plotted as a function of the average power. The slope of the linear fit to the graph is proportional to n_2/A_{eff}. Typical fitted traces and the linear graphs are shown in Figures (5.8) through (5.16). The resulting n_2/A_{eff} as a function of dopant contents are given in Table 5.2.

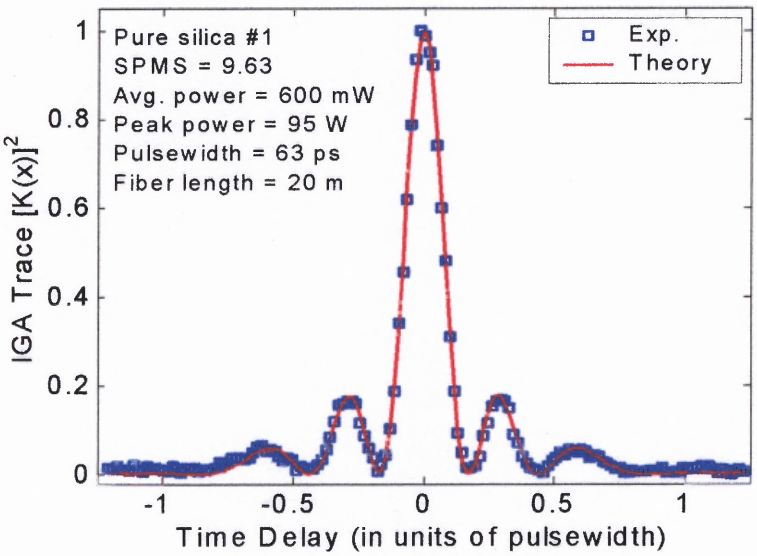

(a) Typical IGA trace for 20 m long Silica fiber

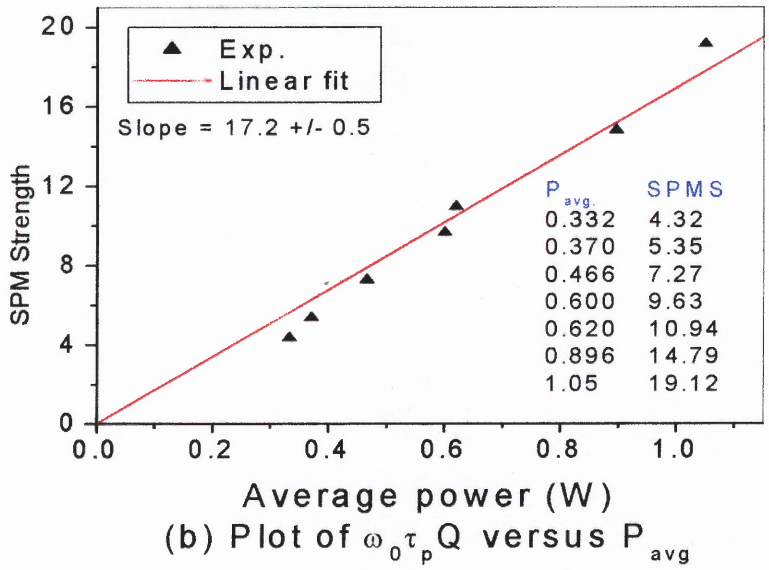

(b) Plot of $\omega_0 \tau_p Q$ versus P_{avg}

Figure 5.8 Typical IGA trace and a plot of SPM strength versus average power for 20 m Silica fiber. (a) Represents IGA trace (b) is a plot of SPMS versus average power

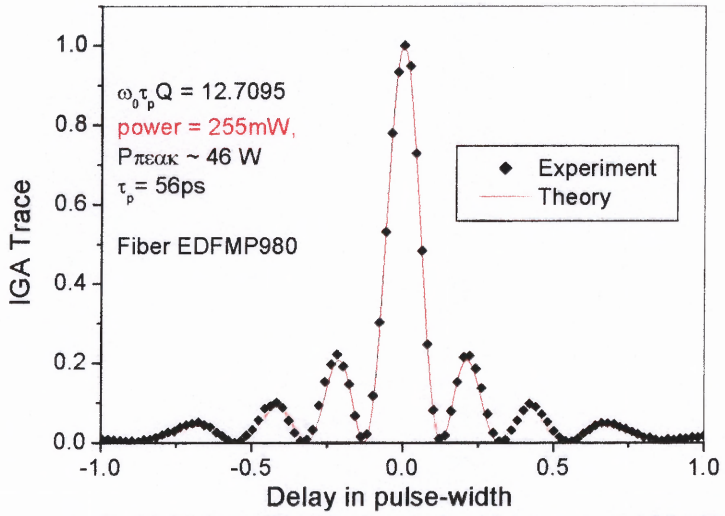

(a)Experimental fit with theory for IGA trace at 255mW

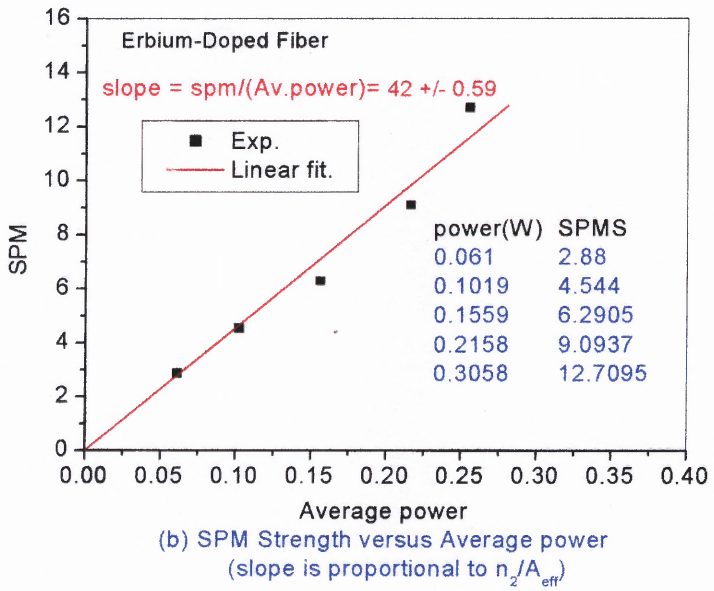

(b) SPM Strength versus Average power
(slope is proportional to n_2/A_{eff})

Figure 5.9 Typical results obtained with erbium doped fiber (18.05 m).
(a) Typical IGA Trace fitted to Equation (4.12)
(b) SPM strength vs Average power for several traces

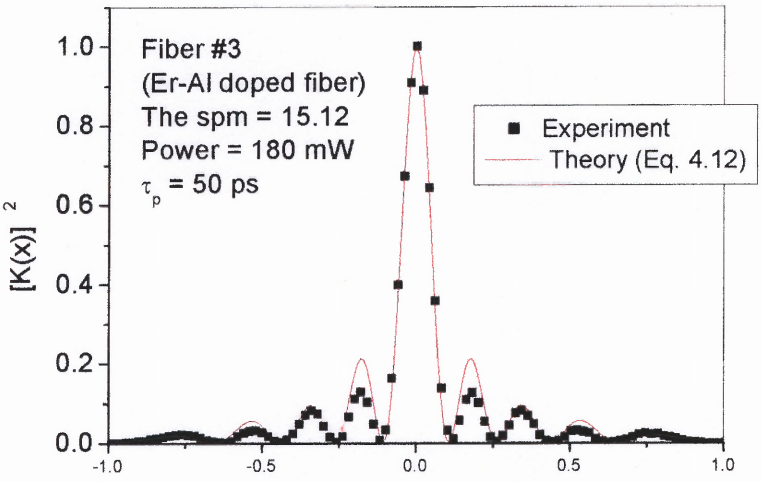

(a) Typical IGA trace for fiber with only Er-Al doping.

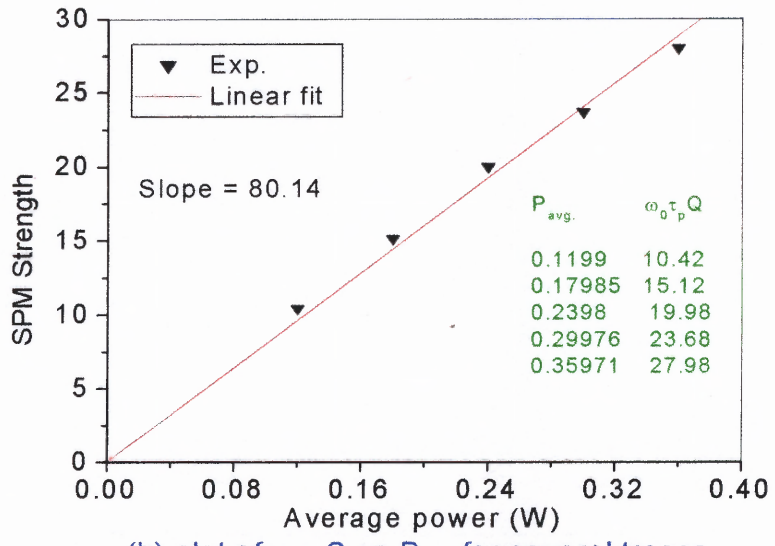

(b) plot of $\omega_0\tau_pQ$ vs P_{avg} for several traces.
Fiber #3 (26 %M of Al, no GeO_2)

Figure 5.10 Plot of result obtained for fiber #3 (Er-Al doped only, 26 %M of Al).

5.4 Discussion of Result and Comparison with Published Results

The measured n_2/A_{eff} and n_2 values in this work are given in Table 5.2. The nonlinear coefficient (n_2/A_{eff}) in the Er-Al-Ge is found to increase with germanium content as well as with the Aluminum and erbium.

An earlier calculation of n_2 from the measured nonlinear coefficient (n_2/A_{eff}) using the A_{eff} at 1.55 for the Er-Al-Ge doped fibers and A_{eff} at 1064 nm for the pure silica indicated that n_2 in erbium (only) doped fiber was higher than n_2 in the pure silica. This analysis was done with the feeling that the mode field diameter (used to calculate the effective area) does not vary significantly with wavelength. The analysis also showed that n_2 in the Er-Al-Ge doped fibers, increased more with GeO_2 content and only slightly with Al and Er concentration in the fiber (6^{th} column in Table 5.2).

It was later found (see Appendix D) that indeed, both MFD and A_{eff} vary significantly with wavelength. This was noted after the author has made MFD and A_{eff} measurements at 1552 nm and 1314 nm and compared the results. For example, the A_{eff} for the pure silica at 1552 nm was found to be 78.77 μm^2 and at 1314 nm the value reduced to 60.76 μm^2, while the value at 1064 nm (obtained from Roger Stolen [164]) was 50 μm^2. This huge variation (and sometimes more) was also observed in all the fibers measured. It therefore became necessary to evaluate n_2 with the A_{eff} at the same wavelength of measurement (1064 nm). In the absence of the equipment for measuring MFD and A_{eff} at 1064 nm, and lack of readily available scaling equation, the author has used the measured values at 1314 nm and 1552 nm to extrapolate the value at 1064 nm (see Appendix D). In doing this, the pure silica fiber whose value is known at these three wavelengths was used as a yardstick for determining the slope of the extrapolation.

Table 5.2 Measured Values of the Nonlinear Refractive Index as a Function of dopants' Concentration in Al-Ge-Er Doped Silica Fibers
Note: (1) n_2 values listed in column 6 were obtained using A_{eff} at 1.55um (2) n_2 values listed in blue (last) column were obtained using A_{eff} at 1064 nm, obtained by interpolation of graphs shown in Appendix D

S/N & Part #	**Er** (cm^{-3})	**Al** %M	**Ge** %M	n_2/A_{eff} (W^{-1})	n_2 (cm^2W^{-1})	n_2 (cm^2W^{-1})
1.Pure * Silica	0	0	0	4.88×10^{-10}	3.84×10^{-16}	2.44×10^{-16} *
2 EDF-MP980	0.80×10^{19}	0	0	1.21×10^{-9}	3.36×10^{-16}	1.78×10^{-16}
3. E071698	0.48×10^{19}	26	0	1.82×10^{-9}	4.72×10^{-16}	2.21×10^{-16}
4. E082595	0.15×10^{19}	2	4	7.30×10^{-10}	3.29×10^{-16}	1.86×10^{-16}
5. E052898	0.24×10^{19}	12	5	1.72×10^{-9}	4.29×10^{-16}	$2.41. \times 10^{-16}$
6. E012397	0.15×10^{19}	12	13	3.09×10^{-9}	5.06×10^{-16}	2.70×10^{-16}
7. E060195	0.88×10^{19}	12	13	3.23×10^{-9}	5.30×10^{-16}	3.02×10^{-16}
8 DCF				2.87×10^{-9}	4.94×10^{-16}	3.00×10^{-16}
9 TrueWave				5.46×10^{-10}	3.28×10^{-16}	2.22×10^{-16}

Table 5.3 Some Published n_2/A_{eff} and n_2 Values for Comparison with Table 5.2

Fiber Type Reference	**Technique**	**Wavelength**	n_2/A_{eff} $(W)^{-1}$	n_2 $(cm^2W)^{-1}$
Pure silica * [66]	SPM (L~200 m)	1064 nm	5.06×10^{-9}	2.53×10^{-16} *
DCF [15]	XPM (L ~ 4km)	1550 nm	2.06×10^{-9}	3.95×10^{-16}
DCF [57]	Cw (L ~ 200 m)	1550 nm	$1.1 1 \times 10^{-9}$	2.46×10^{-16}
Silica core [13]	SPM (L~100)	514.5 nm	2.66×10^{-9}	3.26×10^{-16}

**Measured with the same fiber [164]*

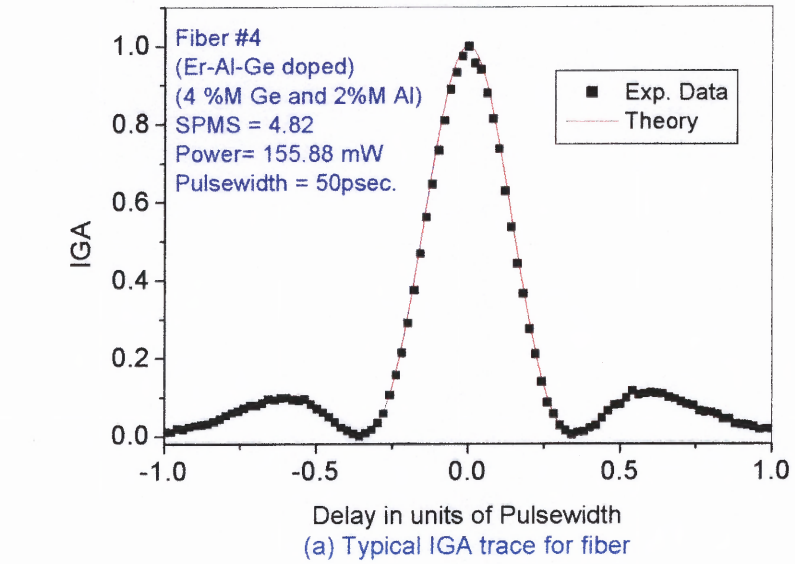

(a) Typical IGA trace for fiber

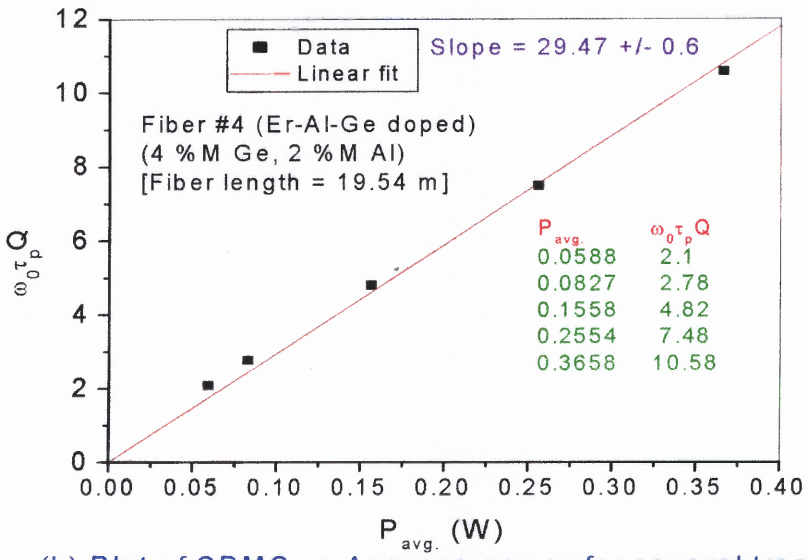

(b) Plot of SPMS vs Average power for several traces

Figure 5.11 Plot of the result obtained for fiber # 4 (Er-Al-Ge doped, 4 %M Ge and 2 % M Al). (a) Typical IGA trace (b) Plot of SPMS vs $P_{avg.}$ for several IGA traces.

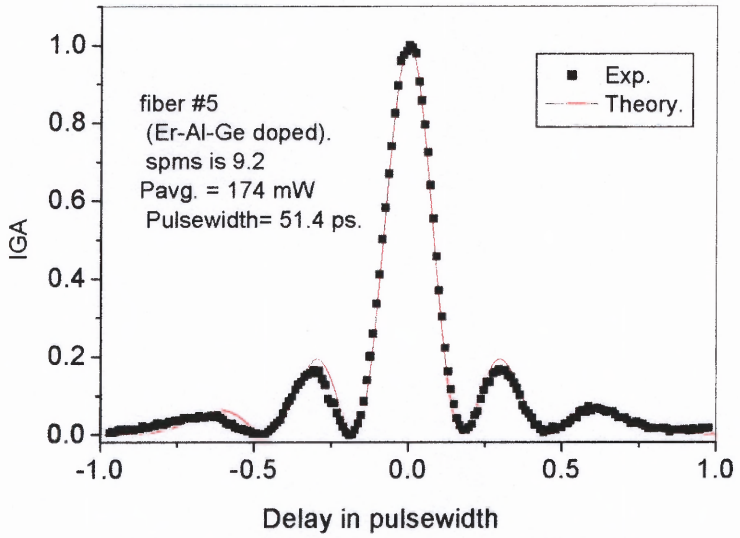

(a) Typical IGA trace measured at 174 mW.

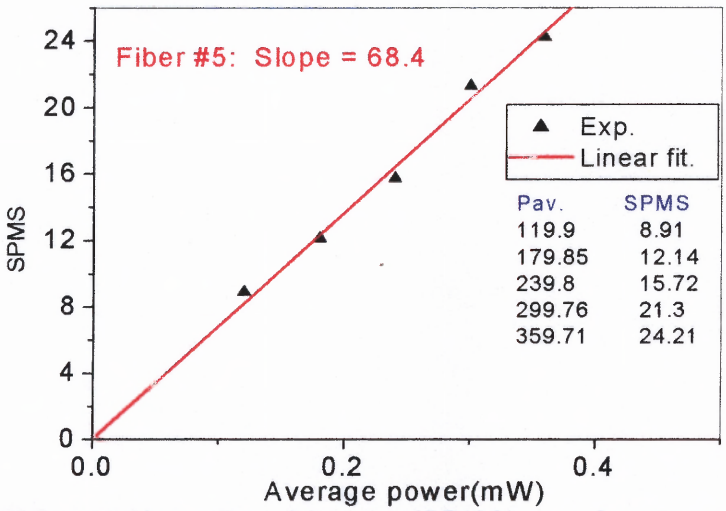

(b)Self Phase Modualtion Strength (SPMS) as a function of Average Power for Er-Al-Ge doped Fiber with 5%M Ge and 12 %M Al.

Figure 5.12 Typical result obtained for fiber #5 (Er-Al-Ge doped fiber with 12 %M Al and 5 %M Ge). (a) typical IGA trace and (b) plot of SPMS vs P_{avg} for several IGA traces

The last column of Table 5.2 shows the result of n_2 obtained using A_{eff} at 1064 nm. Contrary to expectations, it is seen that n_2 of the silica is higher that of the erbium (only) doped fibers and in the Er-Al-Ge doped fibers with little GeO_2. Nevertheless, in the Er-Al-Ge doped fibers where the germania concentration is high (rows 5 and 7), the n_2 is significantly higher than in pure silica, as expected. The n_2 in the DCF (dispersion shifted fiber) in row 8 of Table (5.2) is also higher than in pure silica. These are consistent with earlier reports [52,57]. However, since one expects n_2 to be higher in the erbium (only) doped fiber and in the E-Al-Ge doped fibers with low GeO_2 content than in pure silica, the observed contrary raises some questions on the actual role of erbium in the n_2 of the fiber. If erbium reduces the n_2 of the fiber, this could upset the slight increase due to the GeO_2 and Al in the Er-Al-Ge with low GeO_2 content, thus leading to a smaller net value than expected. It is also possible that this reduction in the value of n_2 in the erbium (only) doped fiber and in the Er-Al-Ge may have arisen due to polarization effect. The silica core fiber is a polarization maintaining fiber, while all the doped fibers are non-polarization maintaining fibers. The value of n_2 is usually higher if polarization is maintained and lower if polarization is scrambled. Although, it is usually assumed in IGA experiments that polarization scrambling is not effective, because the fiber length is short, this may not generally hold in the actual experiments. With this observation, it may be necessary to investigate the role of polarization in IGA experiment for n_2 measurements.

The major source of uncertainties in this work is the effective area measurement. The effective area used at 1064 nm were estimated (as explained in Appendix C) based

on the measurements done at other wavelengths. An additional source of uncertainty is the laser amplitude fluctuation of the Nd:YAG (typically 2-4%), which is translated into

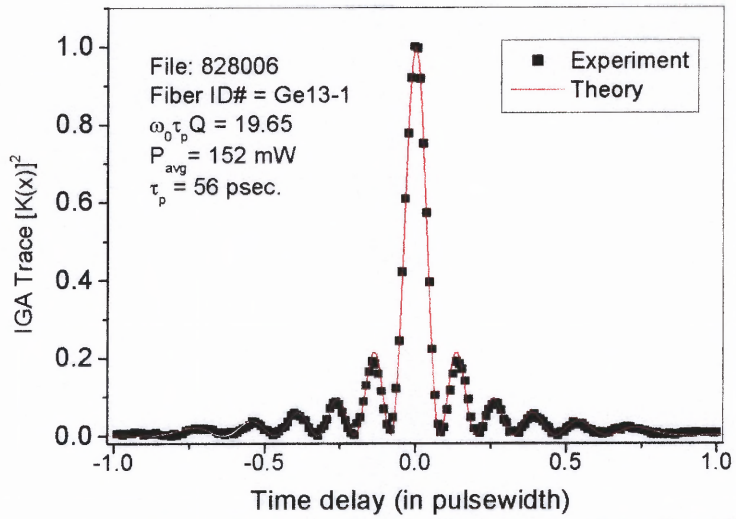

(a) Typical IGA trace fitted to Equation 4.12 for fiber #6
(Er-A-Ge fiber with 13 %M Ge and 12 %M Al)
(Erbium conc. = 0.15 x $10^{19}$$cm^{-3}$)

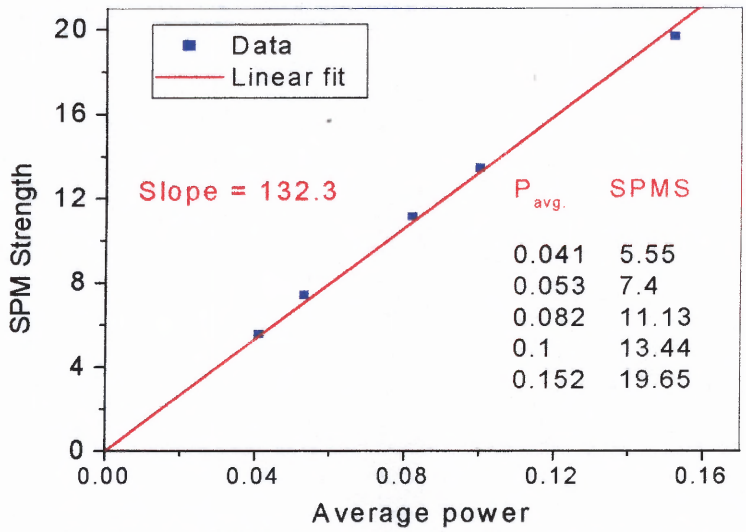

(b)Plot so SPM strength versus average power for several fitted IGA traces.

Figure 5.13 Plot of typical measured result for Er-Al-Ge doped fiber #6 (13 %M Ge, 12 %M Al and Erbium concentration = 0.15 x 10^{19} cm^{-3}).
(a) Measured IGA trace fitted to the model, Equation (4.12)
(b) Plot of SPM strength vs Average power (slope is proportional to n_2/A_{eff})

fluctuations in the average power. This is minimized by averaging the results of several measurements, through a plot of a linear graph of SPM strength Vs average power, and using the slope to calculate n_2. The error in the slope is typically less than 2%.

Table 5.3 shows some reported values of n_2 measurements in different fiber, using different techniques. The value of n_2 = 2.44 x10^{-16} cm^2/W obtained with the IGA technique is in good agreement within 5% with earlier measurement (n_2 = 2.53 x10^{-16} cm^2/W) using SPM in the same fiber [164, 66]. The IGA measured value for the DCF is also in good agreement with the published results for the DCFs shown in Table (5.3).

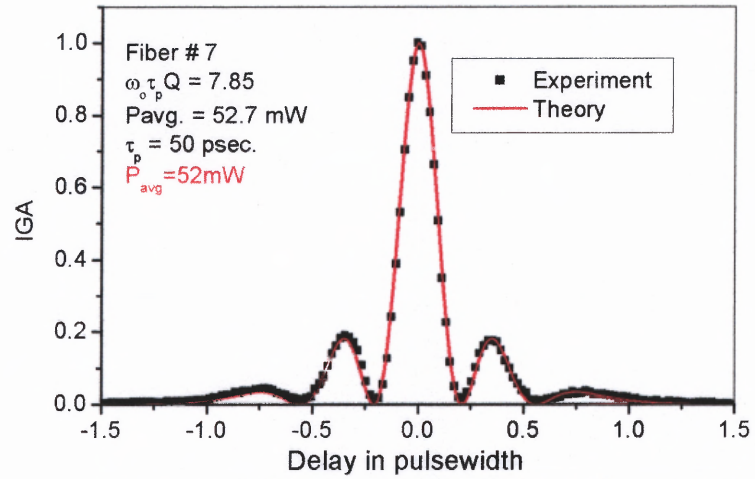

(a) Measured IGA trace at 52mW fitted to Equation (4.12)
(13 %M Ge, 12 %M Al, Er^{3+} conc. = 0.88 x $10^{19}m^{-3}$)

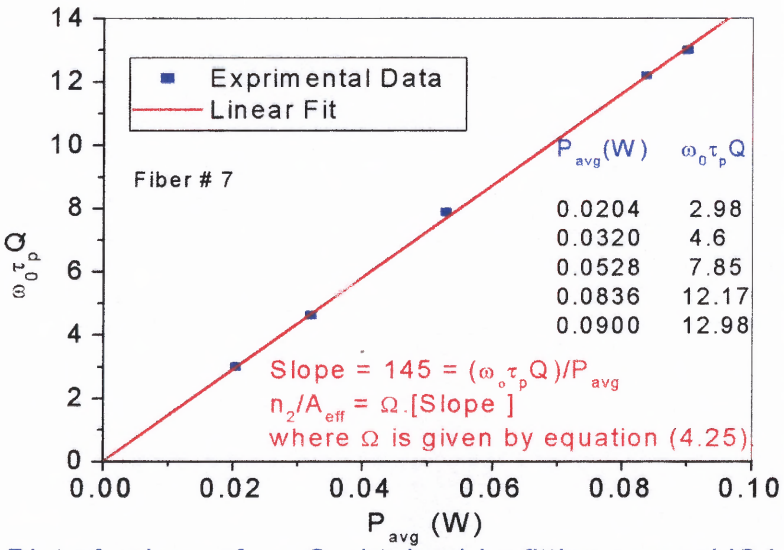

(b) Plot of values of $\omega_o\tau_p Q$ obtained by fitting several IGA traces taken at different powers.

Figure 5.14 Plot of typical results obtained in Er-Al-Ge doped fiber (with 13%M Ge, 12%M Al and Er^{3+}concentration = 0.88 x 10^{19} cm^{-3}).
(a) IGA trace fitted to Equation (4.12)
(b) Plot of SPM strength vs Average power for several fitted traces

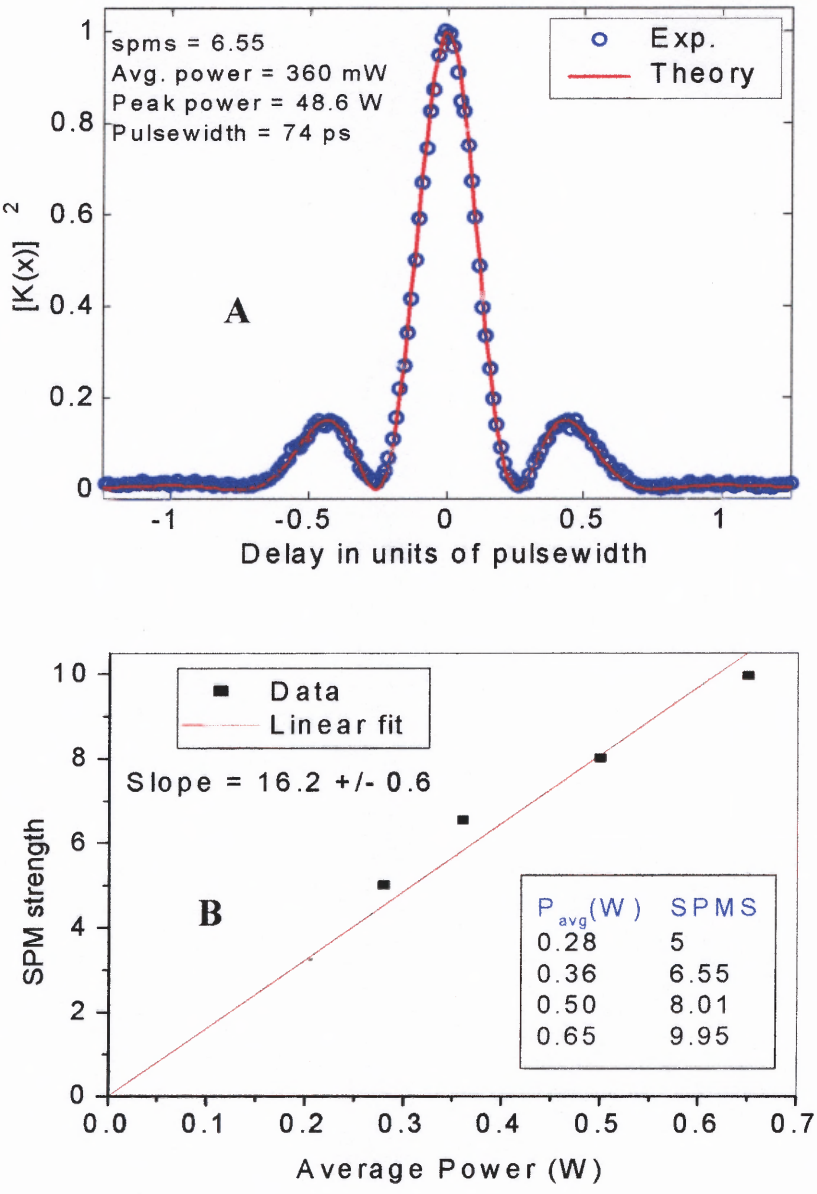

Figure 5.15 Typical results obtained for True Wave fiber
(a) IGA trace fitted to Equation (4.12)
(b) Plot of SPM strength vs average power (Slope is proportional to n_2/A_{2ff})

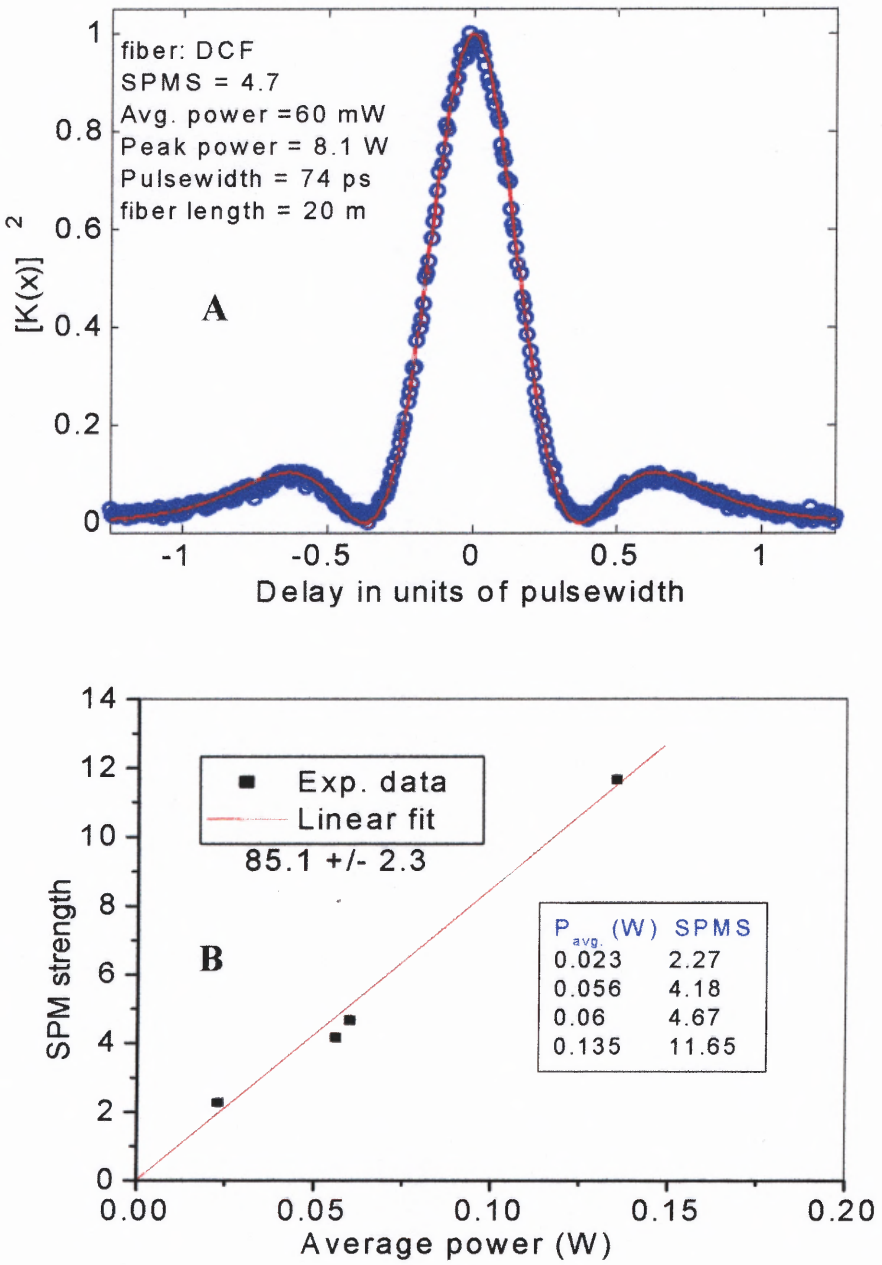

Figure 5.16 Typical results obtained for DCF showing (a) IGA trace fitted to Equation (4.12) and (b) SPM strength vs average power (Slope is proportional to n_2/A_{ff}).

CHAPTER 6

MEASUREMENT OF THE RAMAN GAIN COEFFICIENT IN OPTICAL FIBERS USING INDUCED GRATING AUTOCORRELATION: THEORY AND EXPERIMENT

6.1 Introduction

One of the most important nonlinear effects in optical fibers that greatly influence optical communications is stimulated Raman scattering. While this phenomenon is known to cause noise and cross-talk in optically amplified transmission systems [12], it is equally the "key" process that drive the newly emerging Raman fiber amplifiers and Raman fiber lasers [41-44]. The efficiency of performance of these systems depends on the stimulated Raman gain through the SRS process. Raman gain is proportional to the Raman gain coefficient, which is specific to the fiber material among other factors; such as pump wavelength, effective core area and fiber length. Different experimental techniques have been used to measure the Raman gain coefficient in optical fiber [158-160]. The use of IGA technique to measure the Raman gain coefficient is a new development, which is part of the investigations embodied in this thesis. The incentive to this stemmed from a recent observation made by the author [70] while performing experiments on n_2 measurements in Er-Al-Ge doped single mode fiber with high germania content. It was observed that the IGA trace was distorted in a fiber with high germania doping, even at moderate power inputs, and the resulting trace deviated significantly from the theoretical fit modeled in the context of pure SPM (see Chapter 4). This observation resulted in the subsequent modification of the original IGA model and its subsequent application in the measurement of Raman gain coefficient of fibers. These investigations are reported in this chapter.

6.2 Observation of Distortion of IGA Trace by Stimulated Raman Scattering and Initial Breakdown of the Standard IGA Model Based on Pure SPM

6.2.1 The Observed Deviation and Possible Cause(s)

While the author has obtained an excellent agreement between theory and experiment for IGA measurements on Er-Al-Ge fibers with low germania contents (0 – 13 %M), the result obtained from high germania doped (>28 %M) specie showed clear deviations from the standard IGA model. The standard IGA model (see chapter 4) assumes that there is no GVD within the typically-used 20 m long fibers, and that there is no contribution to the nonlinearity from SRS and XPM. The observed deviation is characterized by the lifting of the base region of the central peak of the IGA trace and outward shifting of the sidelobes. There is also a gradual depletion of the sidelobes (see Figure 6.1).

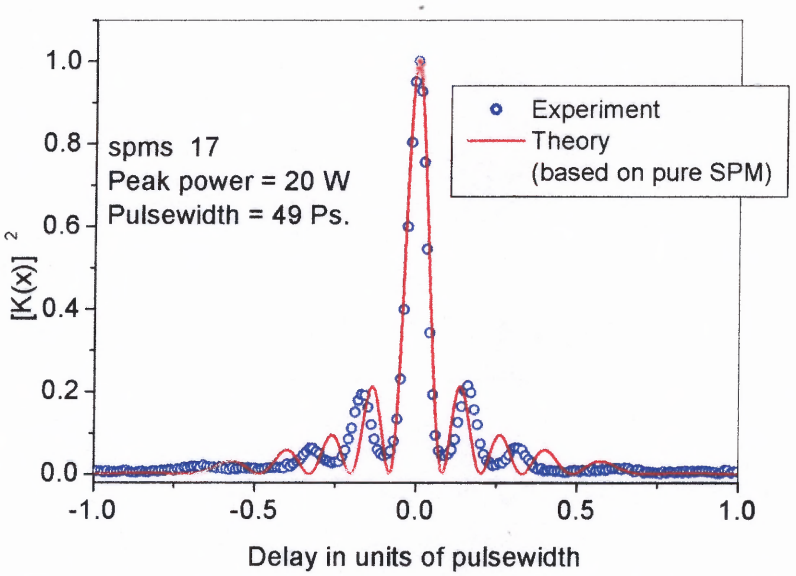

Figure 6.1 Typically measured IGA trace fitted with the standard IGA model for high germania doped fiber [fiber length ~ 20 m].

To investigate this observation further and in attempts to nail down the cause of this deviation, the author has systematically performed IGA measurements in two well-characterized fibers: (a) silica core fiber [164] (of lengths 20 m & 100 m), and (b) a DCF (dispersion compensating fiber) [165] , whose Raman proprieties have been previously studied [157, 163]. IGA measurement performed on the 20 m long silica core fiber from low (< 20 W peak power) to high (>70 W peak power) showed no deviation. With the 100 m long fiber, GVD is negligible because this is still far below the dispersion length of silica fiber. However, fiber loss may not be neglected. Thus, with a loss of 1.2 dB/km (at 1.064 μm), the effective length (see Equation 2.29) was calculated to be 98.63 m. Normal IGA trace that fit the standard pure SPM model were obtained with this fiber at moderate powers but at high power (typically 40 W), deviations were observed similar to the case of high germania fibers. The IGA traces measured in the DCF also showed good fit with the standard IGA model at low powers but deviated as the power was increased. Although, DCF fibers are known to have high negative dispersion [105], the occurrence of normal IGA traces (with sidelobes) at low powers has ruled out the effect of dispersion, so that one is safely working in the limit of zero GVD. In the presence of dispersion, IGA does not exhibit sidelobes [63-64].

Since this deviation appears to be intensity dependent, it must be associated with additional nonlinear process. The other commonly encountered nonlinear processes (apart from SPM) for a single propagating pulse in optical fiber, are stimulated Brillouin scattering (SBS), stimulated Raman scattering (SRS), intra-pulse Raman scattering, self-steepening and two-photon absorption. Some of these processes and the conditions under which they are observed have been explained in details in Chapter 2 of this thesis.

The SBS is known to occur in optical fiber only for cw (continuous wave) beams and for pulses with pulsewidth in the range of nanoseconds and higher [20]. As a result SBS is not a possible suspect, since these experiments were done with short pulses (~ 50 to 70 picoseconds). Stimulated Raman scattering is a prime suspect because it is usually effective in both long and short pulses if the appropriated threshold is reached (see Chapter 2, Section 2.5). In addition germania doping is known to increase the Raman gain coefficient in silica fibers [163].

On the other hand, intra-pulse Raman scattering is a process where the Raman gain amplifies the lower frequency component of a pulse by transferring energy to it from the high frequency component of the same pulse. As a result, the pulse spectrum shifts toward the low frequency side as the pulse propagates. This is sometimes referred to as self-frequency shift [166]. However, this phenomenon occurs for ultra-short pulses, with pulsewidth less than 1 picosecond [166]. Thus, because of the fact that the pulses used here are far from this range, the process has to be ruled out. Self-steepening is also another phenomena that occur with ultra-short pulses (< 1 psec) and arises from the intensity dependence of group velocity. In this case, the center of the pulse (which is more intense) moves at a lower speed than the wings. Therefore as the pulse propagate through the fiber, it becomes asymmetric with its peak shifting toward the trailing edge. As a result, the trailing edge becomes steeper and steeper with increasing propagation distance and eventually this leads to the formation of an optical shock [20]. Since the pulsewidth used here is much longer than that for which self-steepening occurs, it is not expected to contribute to the above-observed deviation.

Two-photon absorption has been previously explained in Chapter 2. This effect is automatically ruled out when one considers the long wavelength of the laser used in this work. The band-gap of silica is about 8.3 eV, while the photon energy at 1064 nm is only about 2 eV.

With the exclusion of all the nonlinear effects listed above except SRS, one needs to examine the spectrum, since the Raman has a characteristic frequency shift. Bromage et *al* [163] has shown that the Raman spectrum of GeO_2 and SiO_2 sufficiently overlap in a germania doped silica fiber and exhibits a peak value at about 430 cm^{-1}. On the same scale, the peak for pure silica fiber (containing no GeO_2), is shown (Figure 6.2A) to occur at about 445 cm^{-1} [163]. This is not surprising, since in the bulk, GeO_2 and SiO_2 are known to exhibit Raman peak values at 420 cm^{-1} and 440 cm^{-1} respectively [98]. In silica fibers, the Raman gain increases with increase in germania concentration [97,163]. This is because it reduces the effective core area of the fiber thereby increasing the pump intensity in the core. Secondly it increases the Raman gain coefficient. The Raman gain coefficient of GeO_2 is about one order of magnitude higher than that of SiO_2 [168]. In a recent experiment, Torres et al [167] has obtain very high Raman conversion with only 6 meters length of high GeO_2 doped (~20 %M) silica fiber, using 120 ps pulses from mode-locked Nd:YAG laser operating at 1064 nm(82.5 MHz repetition rate). The Raman peak of SiO_2 were indistinguishable, and appeared at 1117 nm, corresponding to a shift of about 53 nm from the 1064 nm pump, as expected (see Figure 6.2B).

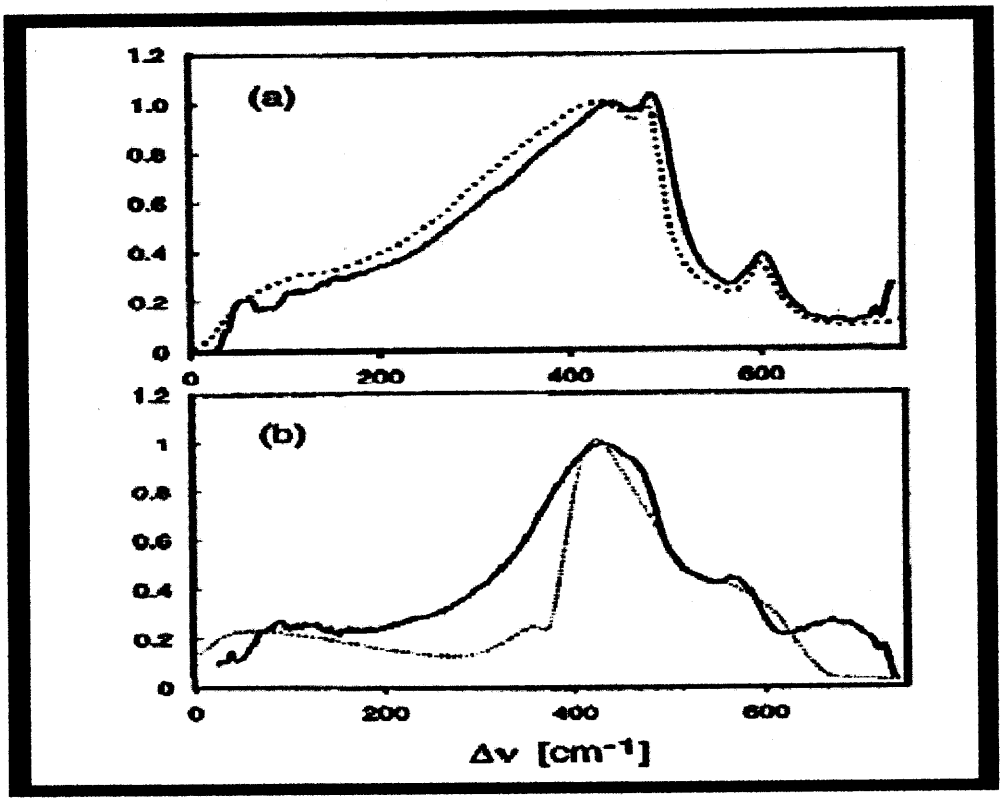

Figure 6.2A Amplitude normalized spectrum of (a) pure silica (Si-O-Si) and (b) binary (Si-O-Ge) as a function of 1455 nm pump and signal[163]
The dashed lines are measurement made on vitreous silica and germania.

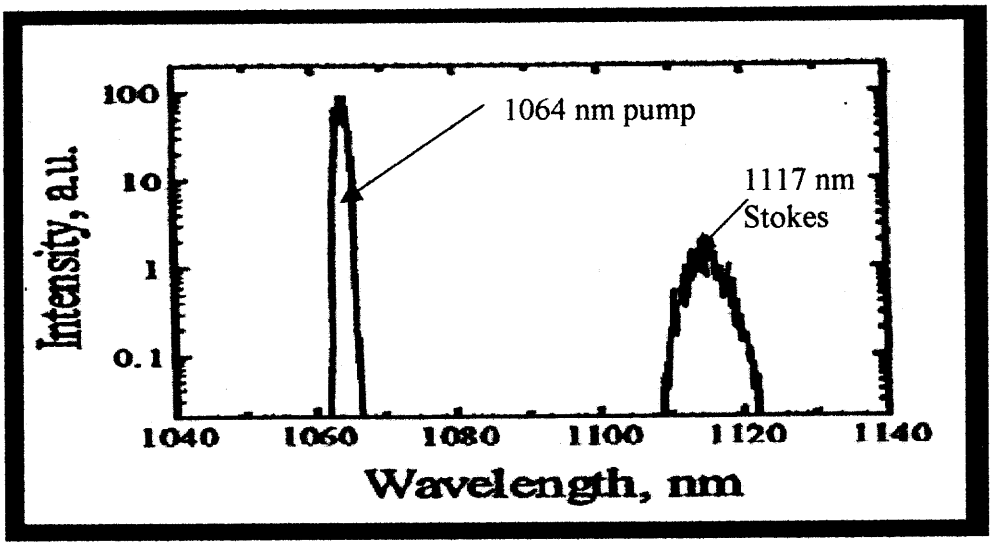

Figure 6.2B Pump and Stokes spectra at the output of a 6-m long high Ge fiber [167].

6.2.2 Measurement of the Pulse Spectrum and Further Evidence of the Role of SRS

The output spectra from different fiber samples were measured using an optical spectrum analyzer (Advantest model Q8381A) with 0.1 nm resolution and also with a McPherson (0.06 nm resolution) spectrometer (model 207). The auxiliary detection system for the spectrometer includes a Judson Technologies' J16 germanium photodiode, coupled to a lock-in amplifier. Typical measured spectra for pure silica core fiber and high germania doped fibers are shown in Figures 6.3 and 6.4. From the spectra, it was noted that the fiber with high germania content revealed a significant conversion of the pump (1064 nm) into stokes pulse (~1117 nm) while the pure silica fiber of the same length (20 m) showed no Raman peak, even at much higher peak power. In the 100 m silica fiber Raman conversion was appreciable at 48 W peak power, but even below this power, the high germania fiber has already produced well-developed second Stokes at 1174 nm. These are indicators that germania enhances stimulated Raman scattering in silica fibers and that the observed distortion on the IGA trace results from the influence of SRS on the pulse. The reduction in the core size of the GeO_2 doped fiber helps it to develop high power density in the core, which favors the SRS process. In addition GeO_2 increasing the Raman gain coefficient of the fiber [98].

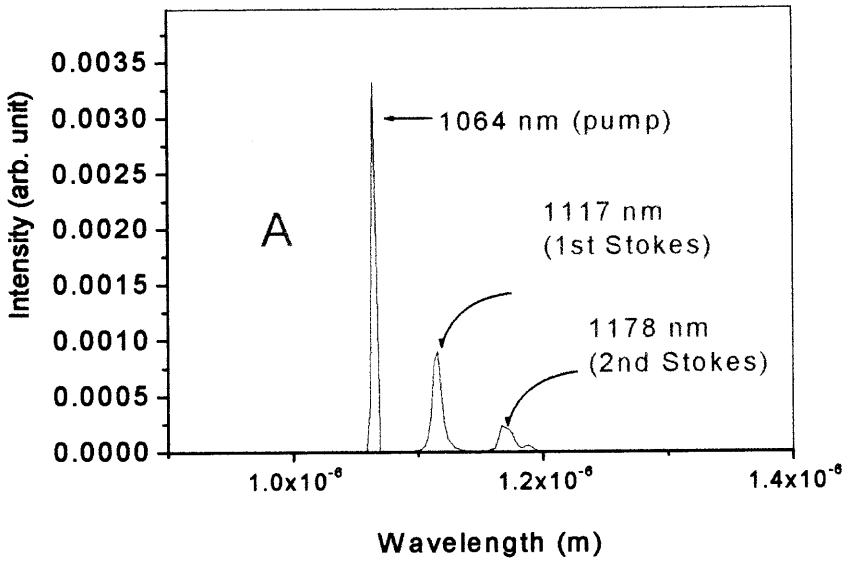

(A) Spectrum of output pulse from High Germania doped fiber (#6B) at 40 W peak power and 8.6 x 10^{12} Wm^{-2} [L~ 20 m].

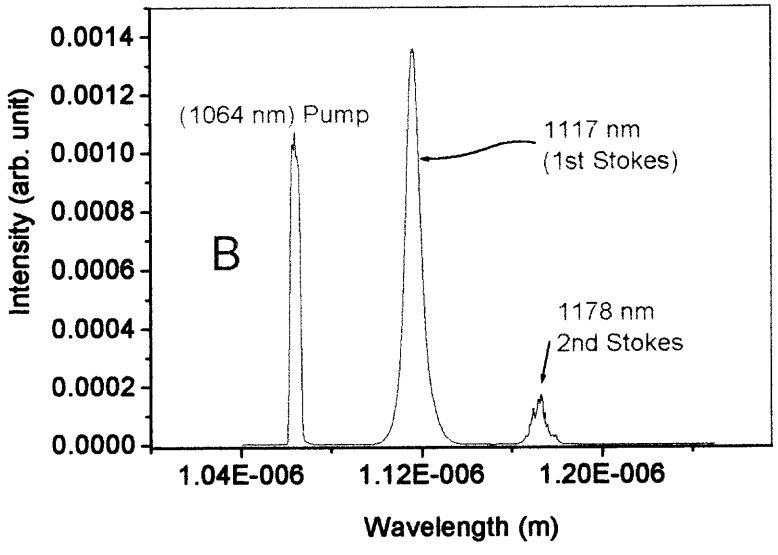

(B) Spectrum of output pulse from High Germania doped fiber (#6C) at 55 W peak power and 9.5 x 10^{12} Wm^{-2} [L~ 20 m].

Figure 6.3 Typical spectra from high GeO_2 doped fibers (fiber properties are listed in Table 6.1).

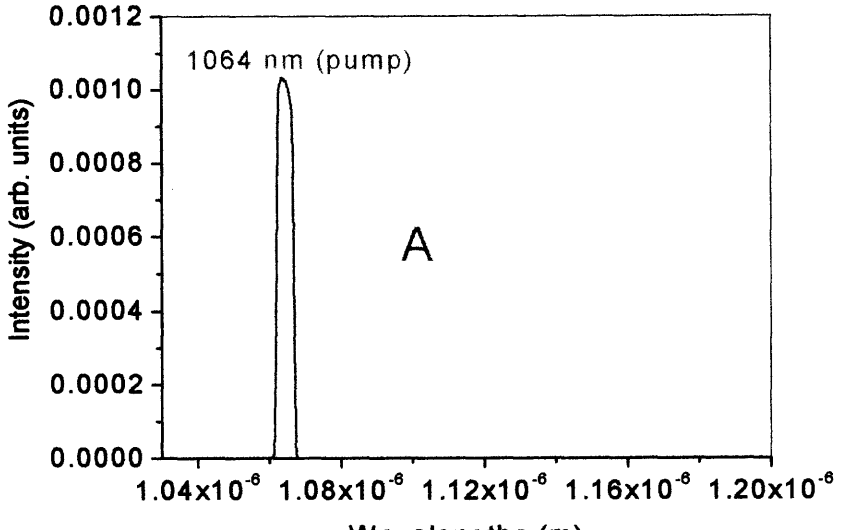

(A) Spectrum of the output pulse from 20m pure silica fiber at peak power of ~ 55 W (intensity 1.1 x 10^{12} Wm^{-2}. This is also typical of spectrum obtained with the 100 m length silica fiber at about 18 W peak power.

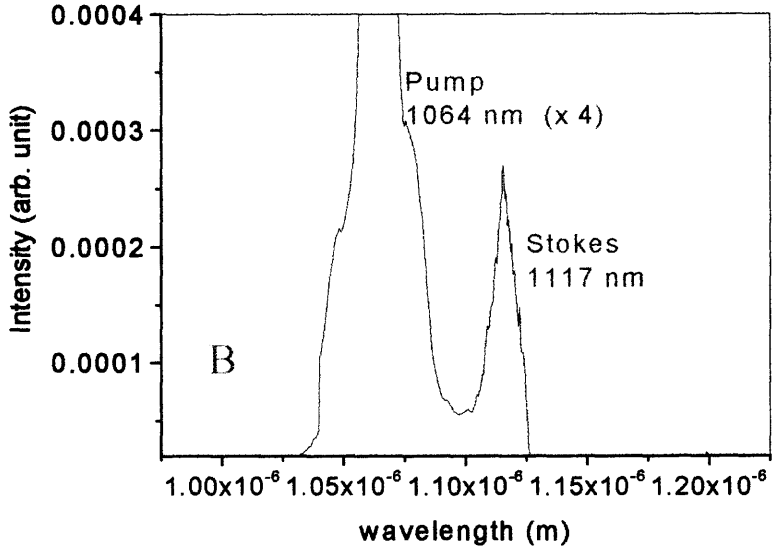

(B) Spectrum of output pulse from 100 m silica fiber [Peak power = 48 W, Intensity = 9.6 x $10^{11}Wm^{-2}$]

Figure 6.4 Spectrum of the out put pulse from pure silica fiber, containing no germania. 20 m and 100 m were examined.

6.2.3 Raman Gain Coefficient of Highly GeO_2 Doped Fibers

The Raman gain coefficient of a high germania doped silica fiber can be predicted from a knowledge of the germania concentration in the fiber. The Raman gain in a germania doped fiber is shown to depend on the relative index difference between the core and the fiber cladding [97]. The core-cladding relative refractive index is proportional to the GeO_2 contents. The Raman gain coefficient can be expressed as [98,167]

$$g_R(cm/W) = \left(\frac{0.94 \times 10^{-11}}{\lambda_p}\right)(1+80\Delta) \tag{6.1}$$

where λ_p is the pump wavelength, measured in μm, and Δ is the relative refractive index between the core and the cladding. Thus the Raman gain also scales inversely with wavelength. The above equation assumes that polarization is maintained in the fiber in the fiber. If the polarization is completely scrambled (as seen in long non-polarization preserving fibers), the Raman gain decreases by a factor of 2.

One can now estimate the Raman gain coefficient of the two high germania doped fibers listed in Table 6.1, which gave the enhanced SRS signal in the spectrum. For fiber #6B, with $\Delta n = 0.041$, $\Delta \approx 0.0275$. Taking $\lambda = 1.064$ μm, the Raman gain coefficient is calculated from Equation (6.1) to be $g_R = 2.83 \times 10^{-11}$cm/W. For the other fiber #6C, $\Delta n = 0.044$ and $\Delta \approx 0.0293$. The calculated Raman gain coefficient is $g_R = 2.98 \times 10^{-11}$ cm/W. The calculated values of g_R in these fibers suggest that the Raman gain coefficient in the two high germania doped fibers are about three times higher than the valued for pure silica - the value of g_R reported by Lin et al [96] for silica fiber is 0.92×10^{-11} cm/W. Such high values of g_R in the doped fibers are expected, since GeO_2 has high Raman gain coefficient, about an order of magnitude higher that SiO_2 [168]. In the next section,

the IGA technique will be modified and used to measure the gain coefficient in these fibers to confirm the above-predicted results.

6.3 Modification of the IGA Model and Measurement of Raman Gain Coefficient in Optical Fiber Using IGA

6.3.1 Modification of IGA Model in the Undepleted Pump Approximation Through the Analytical Solution of the Coupled Nonlinear Schrodinger Equation

One way to take into account the effect of SRS in pulse propagation in optical fibers is to solve the coupled nonlinear Schroedinger equation (NLSE), which is typically written for the pump and the Stokes pulses as simultaneous, coupled-amplitude differential equation. In the absence of SRS (when only the SPM is the sole nonlinear process in the fibers), the simple NLSE suitable for describing picosecond pulses can be written as [20]:

$$\frac{\partial A}{\partial z}+\beta_1\frac{\partial A}{\partial t}+\frac{i}{2}\beta_2\frac{\partial^2 A}{\partial t^2}+\frac{\alpha}{2}A=i\gamma|A|^2A \tag{6.2}$$

where A = A(z,t) is the envelope of the electric field, β_1 is the group velocity dispersion term ($\beta_1 = 1/v_g$; v_g is the group velocity), β_2 is the dispersion parameter{$\beta_2 = d\beta_1/d\omega$}. In the literature, D is sometimes used [22] in place of β_2 and the two are related by:

$$D = -\beta_2(2\pi c/\lambda^2) \tag{6.3}$$

where D is measured in ps/(km-nm) and β_2 is in ps^2/km, γ is the nonlinear coefficient ($\gamma = n_2\omega_0/cA_{eff}$), and α represents the fiber losses. In principle, the NLSE can be derived from the wave equation, but this derivation will be omitted. Such derivation has been treated in details elsewhere [20]. It should be noted that the NLSE is (conventionally) written for the pulse envelope. The electric field, E(z,t) of an optical pulse is related to the pulse envelope A(z,t) by the following expression [20, 105]:

$$E(z,t) = [\exp i(\omega_0 t - k_0 r)]F(x,y)A(z,t) \tag{6.4}$$

where $\exp i(\omega_0 t - k_0 r)$ is the phase term and F(x,y) represents the spatial modal distribution (which is unimportant in this case, since single mode fibers have a confined mode). Therefore, for the analysis here, one can assume that for single mode fibers, $A(z,t) \approx E(z,t)$. It is sometimes more convenient to write the Schrodinger equation with the time measured in a frame of reference moving with the pulse at group velocity v_g (this is called the retarded frame) by making the following transformation:

$$T = t - \beta_1 z = t - z/v_g \tag{6.5}$$

Equation (6.1) therefore reduces to:

$$\frac{\partial A}{\partial z} + \frac{i}{2}\beta_2 \frac{\partial^2 A}{\partial T^2} + \frac{\alpha}{2}A = i\gamma |A|^2 A \tag{6.6}$$

The SRS effect can be included by introducing the coupled amplitude NLSE to account for the propagation of the pump and Stokes pulses in the fiber.

$$\frac{\partial A_p}{\partial z} + \frac{i}{2}\beta_{2p} \frac{\partial^2 A_p}{\partial T^2} + \frac{\alpha_p}{2}A_p = i\gamma_p |A_p|^2 + (2 - f_R)|A_s|^2 A_p - \frac{g_p}{2}|A_s|^2 A_p \tag{6.7a}$$

$$\frac{\partial As}{\partial z} + \frac{i}{2}\beta_{2s} \frac{\partial^2 A_s}{\partial T^2} + \frac{\alpha_s}{2}A_s - d\frac{\partial A_s}{\partial T} = i\gamma_s |A_s|^2 + (2 - f_R)|A_p|^2 A_s + \frac{g_s}{2}|A_p|^2 A_s \tag{6.7b}$$

In the above equations, A_j (j = p or s, representing the pump and Stokes respectively) is the slowly varying amplitude of the pulse envelope; $\gamma_j = n_2\omega_j/cA_{eff}$ is the nonlinear parameter; β_{2j} is the dispersion parameter and f_R represents the fractional contribution of the delayed Raman response to the nonlinear polarization [20]. Typically, f_R is about 0.18 [20,53,173-174]. The nonlinear parameter γ_j and the Raman gain coefficient g_j for the pump and Stokes are related through the wavelengths as follow:

$$g_s \lambda_s = \lambda_p g_p \tag{6.8}$$

and

$$\gamma_s \lambda_s = \lambda_p \gamma_p \tag{6.9}$$

The walk-off parameter d is introduced to account for the group velocity mismatch between the pump and the Raman pulses ($d = 1/v_{gp} - 1/v_{gs}$). One can define a walk-off length (L_w) as the distance in which the Stokes pulse passes through one pump pulsewidth. This is effectively the distance over which the pump and the Stokes pulses overlap. This distance can be given in terms of the walk-off parameter (d) and the pump pulsewidth (τ_p) and as follow:

$$L_W = \left(\frac{|d|}{\tau_p} \right)^{-1} \tag{6.10}$$

The walk-off length depends on both the pulsewidth and the wavelength of the laser as well as the relative refractive (Δ) difference between the fiber core and the cladding. Typically, $L_w \sim 6$ m in silica fibers at 532 nm for a pump pulse of width 36 ps [30] while at 1064 nm, the author has calculated L_w to be 38 ps in silica fibers for a 50 ps pump pulse. For typically high GeO_2 doped fiber (with $\Delta \sim 0.025$), $L_w \sim 20$ m at 1064 nm for 50 ps pulses, since the $d = 2.5$ ps/m for such a fiber [167]. One can further introduce The Raman gain length (L_G) which represents the length scale over which the Raman gain becomes important. This length can also be given in terms of the pump peak power and its Raman gain coefficient g_p [actually, g_p looks like "pump depletion coefficient" since its sign in Equation (6.6) is negative] and it predicts accurately how energy is transferred to the Stokes.

$$L_G = (g_P P_0)^{-1} \tag{6.11}$$

The solution to Equation (6.6) is generally obtained by numerical procedures, but analytical solution is also possible by making some few approximations [169]. Analytical solution is advantageous because it allows one have an expression for the pulse envelope, which can be fitted directly to the experimental data. The author has used the undepleted pump approximation to obtain the analytical solution to Equation (6.6) by following the framework developed in [20] and elsewhere [169]. First, one neglects GVD ($\beta_{2p} = \beta_{2s} = 0$) and fiber loss ($\alpha_p = \alpha_s = 0$). This assumption is justified in the present circumstance due to the short lengths of fibers typically used in IGA experiments. Equation (6.6) therefore simplifies to:

$$\frac{\partial A_p}{\partial z} = i\gamma_p |A_p|^2 + (2 - f_R)|A_s|^2 A_p - \frac{g_p}{2}|A_s|^2 A_p \tag{6.12a}$$

$$\frac{\partial As}{\partial z} - d\frac{\partial A_s}{\partial T} = i\gamma_s |A_s|^2 + (2 - f_R)|A_p|^2 A_s + \frac{g_s}{2}|A_p|^2 A_s . \tag{6.12b}$$

Second, one makes further simplification by assuming that the Stokes' amplitude is small compared with the pump such that $|A_p|^2 >> |A_s|^2$ (this is the so called undepleted pump approximation). Thus all terms containing $|A_s|^2$ in Equation (6.12) can be dropped, so that we have

$$\frac{\partial A_p}{\partial z} = i\gamma_p |A_p|^2 \tag{6.13a}$$

$$\frac{\partial As}{\partial z} - d\frac{\partial A_s}{\partial T} = (2 - f_R)|A_p|^2 A_s + \frac{g_s}{2}|A_p|^2 A_s \quad . \tag{7.13b}$$

These equations have the following solutions:

$$A_p(z,T) = A_p(0,T)\exp\left[i\gamma_p |A_p(0,T)|^2 z\right] \tag{6.14a}$$

$$A_s(z,T) = A_s(0,T+zd)\exp\left\{\left[\frac{g_s}{2} + i\gamma_s(2-f_R)\right]\psi(z,T)\right\} \tag{6.14b}$$

where ψ is an overlap factor given by:

$$\psi(z,T) = \int_0^z \left|A_p(0,T+zd-z'd)\right|^2 dz' \tag{6.15}$$

The Stokes pulse changes both its shape and spectrum as it propagates. The change in shape (temporal change) results from the Raman gain, while the spectral change results from the cross-phase modulation. Because of pulse walk-off, the extent of these changes would depend on the overlap factor ψ(z,T), which takes into account the relative separation between the pump and the Raman pulses along the fiber. This overlap factor depends on the shape of the pulse [20] and thus the integral given in Equation (6.15) needs to be evaluated for a given pulse shape. For the particular case of a Gaussian pump pulse of the form used in this work:

$$A_p(0,T) = E_0 \exp\left\{-2\ln 2\left(\frac{T^2}{\tau_p^2}\right) - i(\omega t + \phi)\right\}, \tag{6.16}$$

one can evaluate the integral shown in equation (6.14) to give the following result:

$$\psi(z,T) = \frac{1}{4}P_0\sqrt{\frac{\pi}{\ln 2}}\left(\frac{z}{\delta}\right)\left[erf\left(2\sqrt{\ln 2}(\tau+\delta)\right) - erf\left(2\sqrt{\ln 2}(\tau)\right)\right] \tag{6.17}$$

where *erf* is the so called error function, P_0 is the peak power ($P_0 \approx |A(0,T)|^2$) and one has introduced the normalized time $\tau = T/\tau_p$ and normalized propagation distance $\delta = zd/\tau_p$, d being the walk-off parameter (in units of ps/m).

At this point, it of interest to examine what happens in the photorefractive crystal with the presence of the pump and the Raman pulses. In the present analysis, one

considers the interference of four beams in the photorefractive crystal in the geometry shown in below (Figure 6.5).

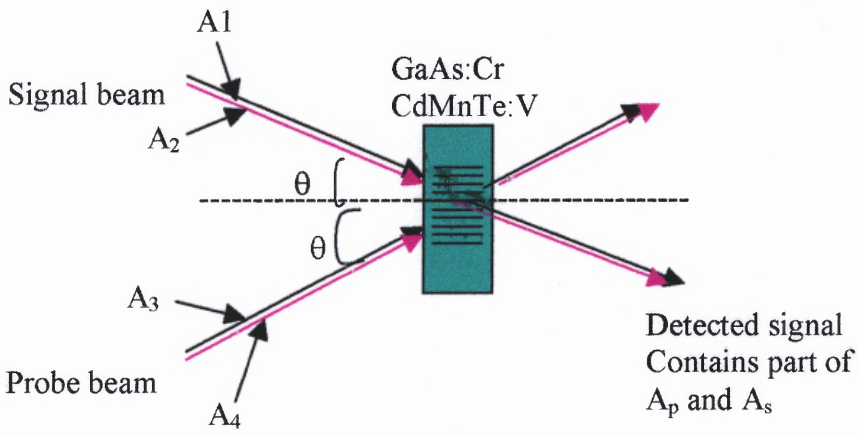

Figure 6.5 The interaction of the pump and the Stokes fields in the photorefractive crystal in the four-wave mixing configuration.

This is because each arm of the two arriving beams contains the pump (1064 nm) and the Stokes (1117 nm) pulses. If one designates the amplitudes of the pump and Stokes parts of the signal beam by A_1 and A_2 respectively, while the pump and Raman part of the probe beam are designated A_3 and A_4. The above configuration is similar to four-wave mixing and can be analyzed within that context. The general problem of four-wave mixing in photorefractive crystal is very complicated because the material response consists of four distinct gratings, namely, one grating due to the interference of beams 1 & 2 with 3 & 4, one grating due to the interference of beams 1 & 3 with 2 & 4, one grating due to the interference of beam 1 with beam 3 and one grating formed from the interference of beam 2 with beam 4. If the phase matching conditions are satisfied:

$$\omega_1 = \omega_3, \quad \omega_2 = \omega_4, \quad \mathbf{k}_2 - \mathbf{k}_1 = \mathbf{k}_4 - \mathbf{k}_3 \tag{6.18}$$

then the problem can be simplified by assuming that of all the gratings present in the system, only one grating (in our case the one created by the interference of beams 1 &2 with 3 &4) gives rise to strong beam coupling. This predominance of one grating is common in many practical situations and is due to the direction, polarization, and coherent relationships of the four beams relative to the photorefractive crystal [170]. If one further assumes that the rise time of the grating is fast compared with the pulse length and that the decay time of the grating is long compared with the pulse length and all delays between pulses in the experiment, then it can be shown that the detected IGA signal can be given by the following expression:

$$W_{\text{det}} \approx \left|\int_{-\infty}^{\infty} A_p(t')A_p^*(t'+\tau)dt'\right|^2 + \left|\int_{-\infty}^{\infty} A_s(t')A_s^*(t'+\tau)dt'\right|^2$$
$$+ \left|\int_{-\infty}^{\infty} A_p(t')A_s^*(t'+\tau)dt'\right|^2 + \left|\int_{-\infty}^{\infty} A_s(t')A_p^*(t'+\tau)dt'\right|^2 \qquad (6.19)$$

where τ is the delay in units of pulse length and A_p and A_s are the pump and Raman pulses. The first term in this expression is just the contribution from pure SPM while the rest of the terms are contributions from the SRS effects through the Raman gain and cross-phase modulation. The above equation is then numerically integrated and the resulting trace fitted to the experimental data. In doing so, Equations (6.14a) and (6.14b) together with Equation (6.17) are substituted and the fitting parameters are factored from the values in the exponents of these equations. These parameters are for convenience identified in dimensionless quantities and represented by:

(a) The self-phase modulation parameter (SPMP) given by:

$$SPMP = \gamma_p^1 z\left|A_p(0,T)\right|^2 \qquad (6.20)$$

where $\gamma'_p = 2\pi n_2/(A_{eff}\lambda_p)$ and $|A(0,T)|^2 \cong P_{peak}$ (ie peak power) and z is the fiber length and the rest have their usual meanings as earlier defined in the text.

(b) The Raman gain parameter (RGP) given by:

$$RGP = g' z|A_p(0,T)|^2 \tag{6.21}$$

where $g' = g_R/A_{eff}$ and g_R is the Raman gain coefficient of the fiber.

(c.) The walk-off term (*WOT*) given by:

$$WOT \equiv \delta = \frac{zd}{\tau_p} \tag{6.22}$$

where d is the walk-off parameter and τ_p is the laser pulsewidth. The first parameter (SPMP) is usually supplied exactly, or guessed approximately from the self-phase modulation strength (SPMS)of an equivalent undistorted IGA trace. The last two parameters are randomly supplied and the fitting routine returns the appropriate values upon convergence. Typically fitted traces using Equation (6.19) are shown in Figure (6.7).

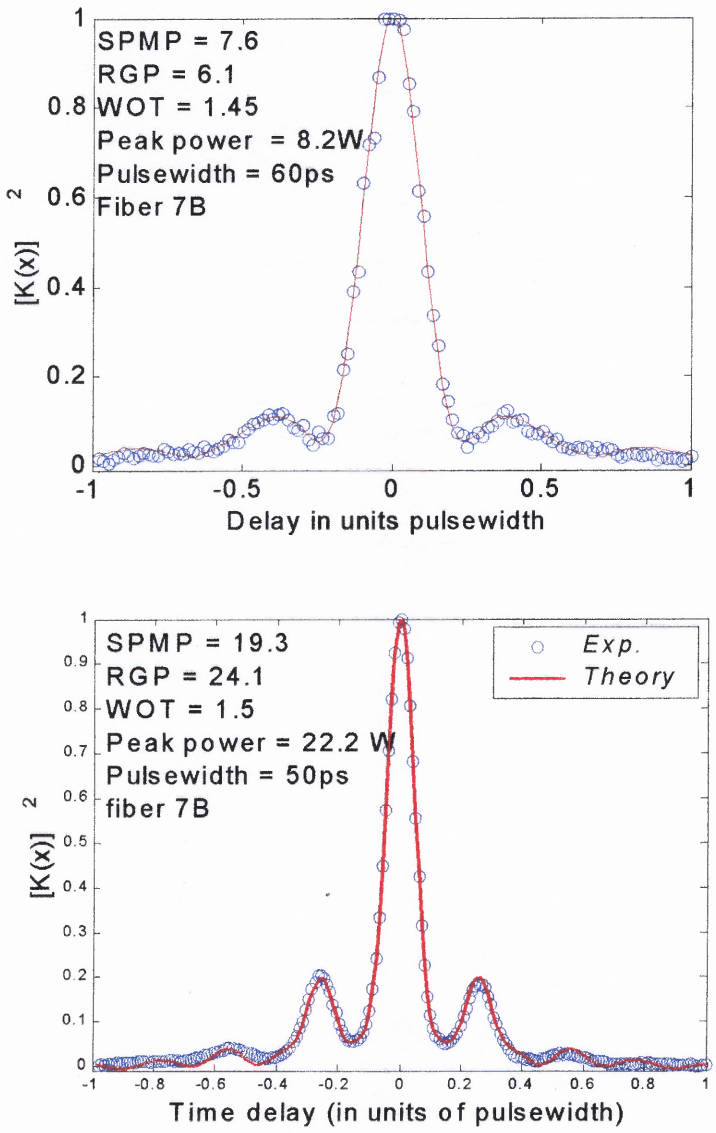

Figure 6.6 Measured IGA traces fitted to the modified IGA model that accounts for SPM and SRS, for fiber 6B with >28% M Ge and 2%M Al.
(fiber length = 20 m, Peak power ~ 9W & 22W respectively, Raman < 25%).

There is excellent agreement between theory and experiment, especially in the region where the Raman conversion is less than 25%. At increased Raman conversion, the distortion is severe and the fit deteriorates (Figure 6.7). This is expected, since the assumption of undepleted pump was made in arriving at the solution. In the expression of Equation (6.21), all the parameters except g_R are usually known from the experiment. Thus, in the region where the fit is good, one may use this to estimate the Raman gain coefficient of the fiber. This will be examined in the next section of this chapter.

Meanwhile, one can now understand the reason for the lifting and depletion of the IGA sidelobes. The SRS gives rise to two different frequency components, which make their way into the photorefractive crystal. The presence of the two frequencies affects the stability of the photorefractive gratings, since interference of difference frequencies usually leads to a moving interference fringes and dynamic grating [171]. A moving grating usually does not support the formation of sidelobes in IGA. At low Raman conversion, the gratings are partially stable since the Stokes pulses are very weak compared to the pump, and few lobes still get formed. As the strength of the Stokes pulses increase, the potential to transform into moving grating intensifies, and lobes deplete. At sufficiently high enough Raman conversion, the contribution of the Stokes in the interference process becomes sufficient to upset the "semi-stable" interference pattern and the grating becomes completely dynamic. At this stage the IGA sidelobes are expected to be completely washed out. In fact, close to this has been experimentally observed in this work (see Figure 6.8).

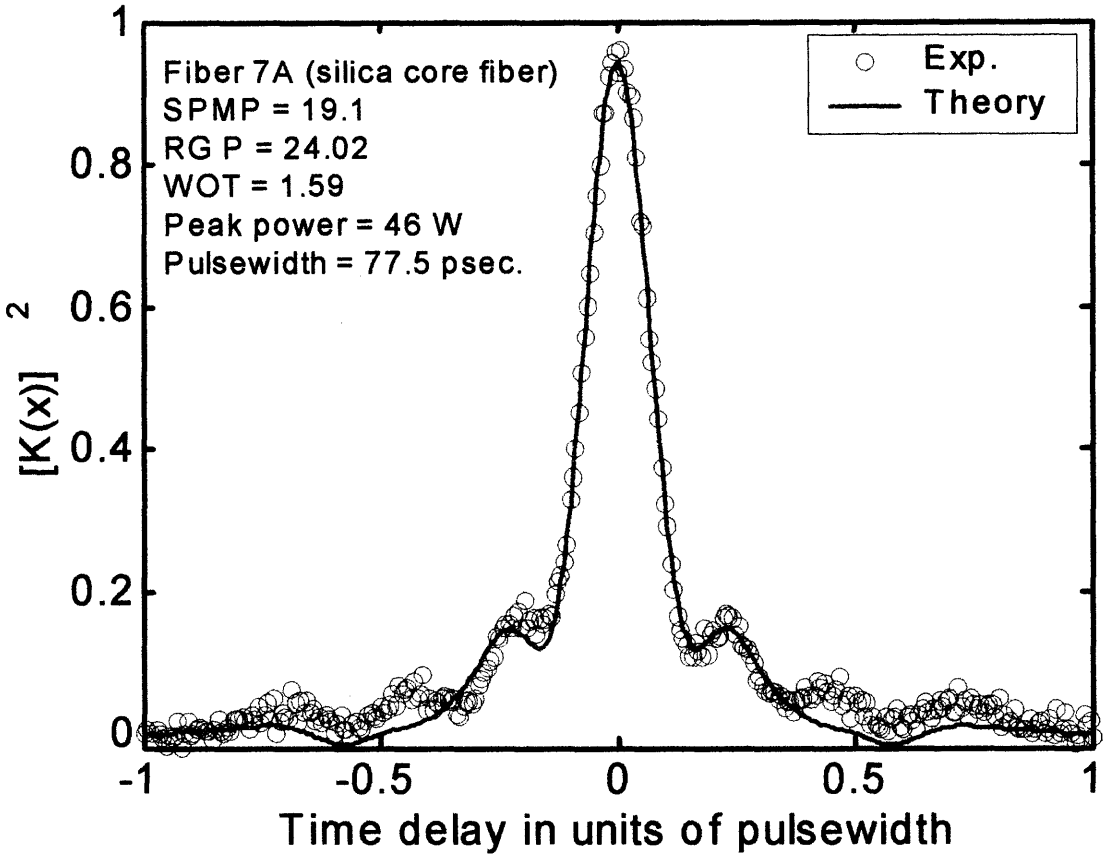

Figure 6.7 Measured IGA trace at about 30 % Raman conversion indicating the breakdown of the undepleted pump IGA model. Fiber length 100 m. (silica core), Peak power = 46 W. The same effect was observed in high Ge doped fiber #7C at peak power of < 36 W.

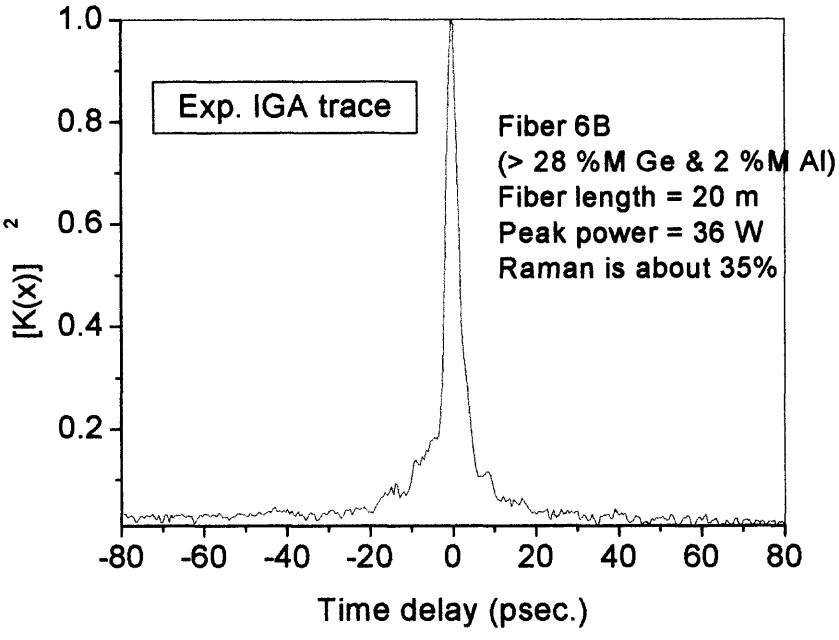

Figure 6.8 IGA trace at high Raman conversion in high Germania doped fibers 7B (fiber length = 20 m, P_{peak} ~ 36W). Similar observation was made in 100m long silica core fiber at P_{peak} ~ 48 W.

6.3.2 Determination of the Raman Gain Coefficient from IGA Data

One of the fitting parameters shown in Equation (6.20) contains the Raman gain coefficient. The rest of the quantities lumped together in the dimensionless fitting parameter are usually known from the experimental apparatus, except the Raman gain coefficient. One can therefore estimate Raman gain coefficient (g_R) this. Writing the g_R, in terms of the other quantities, one obtains:

$$g_R = \frac{RGP}{z|A(0,T)|^2} A_{eff} \tag{6.22}$$

Recognizing that the quantity $|A(0.T)|^2$ is just the peak power while z is the propagation distance in the fiber, which is the same as the effective length (L_{eff}). This equation can then be written as:

$$g_R = \frac{RGP}{P_{peak} L_{eff}} A_{eff} \tag{6.23}$$

where A_{eff} is the effective core area of the fiber. The fitting routine returns RGP, and with the knowledge of the laser parameters, the peak power can be calculated from the average power. Thus g_R can be calculated. It is recommended (for improving the accuracy) to take several IGA traces of the same fiber (with the same length) and plot the resulting RGP versus the peak power. The slope can then be used to estimate g_R. In such a case

$$g_R = \left(\frac{A_{eff}}{L_{eff}} \right) \times slope \tag{6.24}$$

It is also possible to estimate the walk-off parameter *d* from the fit using Equation (6.21).

As an initial test, the author has used this technique to determine the g_R and *d* in four different fibers, including two well-characterized fibers. Fiber properties are listed in Table 6.1. Typical IGA traces from some of the measured fibers are shown in Figures 6.6 through 6.11. The measured g_R and *d* values as determined from the fit are shown in Table 6.2

Table 6.1 Properties of the Fibers whose Raman Gain Coefficients were Measured (Calculated Values Were obtained using Equation 6.1)

Fiber # and Type	Length (m)	Dopants and their concentration	MFD* (μm)	A_{eff}* $(\mu m)^2$	Δn
6A Pure silica core	100	None	8.21	50	0.005
6B Er-Al-Ge doped	20	Er ~ 2.5 x $10^{24}m^{-3}$ Al ~ 2%M GeO_2 > 28 %M	2.42	4.64	0.041
6C GeO_2 doped	20	GeO_2 ~ 29 % M	2.8	5.82	0.044
6D DCF	20	GeO_2 Unknown	3.43	10.44	Not given

**The MFD and A_{eff} were extrapolated from 1.314 μm, 1.450 μm and 1.552 μm (see Appendix D)*

Table 6.2 Raman Gain Coefficients and Walk-off Parameter Determined from IGA Measurements in Four Different Fibers (the Calculated Values are Obtained Using Equation 6.1)

Fiber # and Type	Measured with IGA (λ_p= 1064 nm) g_R (cm/W)	Calculation (λ=1064 nm) g_R (cm/W)	Accepted Value g_R (cm/W)	*d* (ps/m)
6A Pure silica core	6.13 x10^{-12}	-	**9.2 x 10^{-12}** Lin et al 1977 [96]	1.1
6B Er-Al-Ge doped	2.56 x10^{-11}	**2.83 x10^{-11}**		4.3
6C GeO_2 doped	2.77 x 10^{-11}	**2.98 x 10^{-11}**		4.5
6D DCF	11.85 x 10^{-12}	-	**11.41 x 10^{-12}** Bromage 2003 [157]	5.5

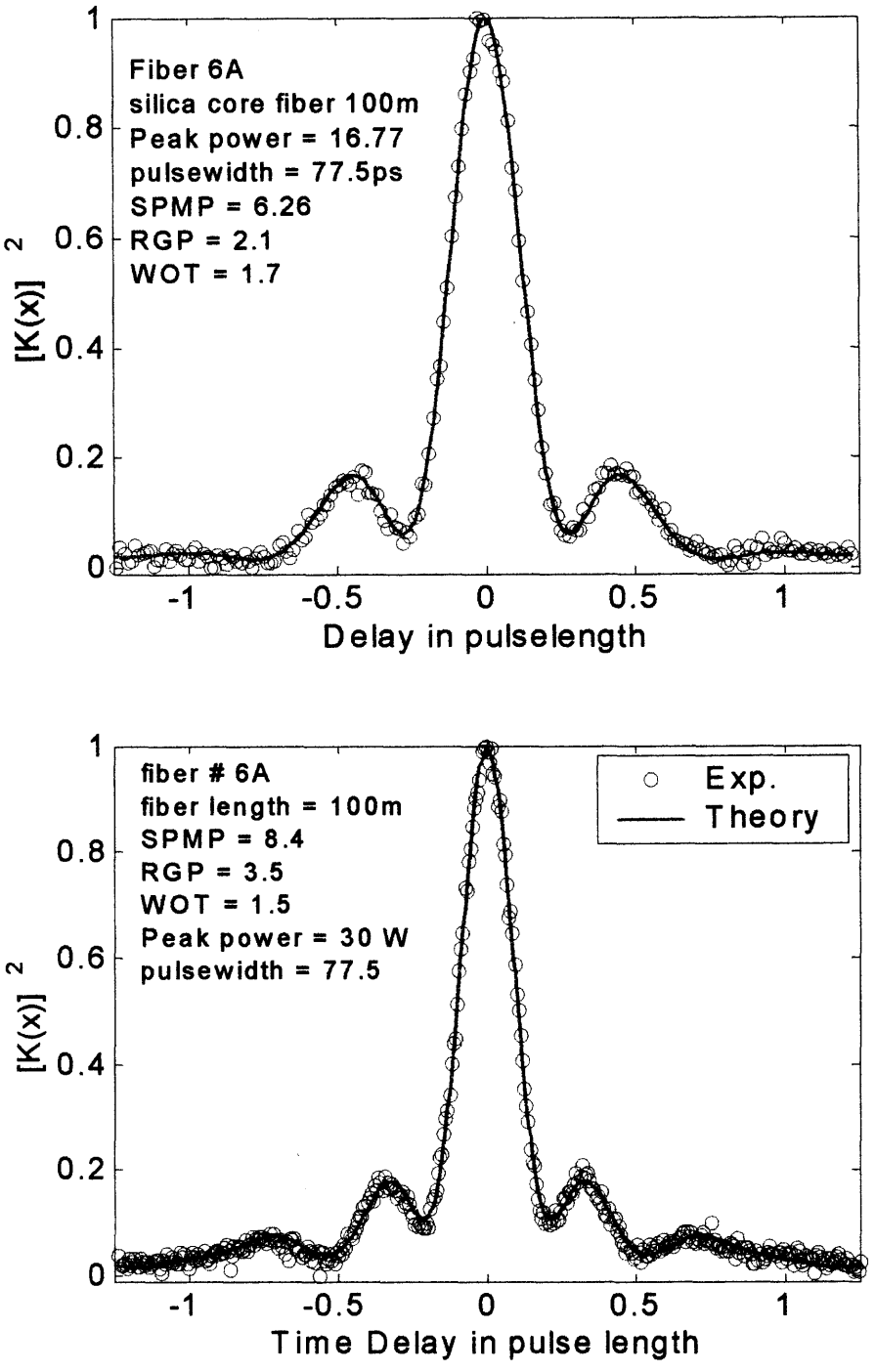

Figure 6.9 Measured IGA traces fitted to the model for 100 m long pure silica core fiber at different power levels.

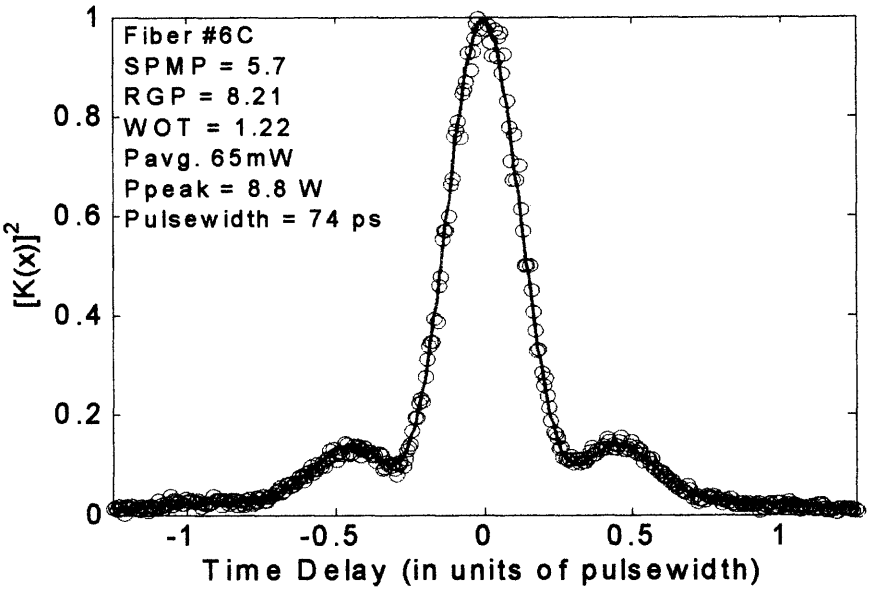

Figure 6.10 Typical IGA trace measured in GeO_2 doped fiber, #6C (Fiber length = 20m, P_{peak} = 8.8W).

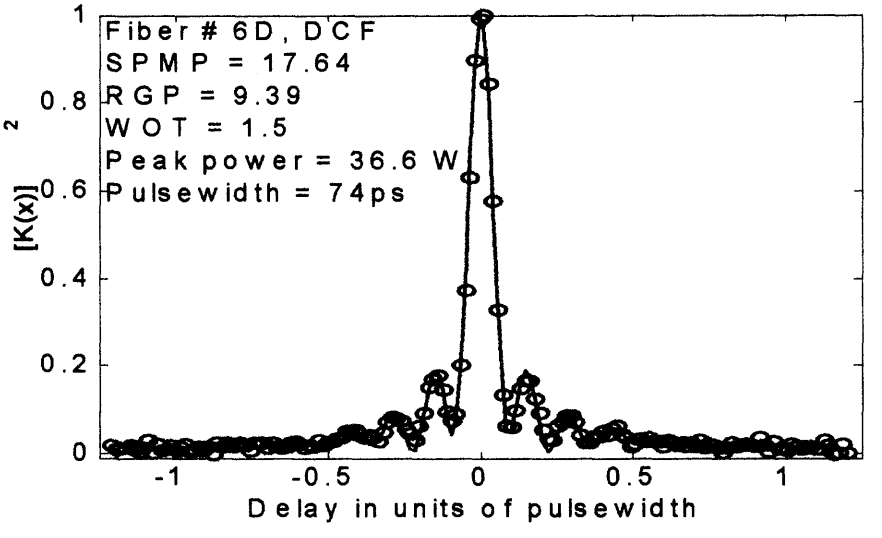

Figure 6.11 Typical IGA trace measured in DCF, #6D (Fiber length = 20m, P_{peak} = .36.6W).

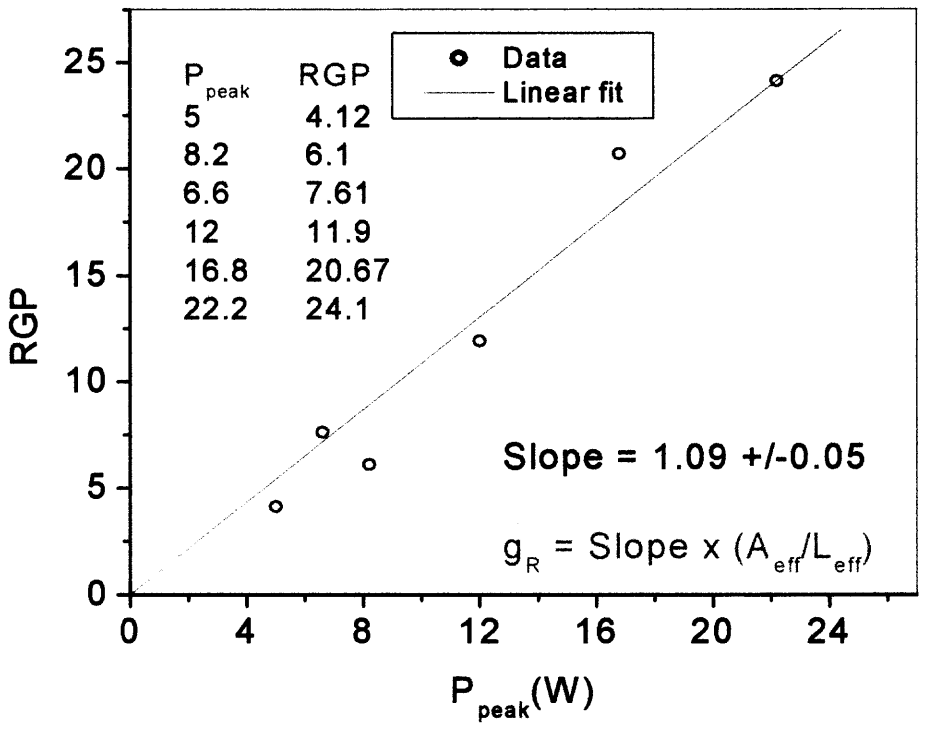

Figure 6.12 Plot of the "Raman gain parameter" (RGP) versus peak power for fiber #6B for estimating g_R (g_R is proportional to the slope) Typical IGA traces for this fiber are shown in Figure 6.6).

6.3.3 Comparison with Published Results

It will be useful at this point to compare the results obtained here with reported values [50,96,157,158,163,167]. In doing this it should be noted that some of these measurements and estimates reported in the literature have been done with different ranges of wavelength. Raman gain coefficient scales inversely with wavelength. For a meaningful comparison, one must scale values measured at other wavelength to 1064 nm, used in this measurement. The scaling equations have been derived by Newbury [160,161] and by Cordina and Fludger [162]. In frequency terms, this equation can be written as [161]

$$g^{+}(\omega_p, \Delta\omega) = (\frac{\omega_p}{\omega_{p0}})^k g^{+}(\omega_{p0}, \Delta\omega), (\ \Delta\omega > 0) \tag{6.25}$$

where g^+ is the Raman gain, and the plus sign indicates gain on the Stokes side. ω_p is the pump wavelength, $\Delta\omega = \omega_p - \omega_s$ is the frequency difference between the pump frequency and the signal (Stokes) frequency ω_s. The exponent k describes the power law scaling of the Raman gain with pump wavelength and ω_{p0} is an arbitrary chosen reference pump frequency. This factor k generally ranges from 2 to 4, and have been determined for a host of fibers [161]. Typical values are 2.3 for SMF-28, and 4.2 for LEAF (large effective area fiber).

In terms of pump and Stokes wavelengths, a similar equation can be written [162]

$$C_R(\lambda, \lambda_s) = \left(\frac{\lambda_p}{\lambda}\right)^{\varepsilon} C_R(\lambda_p, \lambda_s) \tag{6.26}$$

where C_R is the Raman gain efficiency coefficient of the fiber as a function of the signal wavelength λ_s, λ is the new pump wavelength. λ_p is the pump wavelength at which the measurement was taken and ε is the scaling coefficient. Therefore, once C_R is known at a given wavelength, its value at any wavelength can be determined from Equation (6.26). Values of the scaling coefficient ε typically range from 2-5 [162]. Its value for "All wave" fiber (silica core) is 2.8 [162] and this can be used for SM-28, since they have similar properties. The Raman gain efficiency C_R in units of $(Wm)^{-1}$ may be approximately related to the Raman gain coefficient in units of m/W by multiplying C_R by the effective area of the fiber . Table 6.3 shows some reported Raman gain coefficient, which are compared with the measurement done with this technique.

Table 6.3 Comparison of the Raman Gain Coefficient Measured in this Work with Publishedvalues. Scaled Values at 1064 nm were Deduced from the Original Wavelength of Measurement Using Equation (6.26)

Source and Fiber Type	Measured values and wavelength	Scaled value at λ = 1064 nm using Equation (6.26) (cm/W)	Predicted value using (Equation 6.1) (cm/W)
Silica core [Ref. 96]	9.2×10^{-12} cm/ W (@ 1064 nm)	**9.2×10^{-12}**	
[Ref. 50] Silica core	1.5×10^{-11} cm/W @526 nm	**2.1×10^{-12}**	
[Ref 159] Silica core	3.1×10^{-12} cm/W @1550 nm	**8.68×10^{-12}**	
Silica core [158]	1.2×10^{-11} cm/W @795.5 nm	**5.32×10^{-12}**	
Silica core [157,163]	0.39 $(W\text{-}m)^{-1}$ @ 1450 nm	**7.52×10^{-12}**	
DCF [157,163]	3.2 $(W\text{-}km)^{-1}$ @1450 nm	**11.41×10^{-12}**	
IGA DCF	11.85×10^{-12} cm/W @1064 nm	**11.85×10^{-12}**	
IGA Silica core	6.13×10^{-12} cm/W @1064 nm	**6.13×10^{-12}**	
IGA Er-Al-Ge 28% M GeO_2	2.56×10^{-11} cm/W @ 1064 nm	2.52×10^{-11}	2.83×10^{-11}
IGA 30 % M GeO_2	2.77×10^{-11} cm/W @1064 nm	2.61×10^{-11}	2.98×10^{-11}

As seen from the table, reported values of the Raman gain coefficient vary widely. The variation is due some differences in the fibers, Fibers supplied by different manufactures may have some slight differences in the composition and on the wave-guide structure. Another reason for this variation is polarization effect. The Raman gain coefficient depends on the state of polarization of the pump and the Stokes (signal) and also on the polarization property of the fiber. The value of g_R is higher if pump and Stokes have the same polarization state, and if polarization is maintained in the fiber. If polarization is completely scrambled as is the case in long non-polarization preserving fibers, the value of g_R can fall as low as half its actual value in polarization maintaining fiber.

The highest reported g_R is in pure silica in the table is 9.2×10^{-12} cm/W [96] while the least value is 2.1×10^{-12} cm/W. The value obtained with the IGA technique is 6.13×10^{-12} cm/W, which is within the accepted range. An interesting comparison is the measurement made on the same fiber that has been previously characterized. The accepted value [163] of the Raman gain efficiency of 3.2 $(W\text{-}km)^{-1}$ at 1450 nm, which corresponds to $g_R = 11.41 \times 10^{-12}$ cm/W at 1064 nm was measured in the same DCF used in this work. The value obtained from this work for this fiber is 11.85×10^{-12} cm/W. This is in agreement within 4% of the accepted value. The main source of uncertainties in the measurement with this technique is the effective area. The effective area used in the calculations was obtained from interpolation (see Appendix D) from measurements done at other wavelengths (1552 nm. 1459 nm and 1314 nm). Another possible source of error is the laser amplitude fluctuations, which is translated into fluctuations in the average power. The amplitude fluctuation of the Nd:YAG laser used is between 2 - 4%. However, this power fluctuation was minimized by averaging.

For the high germania doped fibers, the calculations using Equation (6.1) predicts that the Raman gain coefficients for the two fibers #6B and #6C should be 2.83 x 10^{-11} cm/W and 2.98 x 10^{-11} cm/W respectively, based on the known germania contents. The IGA technique yielded 2.56 x 10^{-11} cm/W and 2.77 x 10^{-11} cm/W respectively. These are in close agreement with the prediction within 8%. The slight difference arises from experimental uncertainties mentioned above, and perhaps also from polarization effect. The IGA analysis assumed that polarization is maintained in the fiber, which is a reasonable assumption considering the short fiber length used, but this may not generally hold in practice.

6.4 Numerical Modeling of IGA in the Presence of Pump Depletion

One limitation of the analytical solution with the undepleted pump approximation is its failure to predict the IGA traces when the Stokes pulse becomes comparable in strength to the pump (see Figures 6.7 and 6.8). To have an insight into the behavior of the IGA signal in this regime, one has to solve Equation (6.6) numerically.

In solving these equations, fiber loss and dispersion have been neglected but all other terms were retained, so that the appropriate equation now becomes:

$$\frac{\partial A_p}{\partial z} = i\gamma_p |A_p|^2 + (2 - f_R)|A_s|^2 A_p - \frac{g_p}{2}|A_s|^2 A_p \tag{6.24a}$$

$$\frac{\partial As}{\partial z} - d\frac{\partial A_s}{\partial T} = i\gamma_s |A_s|^2 + (2 - f_R)|A_p|^2 A_s + \frac{g_s}{2}|A_p|^2 A_s \tag{6.24b}$$

where the parameters have their usual meanings as earlier defined.

This equation has been solved numerically, using the split step Fourier algorithm [20], and used to simulate the IGA trace of the output pulse. In the simulation, the Raman gain coefficient of pure silica is assumed (9.2 x 10^{-12} cm/W). It is then used as a base value to calculate the Raman gain for a given input power, fiber properties and the SPM strength, with reference to an undistorted IGA trace.. The input power and the Raman gain are then varied until the resulting IGA trace becomes identical to the observed experimental trace. The Raman gain folds at this point are then used to deduce the gain coefficient of the fiber in relative term. Raman gain coefficient five times higher than the gain coefficient for silica fiber was estimated for the high germanium doped fibers.. Typical simulated IGA traces are shown in Figures 6.13 and 6.14. The simulated traces are in qualitative agreement with the experimental observation. By dropping the

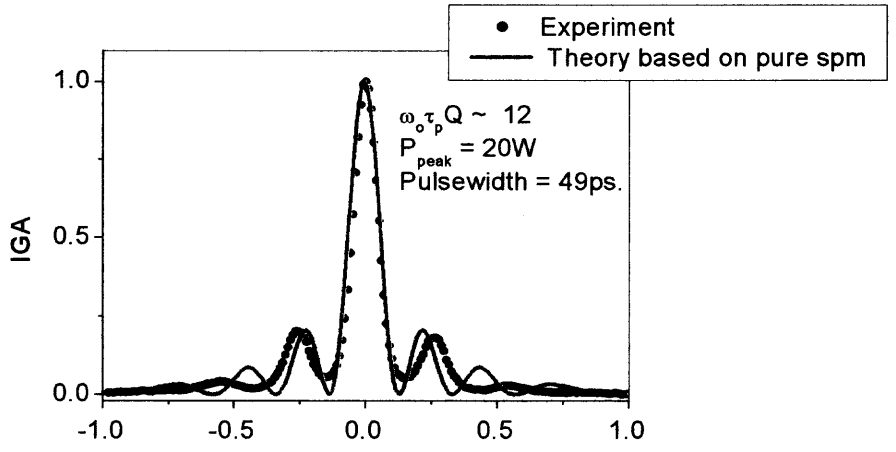

(a) Experimental IGA trace for fiber with 28%M of germania fitted to the pure SPM model. Notice the lifting of the base region of the central peak and gradual depletion of oscillations.

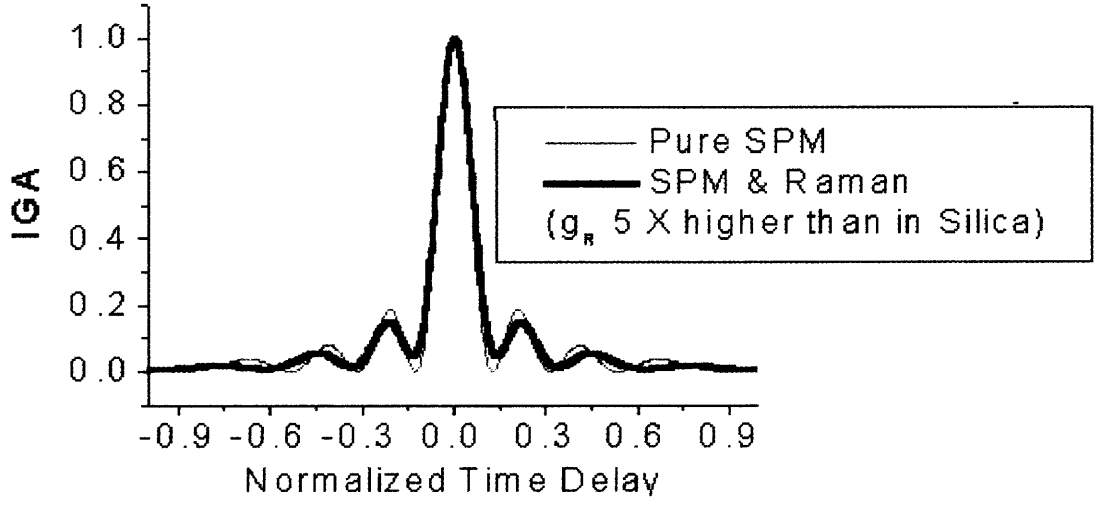

(b) Numerically simulated IGA trace that accounts for SPM and SRS (blue) merged with an IGA trace based on pure SPM model (red). Notice that the numerical trace (blue) clearly shows a lifting of the base region of the central peak and gradual depletion of oscillations, in agreement with experimental trace shown in (a).

Figure 6.13 Comparison of numerically simulated IGA trace with experimental result. The numerical simulated trace exhibits similar structures with the experimental trace, thus indicating that SRS is responsible for the deviation from pure SPM model

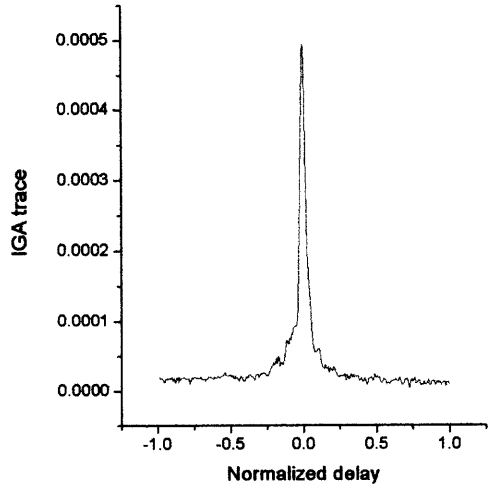

(a) experimental IGA trace for Er-Al-Ge doped fibers with 28% germania (at peak power 36 W)

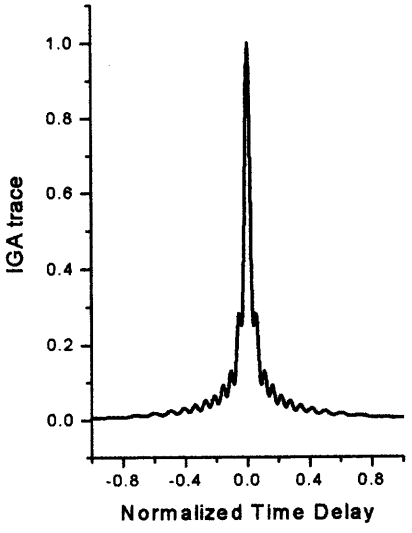

(b) Simulation based on the numerical solution of NSE taking into account SPM and SRS'

Figure 6.14 Experimental (a) and Numerically Simulated(b) IGA traces at high Raman conversion > 35%.

6.5 Discussion of the Result of the Numerical Simulation

It should be mentioned that the aim of the numerical solution is not to provide a direct fitting process with the experimental data, rather, it is to stimulate IGA traces with known input parameters whose shapes are then compared with the experimental IGA trace to establish a qualitative agreement with the observed trend. Such numerical simulation method has been used by Weiner et *al* [172] to study the influence of stimulated Raman scattering on optical pulse compression and by Genty et *al* [175] to investigate spectral modulation due to pulse reshaping in photonic crystal fibers. In all of the above cases, important parameters concerning the experiments have been deduced by comparing the simulated spectra with the experimental data without necessarily performing a fit.

The numerical simulation predicted Raman gain coefficient five times higher than in pure silica for the highly doped germania fibers. If the value of g_R for pure silica fiber is take as 9.2×10^{-12} cm/W, the actual value for g_R predicted is 4.6×10^{-11} cm/W. This is about 35% higher than the value obtained from calculations (2.98×10^{-11} cm/W), using the refractive index difference in one of the highly germania doped fibers and about 40% higher than the measured value of 2.77×10^{-11} cm/W. This increase in the result obtained from the numerical approach may be associated with the condition of pump depletion assumed in the numerical simulations. The inclusion of pump depletion increases the contribution of cross-phase between the pump and the Stokes. This implies increased nonlinear interaction, including the Raman gain. It is therefore not too surprising that the simulation over estimates the Raman gain coefficient. Added to this is the fact that linear polarization of the optical field was assumed to be maintained in the simulation, which may not necessarily be the case in the actual experiment.

One advantage of the numerical approach in this analysis is that it can be used to solve the NLSE and simulate IGA traces when both pump depletion and walk-off effect are both taken into account – a situation that does not lend itself to analytical solution. The Numerical simulation predicts IGA trace even at very high Raman conversion, including in the region where IGA sidelobes get completely washed out as seen in Figure 6.14.

CHAPTER 7

DETERMINATION OF THE SENSITIVITY OF IGA MEASUREMENTS, AND THE RELATIONSHIP BETWEEN IGA TECHNIQUE AND THE SPECTRAL DOMAIN SPM TECHNIQUE

7.1 Introduction

The level of acceptance of any new experimental technique depends on how well its performance and the interpretation of its data relate to other known techniques in the field. Among all the n_2 measurement techniques (see Chapter 3), the spectral domain SPM technique pioneered by Stolen and Lin [13,62], is the most widely used method for measuring the n_2 in optical fibers, and it has a well-established measurement accuracy. The relation between this technique and IGA will be discussed in Section 7.2. A mathematical formulation is derived to establish the link between the two techniques, and it is shown that one can in certain cases predict the results of the spectral domain SPM technique from IGA measurements.

The sensitivity of the IGA, defined by the least detectable phase shift has also been determined and the result is presented in Section 7.3.

7.2 Derivation of the Relationship Between IGA and the Spectral Domain SPM Technique

It is known that SPM causes pulse broadening in the spectral domain that leads to a periodic structure in the power spectrum of the broadened pulse [13,20,176-177]. It was shown by the stationary phase method [176] that the maximum nonlinear phase shift of a modulated pulse can be written as:

$$\gamma \delta n_p = \pi(2m-1) \tag{7.1a}$$

where m is the total number of minima of the spectrum at the Stokes side. The quantity $\gamma\delta n_p$ represents the peak (maximum) nonlinear phase shift, $\gamma = \omega_0 z/c$, and δn_p is the nonlinear refractive index change induce by the field, ω_0 is the laser angular frequency, where the subscript p implies the peak value. The above equation can be written as [179]:

$$\phi_m = \pi(2m-1) \tag{7.1b}$$

where ϕ_m is the maximum phase shift ($\phi_m \equiv \gamma\delta n_p$), m is the number of minima that appear on either the Stokes side or the anti-Stokes side of the power spectrum [2]. The corresponding maximum frequency shift, disregarding variation in amplitude should occur at the inflection point of the phase profile and it is obtained from the time-derivative of the phase. If the inflection point occurs at a time t_i, for a fixed point in space then the maximum frequency shift can be written as [179]:

$$f_m = \frac{1}{2}\frac{d\phi(t)}{dt}\bigg|_{t=t_i} \tag{7.2}$$

where $\phi(t)$ is the time-dependent nonlinear phase shift profile of the pulse.

Now, assuming a Gaussian phase shape of the form:

$$\phi(t) = \phi_m \exp[-4\ln 2\left(\frac{t}{\tau_p}\right)^2] \tag{7.3}$$

where τ_p is the pulsewidth.

$$f_m = \frac{1}{2}\frac{d\phi(t)}{dt}\bigg|_{t=t_i} = \frac{1}{2\pi}\left[\frac{-5.6}{\tau_p^2} t_i \phi(t_i)\right] \tag{7.4}$$

At the point of inflection, $\frac{d^2\phi(t)}{dt^2}\bigg|_{t=t_i}$ must necessarily vanish.

$$\left.\frac{d^2\phi(t)}{dt^2}\right|_{t=t_i} = \frac{1}{2\pi}\frac{d}{dt}\left[\frac{5.6}{\tau_p^2}t_i\phi(t_i)\right]_{t=t_i} = 0 \tag{7.5}$$

Solving, one obtains

$$t_i = \frac{\tau_p}{\sqrt{5.6}} \tag{7.6}$$

But at $t = t_i$,

$$\phi(t_i) = \phi_m e^{-4\ln 2\left(\frac{t_i}{\tau_p}\right)^2} = \phi_m e^{-(2.8)\frac{(\frac{\tau_p}{\sqrt{5.6}})^2}{\tau_p^2}} \tag{7.7}$$

Evaluation of the above expression yields

$$\phi(t_i) = \phi_m e^{-(\frac{1}{2})} = \frac{\phi_m}{\sqrt{e}} \tag{7.8}$$

Equations (7.1b), (7.6) and (7.8) can be substituted into equation (7.4) to obtain the following result:

$$f_m = \frac{1.18(2m-1)}{\tau_p\sqrt{e}} \tag{7.9}$$

where f_m is the frequency bandwidth of the spectrum.

In the Stolen's spectral domain SPM technique [13,52,62] the total spectrum is counted (Stokes and anti-Stokes sides) and the result must be divided by two. His expression for the maximum phase shift measured is therefore given by [52]

$$\Delta\phi_m = \frac{\pi}{2}(2m-1) \tag{7.10}$$

One can combine equations (7.9) and (7.10) to obtain

$$f_m = 1.18\left(\frac{2\Delta\phi_m}{\pi\tau_p\sqrt{e}}\right) \tag{7.11}$$

The above expression can be factorized further to have:

$$f_m = 1.43\left(\frac{\Delta\phi_m}{\pi\tau_p}\right) \tag{7.12}$$

It was shown previously that the frequency bandwidth (Δf) of a SPM broadened spectrum can be given approximately by the relation [64]:

$$\Delta f = 0.45\omega_0 Q. \tag{7.13}$$

where Q is the spectral broadening parameter and ω_0 is the central angular frequency of the laser. Recognizing that, both Δf and f_m are the same, (a measure of the frequency bandwidth of SPM broadened spectrum) Equation (7.13) can then be substituted into Equation (7.12) to have:

$$0.45\omega_0 Q = 1.43\left(\frac{\Delta\phi_m}{\pi\tau_p}\right) \tag{7.14}$$

Rearranging Equation (8.14), one obtains:

$$\omega_0\tau_p Q = 3.18\left(\frac{\Delta\phi_m}{\pi}\right) \tag{7.15}$$

Interestingly, the parameter $\omega_0\tau_p Q$ is what is actually measured in the IGA technique [65-68] called the "self-phase modulation strength", while. $\Delta\phi_m$ is the parameter measured in the spectral domain SPM technique [13,52-53,62], called the "maximum spectral phase shift". Thus equation (7.15) relates the IGA to the spectral domain SPM technique. Re-writing the above equation in the conventional notation, one has:

$$\omega_0 \tau_p Q_m = 3.18\left(\frac{\phi_m}{\pi}\right) \approx \phi_m \equiv \frac{\pi}{2}(2N-1), \qquad (7.15)$$

where N is the number of peaks in the power spectrum for N ≥ 2 (readily identifiable spectral shapes exist for phase shifts of π/2 and π). Q_m is the value of the spectral broadening parameter at the maximum phase shift.

Equation (7.15) relates the IGA technique directly to the spectral domain. At Q = Q_m, the IGA trace should have well defined lobes (zeros) on either side of the central peak. For a typical IGA trace with three well defined lobes on either side of the central peak, $\omega_0\tau_pQ_m$ = 11.13 and the corresponding $\Delta\phi_m$ = 3.5π. This should yield a spectrum with 4 peaks in the spectral domain SPM measurement. A limitation on the sensitivity of the spectral domain SPM measurement is the fact that it allows one to determine the phase shift only in (2N-1) multiples of π/2. This limits the lowest measurable phase shift to 0.5π. In the IGA technique however, one can measure continuous values of $\omega_0\tau_pQ$ at values of Q other than Q_m.

One significant advantage of the continuous value measurement of the phase in the IGA technique is that it is possible to detect values of phase shift lower than 0.5π, which is the current limit of the spectral domain SPM technique. The sensitivity of IGA technique to the measurement of small phase shift will be discussed in the next section.

7.3 Determination of the Sensitivity of the IGA Technique

7.3.1 Definition and Measurement

The sensitivity of the IGA technique is the lowest value of phase shift that can be detected experimentally with this technique. The IGA technique is a useful tool for accurate measurement of pulsewidth just like the famous noncollinear background-free second harmonic generation intensity autocorrelation (SHGA), discussed in chapter four. However, while the SHGA is not sensitive to the phase, IGA is. For a non-phase modulated Gaussian pulse, the IGA trace is identical to the SHGA trace. A self-phase modulated Gaussian pulse would appear the same and exhibit its original pulsewidth under SHGA trace but its IGA trace would show narrowing and sometimes oscillation, to reflect the level of the change in phase of the pulse. This property can be used to determine the smallest level of phase shift imparted onto a pulse that has propagated through the fiber, by comparing the resulting IGA trace with the SHGA trace.

For a Gaussian input pulse in the zero GVD regime, the minimum detectable SPM strength $\omega_0\tau_p Q$ occurs near the limit where the width of the IGA trace approaches the non-collinear background-free intensity autocorrelation width ($\tau_{AUTO} - \tau_{IGA} \rightarrow 0$). Here τ_{IGA} is the FWHM of the central peak of the IGA trace and τ_{AUTO} is the FWHM of the SHGA trace. For a Gaussian input pulse, the pulsewidth is given by $\tau_p = \tau_{AUTO}/\sqrt{2}$.

A prediction was made earlier [66] through simulation that IGA can detect phase shift as low as $\omega_0\tau_p Q \approx 0.6$, by assuming a laser amplitude fluctuation of 5%. This corresponds to $\Delta\phi \approx 0.19\pi$. Careful and systematic measurements were performed to match this prediction and to establish the ultimate sensitivity of the IGA technique.

The measurements were performed in a 20 meters long silica core fiber and at very low power. A variable attenuator was used to attenuate the laser beam before coupling into the fiber. The laser was optimized for stability. The amplitude fluctuation was below 4%. A sensitive digital power meter (Newport model 835, which is good to sub microwatts) was used for the power measurement. IGA traces were taken in the usual procedure earlier described (Chapter 4). The resulting IGA traces are fitted with the IGA model. The autocorrelation trace of the input pulse was also measured.

Figures (7.1) to (7.4) show the series of low power IGA traces plotted in the same scale with a Gaussian fitted SHGA trace of the input pulse, to show the onset of narrowing and how it progressed with slight increases in the power in the fiber.

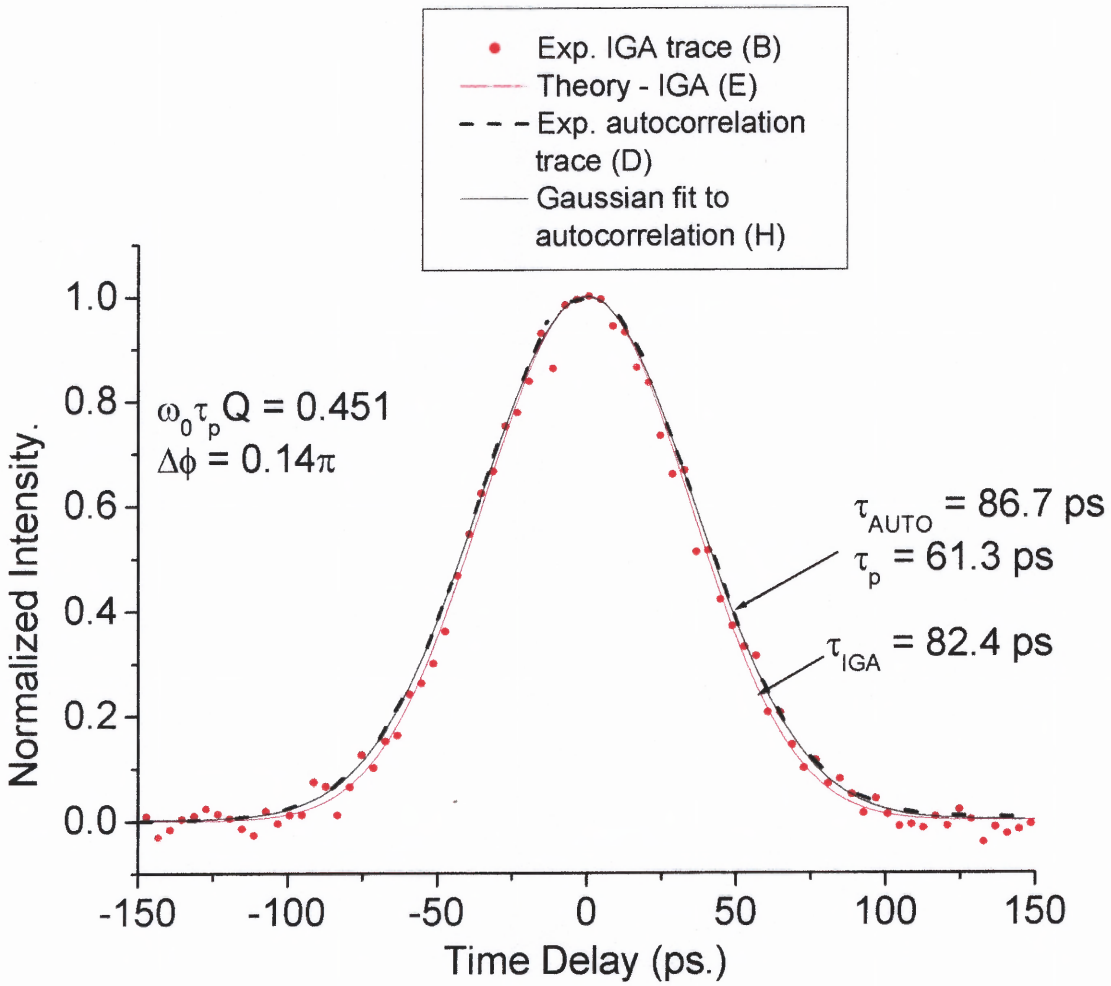

Figure 7.1 Low power IGA trace, and the corresponding Gaussian fitted autocorrelation trace to show the onset of narrowing due to SPM. The minimum detectable SPM strength is 0.451, corresponding to a phase shift of 0.14π [20 m silica core fiber, $P_{avg.} \approx 5$ mW, $P_{peak} \approx 0.82$W].

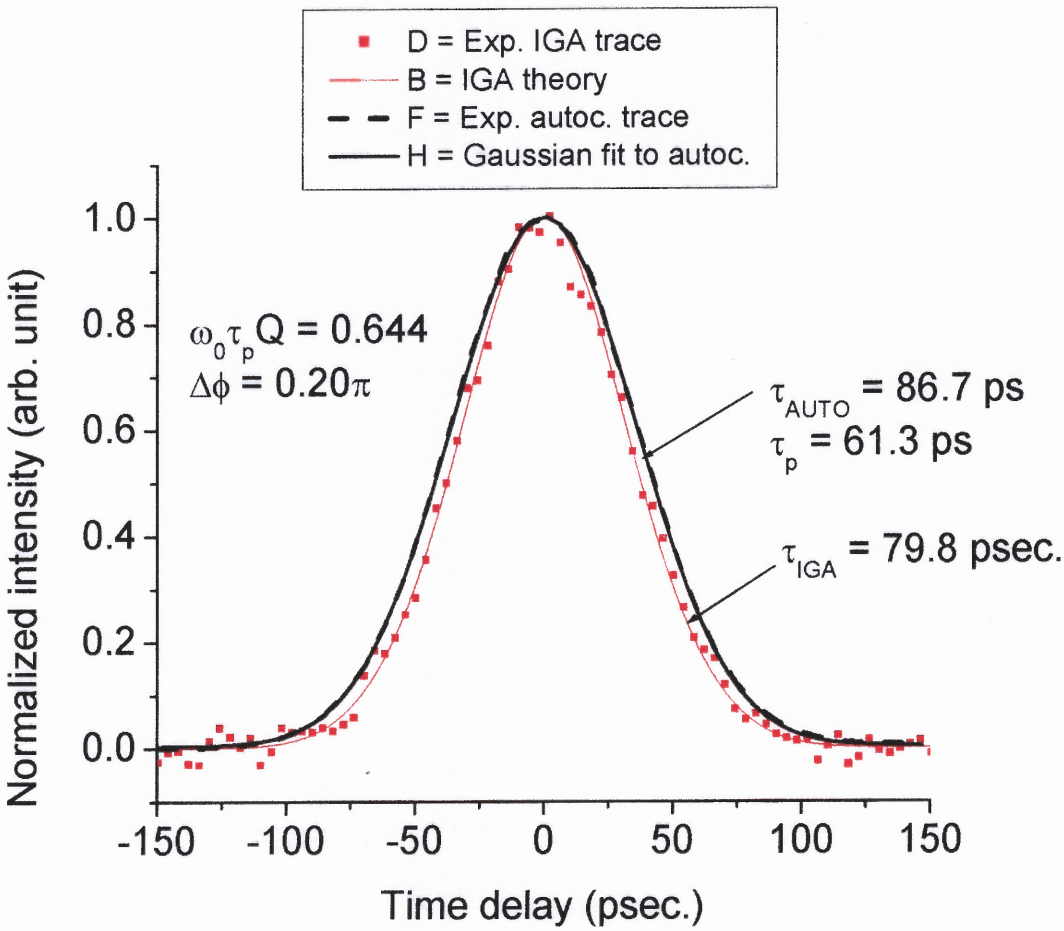

Figure 7.2 Low power IGA trace, and the corresponding Gaussian fitted autocorrelation trace to show gradual narrowing due to SPM. The detected SPM strength is 0.644 for this trace, corresponding to a phase shift of 0.20π [20 m silica core fiber, $P_{avg.} \approx 12$ mW, $P_{peak} \approx 1.92$ W].

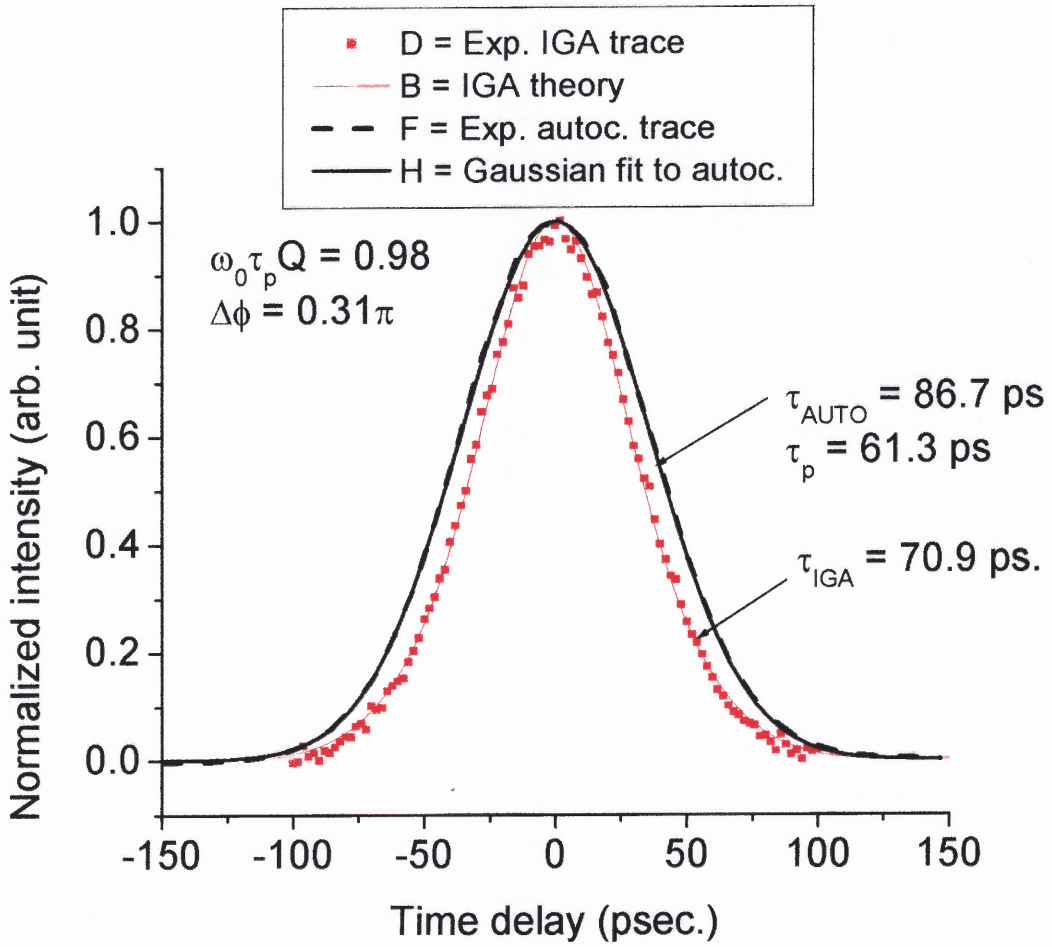

Figure 7.3 Low power IGA trace, and the corresponding Gaussian fitted autocorrelation trace to show the progress of narrowing due to SPM. The measured SPM strength is 0.98, corresponding to a phase shift of 0.31π [20 m silica core fiber, $P_{avg.} \approx 28$ mW, $P_{peak} \approx 4.5$ W].

7.3.2 Discussion of Results

From Figure (7.1), it is clear that one has approached the ultimate limit of phase shift detection using this technique. The minimum SPM strength is shown to be $\omega_0\tau_pQ$ = 0.451, which corresponds to $\Delta\phi = 0.14\pi$. Due to laser amplitude fluctuations, one can barely resolve the difference between the IGA trace and the SHGA trace. Any further attempt to reduce the power leads to a total overlap between the IGA and SHGA. As the power increases, the difference becomes more resolved between IGA trace and the SHGA trace. In Figure 7.2, the two traces are clearly separated and the corresponding self-phase modulation strength is 0.644, which corresponds to $\Delta\phi = 0.20\pi$. The result obtained here is remarkable because it appears to be the most sensitive measurement of the nonlinear phase shift in optical fiber. Although, a comprehensive data on the sensitivity of detection of the different n_2 measurement techniques is not available, one can compare with the spectral domain SPM method, which is currently the most popular technique. The reported minimum measured phase shift with this technique to date is 0.5π. This is so limited primarily due to the fact that one relies on counting of nodes in the spectrum to determine the phase shift, which appear only at integer orders of $\pi/2$. Comparing this with the current result of 0.14π reported here, it is seen that the sensitivity of IGA is over a factor of three better. One may in principle improve the sensitivity of the spectral domain SPM technique by evaluating the integral listed in [13] and fitting the resulting spectrum to the experimental data. In this case, one can obtain a continuous value measurement of the phase.

It should be mentioned that the minimum phase shift theoretically predicted [66] for the IGA technique was $\Delta\phi = 0.19$, which is about 30% higher than the lower limit of the measured sensitivity (0.14π) the measured value, implying that the measured value

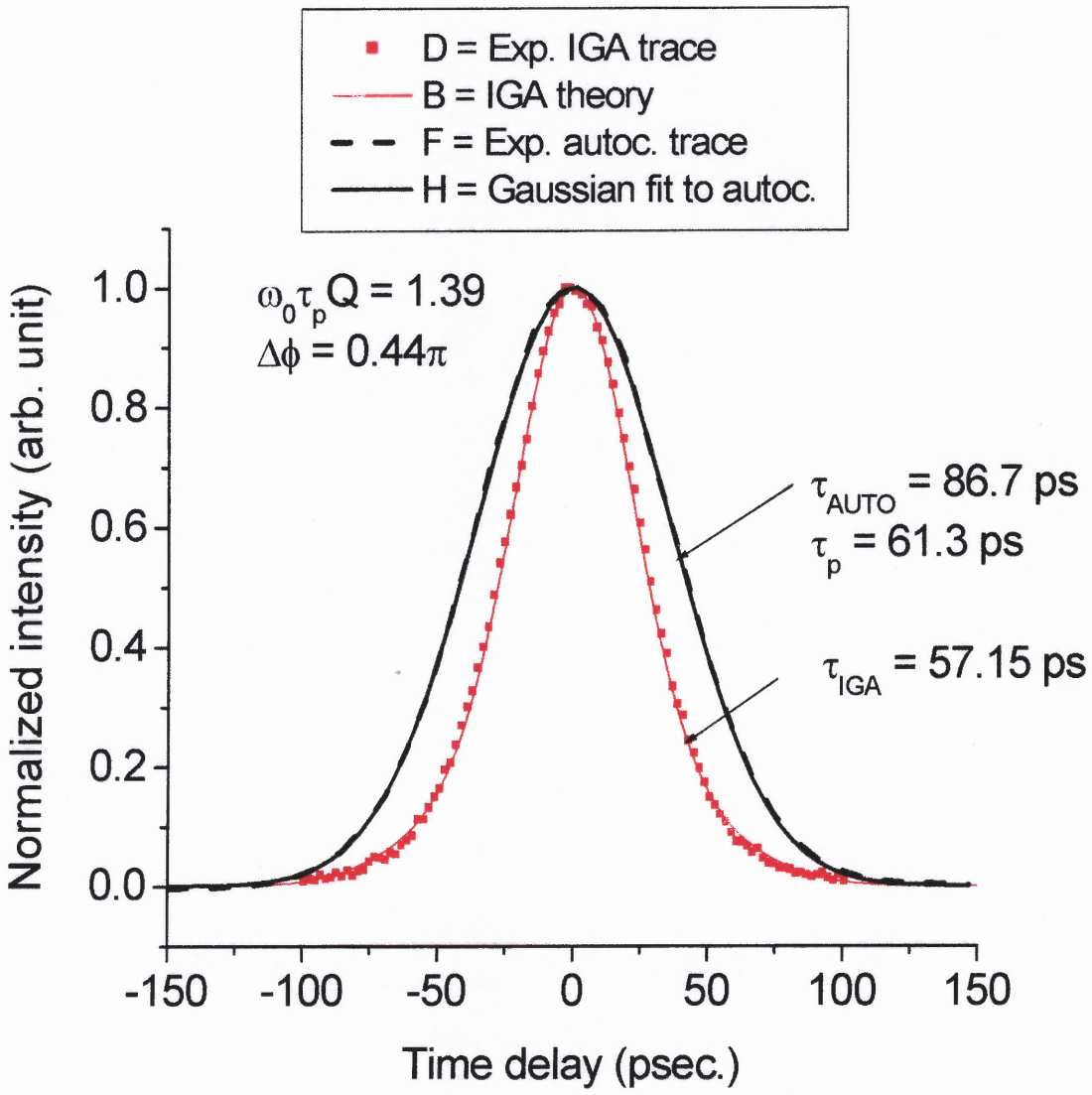

Figure 7.4 Low power IGA trace, and the corresponding Gaussian fitted autocorrelation trace to show increased narrowing due to SPM as the power is increased. The SPM strength for this trace is 1.39, corresponding to a phase shift of 0.44π [20 m silica core fiber, $P_{avg.} \approx 60$ mW, $P_{peak} \approx 9.6$ W].

has pushed further the sensitivity by 30%. The prediction assumed 5% amplitude fluctuation in the theoretical simulation. This is slightly higher than the amplitude fluctuation of the laser at the time of the measurement. Fluctuation in laser amplitude limits one's ability to resolve the difference between the IGA trace and the SHGA trace when the narrowing is substantially low, and reduces the accuracy of the fitting routine. The fitting routine yields the $\omega_0\tau_pQ$ value by establishing a convergence between the experimental data and the IGA model. With a more stable pulse, better resolution and convergence accuracy is obtained, which improves the sensitivity of detection.

At this juncture, it may be useful to specify the power-length product used for this measurement and mention some important numbers. The corresponding laser power that propagated into the 20 m long silica core fiber used in the experiment was approximately 0.82 W of peak power. This implies a power length product of 16.4 W-m. (or 1640 W-cm). The fiber has an effective area of 50 μm^2. This gives a peak intensity of 1.64×10^{10} Wm^{-2} (1.64×10^6 Wcm^{-2}) and intensity-length product of 3.28×10^{11} Wm^{-1} (3.28×10^9 Wcm^{-1}).

CHAPTER 8

CONCLUSION

8.1 Summary

In this study, the photorefractive beam coupling technique, also called induced grating autocorrelation (IGA), has been used to measure the nonlinear refractive index (n_2) and the Raman gain coefficient (g_R) in short lengths ($z \sim 20$ m) of different types of optical fibers, and the dependence of n_2 on the doping profiles of Er-Al-Ge has been investigated. A detailed review of other available techniques [13,15,54-59,107-113] for n_2 measurements given in Chapter 3 has shown that all these techniques typically require hundreds of meters and sometimes, kilometers of fibers for n_2 measurement setup. In measuring n_2 in long fibers, one has to deal with the problems of pulse dispersion and polarization scrambling, which amounts to additional uncertainties in the n_2 measurement. The IGA technique has the advantage of measuring n_2 accurately in short lengths of fibers, thereby avoiding the above mentioned problems, in addition to cost-saving.

In the IGA experiment, a transform limited Gaussian pulse is propagated through a short length of an optical fiber, where it undergoes self-phase modulation (SPM) and other nonlinear distortions, and the output pulse is split into two. The two-excitation pulses are then coupled into a photorefractive crystal, where they interfere and form a photorefractive phase grating. The IGA response is determined by delaying one beam (the probe) and plotting the diffracted intensity of the probe versus the relative delay (τ). Analysis of the IGA response yields information about the nonlinear phase distortions and other calibration parameters of the fiber. The standard IGA model for n_2

measurements as discussed in chapter four was derived from the solution of the wave equation for pulse propagation, in the limit of pure SPM. This model assumed that GVD (group velocity dispersion) and other nonlinear processes such as stimulated Raman scattering (SRS), are negligible. This model has been successfully used to fit the experimental data and determine the n_2 of the fiber from the time dependent phase shift imparted on the pulse..

The breakdown of the standard IGA model was initially observed [70-71] in high GeO_2 doped fibers, where it was noted that the measured IGA trace was distorted and showed clear deviations from the standard IGA model. Investigations into the cause of this deviation revealed that stimulated Raman scattering was responsible. Measurement of the spectrum of the output pulse from these highly GeO_2 doped fibers showed a strong Raman peak (including second Stokes signals), in some cases exceeding 50% conversion at moderate power input.

To account for this deviation, a new model of the IGA has been developed, from the solution of the coupled-amplitude nonlinear Schrodinger equation using both analytical and numerical approaches. The analytical solution was obtained using the "undepleted pump approximation", in which the Stokes signal is treated as a perturbation on the pump. The IGA model developed from this solution accounted for the SRS effects on the IGA trace and allowed the direct determination of the Raman gain coefficient from the fit of the SRS-distorted IGA trace, provided that the Raman conversion does not exceed 25% of the pump. Measurement of Raman gain coefficient was made in four different fibers including pure silica fiber, Er-Al-Ge doped fiber with 28% Ge, a GeO_2 doped fiber with 30% germania and a DCF (dispersion compensating fiber). The results

obtained in all these cases are in good agreement with published results. The numerical approach extends the IGA model further into the region of pump depletion and predicts IGA traces quite well even when the Stokes signal exceeds the pump. This numerical procedure also allows the determination of the Raman gain coefficient of high germania doped fiber, on a relative term with pure silica..

It has also be shown in this work (Chapter 7) that, in the limits of pure self-phase modulation, the IGA technique reduces to the widely accepted spectral domain SPM technique pioneered by Stolen and Lin [13], but is readily applicable to shorter lengths of fiber and is sensitive to smaller phase shifts.

8.2 Scientific Value and Practical Applications

The development of IGA as a new technique for measuring Raman gain coefficient in short lengths of fibers, will have a strong positive impact on scientific research in this field because it is both economical and simple. With the exception of few cases [50], available techniques for measuring Raman gain coefficient in optical fibers have always required the use of very long fibers, $z > 10$ km [159,160,162], while some require the use of two independent laser sources [158,160]. This makes the Raman gain coefficient measurement quite an expensive venture. With the IGA technique, one can measure Raman gain coefficient in 20-100 meter lengths of fiber, using 50-70 picosecond pulses at a single wavelength (1064 nm). In addition, one minimizes the effect of polarization scrambling, since the fiber length is short. These advantages that results from g_R measurement with the IGA technique is also true in the case of n_2 measurements.

System designers require n_2 data of different telecommunication fibers for predicting and, improving the performance of optical communication systems. In today's telecommunication market, fiber manufacturers are sometimes required to specify the numerical value of the n_2 of their fibers. The results of the n_2 measurements obtained in different fiber types in this work will serve to provide these much needed data. The IGA technique, combining its accuracy with its ability to measure n_2 and g_R in short fiber lengths, will now make it possible for these parameters to be measured directly in standard EDFAs. The typical lengths of EDFAs are about 15-25 m.

8.3. Recommendations for Future Studies

There are many new challenging areas in which IGA can be of use. For example, the study of nonlinear optical properties of holey fibers [HFs] is an emerging area of research interest in which IGA can be applied. Unlike conventional fibers, which use different core and cladding materials, HFs can be made from a single material. Light is guided in holey fibers owing to an effective volume average index difference between the center, which forms the core, and the surrounding region, which contains air holes that act as the cladding. One of the pioneering attempts [179] to measure the nonlinearity in this fiber has indicated that the nonlinear coefficient (n_2/A_{eff}) in this class of fibers is about four times higher than that of DSF (dispersion shifted fiber).

Measurement of the Raman gain coefficient and n_2 in tellurite glass fibers is still an open challenge. Measurement of the Raman gain coefficient has only recently been reported [180] in the bulk sample of tellurite glasses, which showed that the g_R is about

30 times higher than in fused silica. This indicates that tellurite fibers would be a good candidate for Raman amplification.

Another very interesting research opportunity would be to extend the IGA technique into the femtosecond regime. With such short pulses, the IGA would require even much shorter fiber lengths and low average power. However this may not be all that simple as it sounds, because with femtosecond pulses, additional nonlinear effects such as intra-pulse Raman scattering and self-steepening may become important. In addition, the pulse shape would no longer be Gaussian, and the IGA model must be modified for hyperbolic secant pulses.

Finally, the author recommends that polarization dependent measurements of the nonlinear refractive index and the Raman gain coefficient in optical fibers be performed using the IGA technique. This is necessary in order to confirm that the assumption of non-polarization scrambling in IGA experiments, owing to short fiber lengths is not an over simplification.

APPENDIX A

DIFFERENT MECHANISMS THAT CAN PRODUCE NONLINEAR REFRACTIVE INDEX (n_2) IN OPTICAL MATERIALS

A.1 Introduction

Although, the nonlinear refractive index (n_2) studied in this work is known to arise from the so called "electronic Kerr effect" (which results from the nonlinear electronic polarizability), it is important to note that there are other physical mechanism that can as well lead to nonlinear refractive index (n_2), with different response times. In this Appendix, the different mechanisms that can contribute to the nonlinear refractive index (n_2) in optical materials are briefly described, together with their relative magnitudes and response times.

A.2 Electronic Kerr Effect

One of the most important mechanisms that produce the nonlinear refractive index is the electronic Kerr effect, which results from the nonlinear electronic polarizability. This was the case discussed in Section 2.1. This effect which arises from an optically induced distortion of the electronic charge distribution, is essentially instantaneous with response time $\tau \sim 10^{15}$ seconds, and it is in general considerably small in magnitude. Typically, $n_2(\text{electronic}) \sim 10^{-13}$ (esu) $\cong 10^{-16}$ cm^2W^{-1} (see Chapter 5). This effect occurs in solids and in fluids composed of *isotropic* molecules [72,182-183].

A.3 Orientational Kerr Effect

The orientational Kerr effect occurs in fluids (liquids and gases) composed of *anisotropic* molecules, whose optical polarizabilities in different coordinate directions are unequal. A good example is a symmetric top molecule whose polarizability along its axis (α_{zz}) is not equal to its polarizability perpendicular to its axis (α_{xx}).

In the absence of an electric field, the molecules are oriented in random directions, so that the index of refraction is isotropic (has the same value in different directions or axis). When an optical field is applied, it induces a dipole moment in the direction of the field. The field can further interact with this induced moment to exert a torque on the molecules proportional to $(\alpha_{zz} - \alpha_{xx})E^2$. Since the induced moment and the field has the same frequency and phase, this torque will have a dc component which will tend to rotate the molecules into alignment with the field. The incremental rotation of a molecule produces a change in index of refraction parallel to the electric field. This index change is given by [72,184]:

$$\delta n = \frac{3}{2}\delta n_s\left[\cos^2\theta - \frac{1}{3}\right] \tag{A.1}$$

where

$$\delta n_s = \frac{4\pi}{3}\frac{(n_0^2+2)^2}{9n_0}N(\alpha_{zz}-\alpha_{xx}) \tag{A.2}$$

N is the density of molecules, θ is the angle between the molecule and the electric field, and n_0 is the linear index of refraction. The average is over all orientations with a weighting factor of a Boltzmann distribution which reflects the interaction energy:

$(\alpha_{zz} - \alpha_{xx})E^2\cos^2\theta$. For complete alignment, ($E \rightarrow \infty$) and ($\theta = 0 \rightarrow \cos\theta = 1$), so that $\delta n = \delta n_s$.

For a small fractional alignment, the nonlinear refractive index is given by

$$n_2 = \left[\frac{(n_0^2+2)^2}{9n_0}\right]^2 \left(\frac{4\pi}{45}\right)\frac{N(\alpha_{zz}-\alpha_{xx})^2}{kT} \tag{A.3}$$

Typically, n_2 is of the order of 10^{-11} (esu) ~ [10^{-14} cm^2W^{-1}], with a response time of the order of 10^{-12} seconds. Note that if the optical field is circularly polarized instead of linear, the change in index of refraction is only one fourth as large.

A.4 Electrostriction

Electrostriction is the density change of an optical material due to the stress caused by intense electromagnetic waves. This change in density alters the index of refraction of the material. The magnitude of the steady state nonlinear refractive index due to electrostrictive process can be given by [72]:

$$n_2(electrostriction) = \frac{n_0\beta}{2\pi}\left(\rho\frac{\partial n}{\partial \rho}\right)^2 \tag{A.4}$$

where ρ is the density and β is the bulk compressibility. The magnitude of n_2 is typically large (~ 10^{-14} cm^2W^{-1}). The speed of response is however very slow (~ 10^{-9} s) [185], since the growth of the density change is governed by acoustic propagation. In deed, the response time is approximately given by the beam cross section divided by the speed of sound.

A.5 Thermal Effect

Nonlinear index change can also result from thermal effect. There are two components to the thermal induced index change, one arising from purely thermal effect at constant volume (such as entropy change) and the other arising from thermal expansion. The two contributions can be represented by [72]:

$$\frac{dn}{dT} = \left(\frac{\partial n}{\partial T}\right)_V + \left(\frac{\partial n}{\partial \rho}\right)_T \frac{\partial \rho}{\partial T} \tag{A.5}$$

where T is temperature and ρ is the material density. The first term is due to change in entropy, and occurs very fast, but it is usually very small in magnitude. The last term represents the contribution form thermal expansion, which can be quite large, but has a slow response time. The relaxation of both contributions is determined by the diffusion of heat away from the optical beam, and it is generally slow (~ 10^{-3} to 1 s). Thermal induced n_2 is usually not important for picosecond pulses except where the effect is integrated over the entire pulse train. Generally, thermal n_2 is negative and produces self-defocusing effect.

A.6 Other Mechanisms

A contribution from nonlinear index can also arise from several other mechanisms. For example, in gases composed of spherically symmetric molecules (such as argon. Krypton etc) molecular collisions can give rise to nonlinear index. Collision between two molecules can lead to a distortion in their electronic distributions such that the polarizability of the pair may have a small anisotropic component. The can result to a nonlinear index analogous to the molecular orientational Kerr effect. The relaxation time of this effect is typically in the range of 10^{-12}s - 10^{-13}s.

Photorefractive effect can also produce a change in index of refraction in electro-optic materials under an applied optical field. The photorefractive effect often leads to a strong nonlinear response, which usually cannot be described in terms of the third order nonlinear susceptibility, because the nonlinear polarization does not depend on the applied field strength in the same manner as the other mechanisms listed. In addition, its response time depends on the intensity of the optical field. A contribution to n_2 can also arise from an optically induced polarization in absorbing polar materials, in which the dipole moment of an excited state differs from the ground state [186].

Table A.1 Different Mechanisms Leading to a Nonlinear Refractive Index, Including Typical Values and Response Times [119,185]

Mechanism	n_2 (cm^2W^{-1})	Response time
Electronic polarization	10^{-16}	10^{-15}
Molecular orientation	10^{-14}	10^{-12}
Electrostriction	10^{-14}	10^{-9}
Thermal effect	10^{-6}	10^{-3}
Saturated atomic absorption	10^{-10}	10^{-8}
Photorefractive effect	Large ($\sim 10^{-3}$)	Intensity dependent (10^{-4} for 1 W/cm^2)

APPENDIX B

VARIOUS UNITS FOR EXPRESSING THE CONCENTRATION OF DOPANTS IN OPTICAL FIBER

In this appendix the author whishes to explain the different units that are used to specify the quantity of dopants in an optical fiber and how they are calculated. The concentration of dopants in optical fiber is usually expressed in various units [133], such as parts per million mole (ppm), percentage molar concentration (%M), ions/cm^3 etc. Most of these dopants are available in the form of the compounds of the oxides or chlorides. Silica itself consists of as silicon oxide (SiO_2). Table (B.1) shows these compounds with their molecular weight.

Table B.1 Some Common Compounds Used as Dopants in Optical Fiber

Name of compound	Chemical formula	Molecular weight (Z) g.
Silicon oxide (silica)	SiO_2	60.1
Erbium oxide	Er_2O_3	382.6
Aluminum oxide	Al_2O_3	102.0
Aluminum chloride	$AlCl_3$	133.4
Germanium oxide (Germania)	GeO_2	104.6
Phosphorus oxide	P_2O_5	142.0

(i) Percentage molar concentration (%M): This indicates the molar fraction of a given dopant in relation to one mole of the total combination as contained in the glass fiber. Let x(d) be the fractional molar concentration of a given dopant (oxide or chloride) composing the glass and x(s) the fractional molar amount of silica, then

$$\sum_{i}^{\#} x_i(d_i) + x(s) = 1 \qquad \text{(B.1)}$$

Hence, the percentage molar concentration of a dopant (d) is given by

$$\frac{x_i(d_i)}{\sum_{i=1}^{\#} x_i(d_i) + x(s)}.100\% = x_i(d_i).100\,(\%\text{M}) \qquad \text{(B.2)}$$

If Z is the molecular mass (or atomic mass) of the constituents, the total weight of the composite glass is given by:

$$W = x(siO_2).Z(SiO_2) + x_1(d_1).Z(d_1) + x_2(d_2).Z(d_2) + \text{-------} + x_{\#}(d_{\#}), \qquad \text{(B.3)}$$

Where $x(siO_2)$ is the molar fraction of silica and $Z(SiO_2)$ is the molecular mass of silica; $x_1(d_1)$, $x_2(d_2)$, $\ldots x_{\#}(d_{\#})$ are the molar fractions of the different dopants with molecular (or atomic) masses $Z(d_1)$, $Z(d_2)$, $\ldots$ $Z(d_{\#})$.

(ii) Number of molecules per cc or ions per cc (cc = cubic centimeter).

Let D be the density of the composite glass and $\mathcal{N}_a$ = Avogadro's number ($\mathcal{N}_a = 6.02 \times 10^{23}$), the number of molecules per cubic centimeter for each dopant is given by:

$$N(d) = \left(\frac{x(d).D.N_a}{W}\right) \text{cm}^{-3} \qquad \text{(B.4)}$$

Example:

For the case of silica (SiO_2), $N(SiO_2) = \left(\frac{x(SiO_2).D.N_a}{W}\right) \text{cm}^{-3}$,

For germania (GeO_2), $N(GeO_2) = \left(\frac{x(GeO_2).D.N_a}{W}\right) \text{cm}^{-3}$,

For Erbium oxide (Er_2O_3), $N(Er_2O_3) = \left(\frac{x(Er_2O_3).D.N_a}{W}\right) \text{cm}^{-3}$

The number of Erbium ions per cc can be given by:

$$N(Er^{3+}) = \left(\frac{x(Er_2O_3).2D.N_a}{W}\right) \text{ions/cm}^3.$$

This is sometimes called the erbium ion density $\rho(Er^{3+}) \cong N(Er^{3+})$.

(iii) Parts per millions in molar concentration (ppm): This is defined for a given dopant *d* as:

$$\rho(d)_{ppm} = \left[\frac{N(d)}{N(SiO_2)} \times 10^6\right] ppm \qquad \text{(B.5)}$$

***Example*:** The ppm of Er_2O_3 is $\rho(Er_2O_3)_{ppm} = \left[\frac{N(Er_2O\ )}{N(SiO_2)} \times 10^6\right] ppm$.

In terms of Er^{3+}, it becomes: $\rho(Er_2O_3)_{ppm} = \left[\frac{W.N(Er^{3+})}{2.D.N_a x(SiO_2)} \times 10^6\right] ppm$

(iv) Density of molecules in grams per cc (g/cm^3):

For each constituent compound or ion, one can obtain the concentration or density of the molecules in grams per cc as follow:

$$\rho(d)_{g/cm^3} = \left(\frac{N(d)Z(d)}{N_a}\right) = \left[\frac{x(d).Z(d)}{W} \times D\right] g/cm^3 \qquad \text{(B.6)}$$

For silica (SiO_2), this can be written as:

$$\rho(SiO_2)_{g/cm^3} = \left(\frac{N(SiO_2)Z(SiO_2)}{N_a}\right) = \left[\frac{x(SiO_2).Z(SiO_2)}{W} \times D\right] g/cm^3$$

(v) Percentage weight in total concentration (wt%):

This is defined by:

$$\rho(d)_{wt\%} = \left(\frac{\rho(d)_{g/cm^3}}{D} \times 100\right) wt\% \equiv \left[\frac{x(d).Z(d)}{W} \times 100\right] wt\% \qquad \text{(B.7)}$$

For Er_2O_3, one has:

$$\rho(Er_2O_3)_{wt\%} = \left(\frac{\rho(Er_2O_3)_{g/cm^3}}{D} \times 100\right) wt\% \equiv \left[\frac{\rho(Er^{3+})_{ions/cm^3}.Z(Er_2O_3)}{2.D.N_a} \times 100\right] wt\%$$

(vi) Parts per millions weight (ppm wt):

One can define the parts per millions weight by:

$$\rho(d)_{ppmwt} = \left(\frac{\rho(d)_{g/cm^3}.2Z(ion)}{D.Z(d)} \times 10^6\right) \text{ppm wt,} \qquad \text{(B.8)}$$

where Z(ion) is the atomic mass of the 'active' ion of the molecule.

Example: For Erbium, one can write:

$$\rho(Er_2O_3)_{ppmwt} = \left(\frac{\rho(Er_2O_3)_{g/cm^3}.2Z(Er^{3+})}{D.Z(Er_2O_3)} \times 10^6 \right) \text{ppm wt,}$$

and

$$\rho(Er^{3+})_{ppmwt} = \left(\frac{\rho(Er^3)_{ions/cm^3}.Z(Er^{3+})}{D.N_a} \times 10^6 \right) \text{ppm wt.}$$

(vii) Estimating Erbium concentration from absorption data:

If the absorption and cut-off wavelength of an Er-doped fiber is known, the Er^{3+} concentration (ions/cm^3) can be deduced approximately from the following relation:

$$\text{Erbium concentration (ions/cm}^3\text{)} = \frac{absorption}{(overlap) \times (cross - section)}, \qquad \text{(B.9)}$$

where the absorption is usually expressed in dB/m and the absorption cross-section is in m^{-2}. The overlap factor is a parameter that specifies the overlap between the mode intensity and erbium ion distribution in the fiber. It is a dimensionless number. Typical values of overlap parameter for Er-Ge-Al doped fibers are 0.64 at 980 nm pumping, 0.46 and 0.4 at 1480 nm and 1550 nm pumping respectively [134].

Example:

For a Er-Al-Ge doped silica fiber with absorption α = 10dB/m at 1530 nm. The erbium concentration in this fiber can be estimated as follow: Use published overlap value closet to 1064 nm. Published data on overlap parameter.

Convert absorption from dB/m to np/m: α (np/m) = α(dB/m) × (0.23).

$\therefore$ for 10dB/m, α(np/m) = 10 $\times$ 0.23 = 2.3/m

Use published cross-section for GeO_2-Al_2O_3-SiO_2 fiber [135] ~ 1.7 $\times$ 10^{-25} m^{-1} (at 980 pumping)

$\therefore$ Er^{3+} concentration (m^{-3}) = 2.3/(4.7 x 10^{-25}) = 4.82 x 10^{24} m^{-3}.

APPENDIX C

DEPENDENCE OF Δn ON GeO_2 CONCENTRATION

In this appendix, the author displays a plot of refractive index difference between the core and cladding versus the germania concentration. The plot shows that Δn is directly proportional to GeO_2 concentration [181] and can be used to estimate Δn from known GeO_2 concentration or to obtain GeO_2 concentration when Δn is given. The intercept represents the refractive index of silica glass.

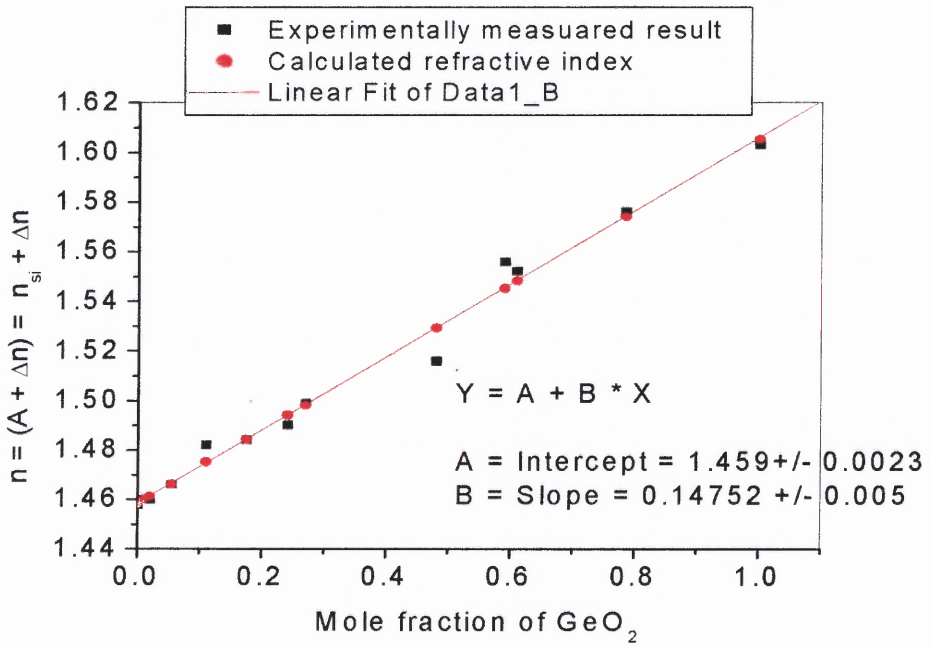

Figure C.1 Plot of core-cladding refractive index difference as a function of GeO_2 concentration. Values plotted here are adapted from [181].

APPENDIX D

ESTIMATING FIBER MODE-FIELD DIAMETER (MFD) AT 1064 nm FROM MEASURED VALUES AT 1314 nm, 1450 nm AND 1552 nm

In this appendix, the author discusses the process used for estimating the MFD at 1064 nm from measurements made at 1552 nm and 1314 nm. The MFD and A_{eff} for the fibers were measured at 1314 nm and 1552 nm, at OFS laboratory (with the help of Dr. Bill Reed), because these are the operational wavelengths of the available equipment for the measurement (Section 5.2.1). Some MFD and A_{eff} values at 1450 nm for some of the fibers were also supplied [157,165].

Since the n_2 and g_R measurements in this work were performed at 1064 nm (see Chapters 4 to 6), the MFD and A_{eff} of these fibers need to be known at 1064 nm since these parameters (A_{eff} and MFD) have been observed to vary significantly with wavelength. Attempts made to obtained some few references that appeared to have discussed direct empirical formula for this was not successful within a reasonable time frame. The author has thus used the measured values of MFD at the above wavelengths to estimate its value at 1064 nm for each fiber. In doing this, a typical case where the A_{eff} and MFD are known at 1552 nm, 1314 nm and 1064 nm [fiber #1(pure silica)] was used to determine the variation trend, which was found to fit well with a second-order polynomial of the form:

$$y(x) = A + B_1*x + B_2*x^2 \qquad (D.1)$$

where A is the intercept on y at $x = 0$ and B_1 and B_2 are constants. Typical fitted results are shown in Figure (D.1).

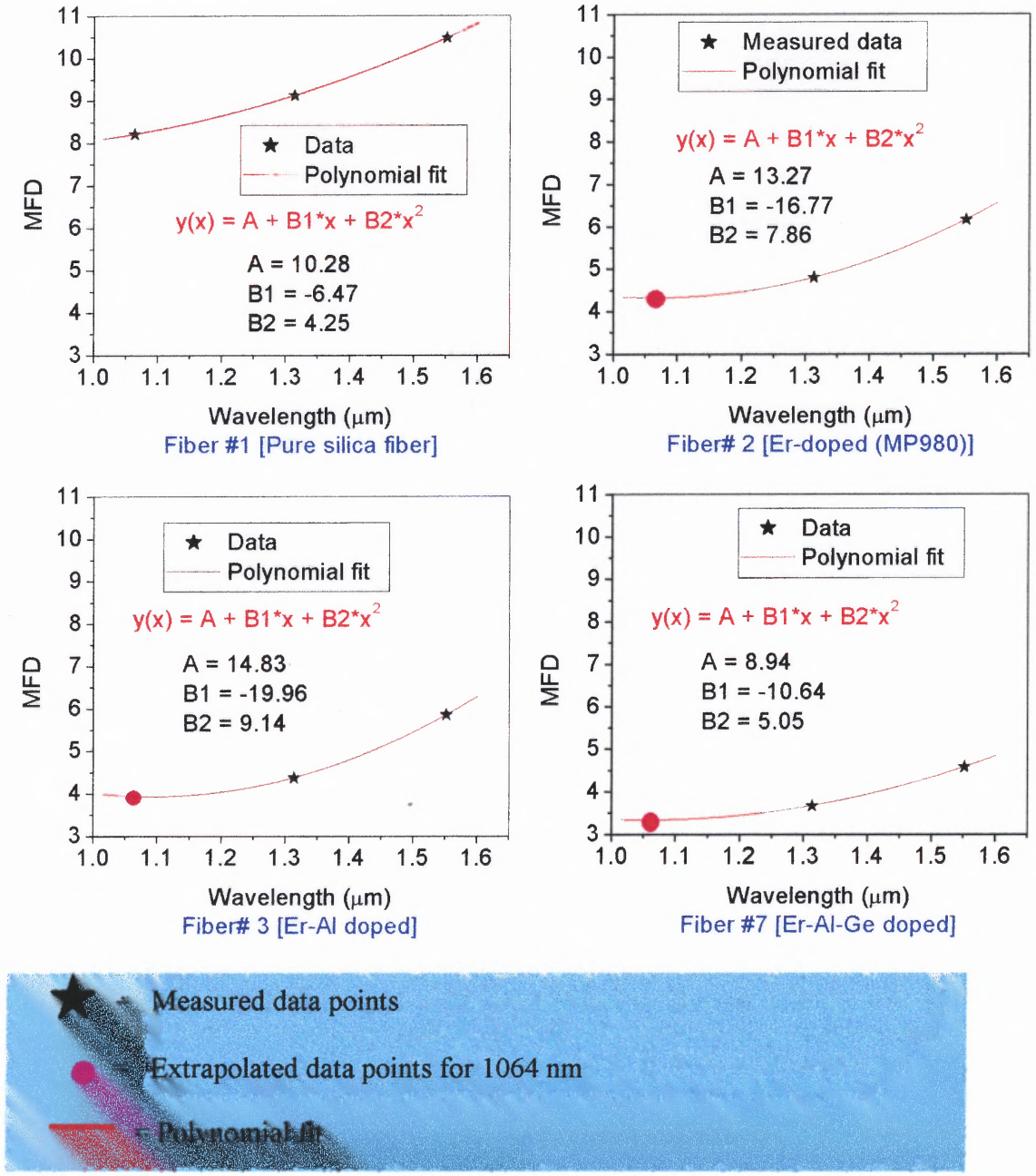

Figure D.1 Typical graphs showing the variation of MFD with wavelength, used to estimate MFD values at 1064 nm.

APPENDIX E

MATLAB FITTING PROGRAM FOR IGA (PURE SPM CASE)

This program is used to fit the experimental data with the IGA model (Equation 4.12).

```
function f2=IGA(z)
global Xval a2 a1 d;
f2 = exp(-1.39*(z.^2 + (Xval+z).^2)).*exp(a2*i*(exp(-2.77*(z+Xval).^2) - exp(-
2.77*(z).^2)));

function fitmaster1(spm)
global Xval a2 Data h err;
j=1;
iterno = 1;
% open the data file
fid = fopen('IGA.DAT','r');
while ~feof(fid)
   x1 = fgetl(fid);
   igaval = sscanf(x1,'%f');
   Data(j,1) = igaval(1);
   Data(j,2) = igaval(2);
   j = j+1;
end
fclose(fid);
parm = [0];
a2 = spm;
parm(1)=spm;
t = Data(:,1);
y = Data(:,2);
plot(t,y,'b.');

% plot x-axis scale from (-1.5 to 1.5)
% use fitminsearch to locate the point of convergence between theory and experiment
axis([-1.5 1.5 -.08 1.05]);
hold on;
h = plot(t,y,'r');
set(h,'EraseMode','xor');
   options = optimset('Display','off');
   lambda = fminsearch('fitfun1a',parm,options);
   lambda(1)
hold off;

% End of program
```

APPENDIX F

MATLAB FITTING PROGRAM FOR THE MODIFIED IGA MODEL (SPM & RAMAN)

This is the computer program for solving Equation (6.19) in the modified IGA model, and for fitting the model to the experimental data. The program is written in MATlab codes and it uses the function called "fminsearch" to locate the point of minimum the difference between the theoretical IGA trace and the experimental trace. At this point of convergence, the program returns the corresponding Raman gain parameter (RGP) and the walk off term (WOT).

```
% Evaluate the SPM contribution
IGA1c.mfunction f2=IGA1c(z)
global Xval a2 a1 d;
f2 = exp(-1.39*(z.^2 + (Xval+z).^2)).*exp(a2*i*(exp(-2.77*(z+Xval).^2)) - a1*i*(exp(-
2.77*(z).^2)));

%Evaluate the Stokes contribution
IgRam.m
function f3=IgRam(q)
global Xval a2 a1 d;
wr=0.952;
f1a = exp(-1.39*q.^2).*exp(i*a2*exp(-
2.77*q.^2)).*exp((a1*0.266/d)*(erf(1.66*(q+Xval)) - erf(1.66*(q-d+Xval))))...
   .*exp((-i*wr*a2*1.06/d).*(erf(1.66*(q+Xval)) - erf(1.66*(q-d+Xval))));
f1b = exp((a1*0.266/d)*(erf(1.66*q) - erf(1.66*(q-
d)))).*exp((i*wr*a2*1.06/d)*(erf(1.66*q) - erf(1.66*(q-d))))...
   .*exp(-1.39*(q+Xval).^2).*exp(-i*a2*(exp(-2.77*(q+Xval).^2)));
f3 = f1a + f1b;

%Evaluate the cross-terms
function f=RAM(y)
global Xval a2 a1 d;
wr=0.952;
f =exp((a1*0.266/d)*(erf(1.66*y) - erf(1.66*(y-d)) + erf(1.66*(y+Xval)) - erf(1.66*(y-
d+Xval)))) ...
   .*exp((i*wr*a2*1.06/d)*(erf(1.66*y) - erf(1.66*(y-d)) - erf(1.66*(y+Xval)) +
erf(1.66*(y-d+Xval))));
```

```
Fit with the exp. data
function fitmaster2(spm,rgp,wot)
global Xval a2 a1 d Data h jref iterno err;
j=1;
jref=1;
iterno = 1;
%open the data file
fid = fopen('newtest.DAT','r');
%fout = fopen('Parmout.DAT','w');
while ~feof(fid)
   x1 = fgetl(fid);
   igaval = sscanf(x1,'%f');
   if igaval(1) == 0
      jref = j;
   end
   Data(j,1) = igaval(1);
   Data(j,2) = igaval(2);
   j = j+1;
end
fclose(fid);
parm = [0 0 0];
a2 = spm;
a1 = rgp;
parm(1)=spm;
parm(2)=rgp;
parm(3)=wot;
d=wot;
t = Data(:,1);
y = Data(:,2);
plot(t,y,'bo');
axis([-1.5 1.5 -0.01 1]);
hold on;
% h = plot(t,y,'r.');
h = plot(t,y,'r');
set(h,'EraseMode','xor');
%for i=1:48
   %parm(3)=0.2 + i/10;
   options = optimset('Display','off');
   lambda = fminsearch('fitfun',parm,options);
hold off;

% End of program
```

APPENDIX G

C -PROGRAM FOR THE NUMERICAL SIMULATION

This is the main program written in C, for the numerical solution of NLSE for the IGA simulation. This program calls three external functions: four1.c, hNL.c and correl.c, whose targets are defined.

```
/* Compliling command: "cc -o essai system2.c hStep.c fft.c hNL.c -lm" */

#include<stdio.h>
#include<math.h>

FILE *inPulsefileP, *overlapP, *outfileRealP, *outfileImP, *outfileP,
   *outSpectrumP,
   *inPulsefileS, *overlapS, *outfileRealS, *outfileImS, *outfileS,
   *outSpectrumS;

#define PI  3.14159
#define N 32768  /* N is the number of sample points of the Input pulse */
          /* T=128.0  Temporal Range from 0 to T; Center is t0=64  */

main()
{
 long int   i, j, iterations, entry,nn,num;
 float temp1P, temp2P,temp1S,temp2S,temp1,temp2;
 float correlation[2*N], correlationa[2*N], ans[2*N];
 float pulseP[2*N],pulseS[2*N], dispersionP[2*N],
       dispersionS[2*N],h, outPulse[2*N],sampling[N],x,y,z;
 float exitFFT[2*N], entry1, entry2, t,T=128.0,t0=64;
 float W=128.0,df,freq[N],disp[N],intensity[N],intensityC[2*N],spectrum[N];
 /* Bandwitdth: from -W to W; df=2 W/N      */
 /* Note: N=2 W T per Definition; Choose W & T to be integer power of 2 */
/* here: effective length = propagation length  (because absorption=0 */
/* where distance =  propagation length in Walk-off-length units */

float Fiber_Length;  /* PROPAGATION DISTANCE */
float fR=0.18; /*fractional contribution of Raman response to NL Pol. */
float LDW; /* dispersion-length/Walk-off-length   */
float LNW; /* Nonlinear-length/Walk-off-length   */
float LGW; /*Gain-length/Walk-off-length   */
float Peff=2*10.0e-7;  /* effective Power of the Noise at Input */
float nlinLength;   /* Pump Nonlinear Length (in meter) */
float LambdaP;      /* Pump Wavelength (in micrometer) */
float LambdaS;      /* Stokes Wavelength (in micrometer) */
```

```
float Ratio;       /* LambdaP/LambdaS */
float Aeff;        /* effective  core Area of Fiber (in micrometer^2) */
float Power;       /* peak power of incoming radiation (in Watt) */
float n2;          /* NL index of refract. (in 10^(-20) meter^2/Watt) */
float pulseWidth;  /* pulse width (in ps) */
float RamanLength; /* Pump Raman-Gain Length (in meter) */
float GainP;  /* Pump Raman-gain coefficient Pump */
float GainS;  /* Stokes Raman-gain coefficient Pump */

/* Definition of external functions follows */
/* they have to be compiled together with this main program!  */
 void  four1(float data[],int nn,int isign);
            /* four1: DISCRETE FOURIER TRANSFORM */
            /* LOCATED in File: fft1.c */
 void  hNL(float pulseP[], float pulseS[], int dim, float h, float LGW, float
 LNW, float Ratio);
/* hNL: NONLINEAR contribution to propagation; (SPM & Raman)
            LOCATED in hNL.c */
 void  correl(float data1[], float data2[], int nn,  float correlation1[]);
/* correl: CORRELATION between data1 and data2 */

 /* Now we open Files. Results of computation will be stored there
  in ASCII-format in form of a Table.
   "w" means that they are open as writing files   */
 outfileRealP=fopen("fourierRealPump2.dat","w"); /* real part of Envelope*/
 outfileImP=fopen("fourierImPump2.dat","w");  /* Im. part of Envelope */
 outfileP=fopen("IntensityPump2.dat","w");   /* Intensity of Envelope */
 outSpectrumP=fopen("SpectrumPump2.dat","w");
 inPulsefileP=fopen("inputPulsePump2.dat","w");
 overlapP=fopen("CorrelationPump2.dat","w");

/* Now, Parameters of the Fiber can be input by the user of the program */
printf("\n\n Ratio of Pump-to-Stokes Wavelength: Ratio=");
scanf("%f", &Ratio);
printf("\n\n dispersion-length/Walk-off-length: LDW=");
scanf("%f", &LDW);
printf("\n\n Nonlinear-length/Walk-off-length: LNW=");
scanf("%f", &LNW);
printf("\n\n Gain-length/Walk-off-length: LGW=");
scanf("%f", &LGW);
print("\n\n Fiber-Length in Walk-off-length units: Fiber_Length=");
scanf("%f", &Fiber_Length);

 for(i=0;i<N;i++)  /* Pump-Pulse def -Gaussian- and sampled */
 {
  t=T*i/(N-1)-t0;
```

```
  x=t*t;
  sampling[i+1]=exp(-0.5 * x);
  fprintf(inPulsefileP, "%f\n", sampling[i+1]);
 }
 fclose(inPulsefileP);

 for(i=1;i<N+1;i++)
 {
  pulseP[2*i-1]=sampling[i];
  pulseP[2*i]=0.0;
 }
/* At this point: Input Pump-Pulse completely defined!  */

 for(i=0;i<N;i++)      {
   sampling[i+1]=sqrt(Peff);
   fprintf(inPulsefileS, "%f\n", sampling[i+1]);
   }
 fclose(inPulsefileS);

 for(i=1;i<N+1;i++)
  {
   pulseS[2*i-1]=sampling[i];
   pulseS[2*i]=0.0;
   }
/* At this point: Input Stokes-Pulse completely defined!  */

 df=2*W/N;   /* frequency step */
 printf("\n\nThe frequency step is df=%f",df);

 for(j=0;j<N/2;j++)  /* Frequencies are defined  */
  {
   freq[j]=j*df;
  }

 for(j=N/2+1;j<N;j++)
  {
  freq[j]=j*df-2*W;
  }
  freq[N/2]=W;

 printf("\n\n Please, enter the step size h: ");
 scanf("%f",&h);
 z=Fiber_Length/h;
 nn=z;

printf("\n%d iterations (%f in float) have to be performed!", nn,z);
```

```
 printf("\n enter a number to continue (AND WAIT FOR RESULTS)!");
 scanf("%d",&num);

/* Loop: IMPLEMENTATION of symmetric split Step method (Pump & Stokes)   */

 for(j=0;j<nn;j++)  /* NUMBER of STEPS to be performed is nn  */
 {
      hNL(pulseP,pulseS, N,h,LGW,LNW, Ratio);   /* NL & Raman over h   */
   hStep(pulseP,dispersionP, N);  /*  PUMP DISPERSION over h/2 */
   hStep(pulseS,dispersionP, N);  /*  STOKES DISPERSION over h/2 */
 }


for(i=1;i<N+1;i++)      /* Store output PUMP pulse envelope in two files */
 {
  fprintf(outfileRealP, "%f\n", pulseP[2*i-1]);  /* Real part */
  fprintf(outfileImP, "%f\n", pulseP[2*i]);      /* Imaginary part */
 }
fclose(outfileRealP);
fclose(outfileImP);

/* Intensity of the Output PUMP Pulse is computed  */
for(j=1;j<N+1;j++)
 {
  intensity[j]=pulseP[2*j-1]*pulseP[2*j-1]+pulseP[2*j]*pulseP[2*j];
  fprintf(outfileP,"%f\n",intensity[j]);
 }
fclose(outfileP);

for(i=1;i<N+1;i++)      /* Store output STOKES pulse envelope in two files */
  {
  fprintf(outfileRealS, "%f\n", pulseS[2*i-1]);
  fprintf(outfileImS, "%f\n", pulseS[2*i]);          }
fclose(outfileRealS);
fclose(outfileImS);

/* Intensity of the Output STOKES Pulse is computed  */
 for(j=1;j<N+1;j++)
   {
   intensity[j]=pulseS[2*j-1]*pulseS[2*j-1]+pulseS[2*j]*pulseS[2*j];
   fprintf(outfileS,"%f\n",intensity[j]);
   }
 fclose(outfileS);

/* PUMP Power Spectrum */
```

```
four1(pulseP,N,1) ; /*Fourier Transform Output PUMP Pulse */
for(j=1;j<(N/2)+1;j++)
 {
  temp1=pulseP[2*j-1];
  temp2=pulseP[2*j];
  spectrum[j+(N/2)]=sqrt(temp1*temp1+temp2*temp2);
 }
 for(j=(N/2)+1;j<N+1;j++)
 {
 temp1=pulseP[2*j-1];
 temp2=pulseP[2*j];
 spectrum[j-(N/2)]=sqrt(temp1*temp1+temp2*temp2);
 }
 for(j=1;j<N+1;j++)
 {
 fprintf(outSpectrumP, "%f\n",spectrum[j]);
 }
 fclose(outSpectrumP);

  /* STOKES Power Spectrum */
   four1(pulseS,N,1) ; /*Fourier Transform Output STOKES Pulse */
   for(j=1;j<(N/2)+1;j++)
    {
    temp1=pulseS[2*j-1];
    temp2=pulseS[2*j];
    spectrum[j+(N/2)]=sqrt(temp1*temp1+temp2*temp2);
    }
   for(j=(N/2)+1;j<N+1;j++)
    {
     temp1=pulseS[2*j-1];
     temp2=pulseS[2*j];
     spectrum[j-(N/2)]=sqrt(temp1*temp1+temp2*temp2);
    }
   for(j=1;j<N+1;j++)
    {
     fprintf(outSpectrumS, "%f\n",spectrum[j]);
    }
   fclose(outSpectrumS);

 /* IMPORTANT Reminder: pulse[] is now Spectrum of output pulse */
 /* correlation = FT of Power Spectrum */
 /* Note that "Power Spectrum" = Square of "Spectrum"     */
 /* Whereas "Spectrum"=FT of "Pulse envelope" in time domain */
/* IGA = Square of correlations overlapped*/.

/*End of program*/
```

REFERENCES

1. T. H. Maiman, "Stimulated optical radiation in ruby masers", *Nature*, **187**, p. 493 (1960).

2. A. L. Schawlow and C. H. Townes, "Infrared and Optical Masers," *Phys. Rev.* **112**, p. 1940 (1958).

3. F. P. Kapron, D. B. Keck and R. D. Maurer, "Radiation losses in glass optical waveguides," *Appl. Phys. Lett.* **17**, p. 423 (1970).

4. M. Horiguchi and H. Osanai, spectral losses of low-OH-content optical fibers," Electron. Lett. **12**, p. 310 (1976).

5. D. N. Payne and W. A. Gambling, Electron. Lett. **10**, p. 289 (1974).

6. T. Miya, Y. Terunuma, T. Hosaka and T. Miyashita, Electron.Lett. **15**, p. 106, (1979).

7. R. J. Mears, L. Reekie, I. M. Jauncie, and D. N. Payne, "High-gain rare-earth doped fiber amplifier at 1.54 μm," in Optical Fiber Communication conference, **3**, 1987 OSA Technical Digest Series (Optical Society of America, Washington DC, 1987).

8. R. J. Mears, L. Reekie, I. M. Jauncie, and D. N. Payne, Electron. Lett. 23, p. 2026 (1987).

9. E. Desurvire, J. R. Simpson and P. C. Becker, Opt. Lett. **12**, p. 888 (1987).

10. F. Forghieri, R. W. Tkach, and A. R. Chraplyvy, "Fiber nonlinearities and their impact on transmission systems," in *Optical Fiber Telecommunications,* **IIIA**, edited by I. P. Kaminow and T. L. Koch, (Academic Press, San Diego, California 1997), pp. 196-264.

11. D. Marcuse, A. R. Chraplyvy and R. W. Tkach, "Effects of fiber nonlinearities on a long-distance transmission," *J. Lightwave Technol.* **9**, pp.121-128 (1991).

12. A. R. Chraplyvy, "Limitations on lightwave communications imposed by optical-fiber nonlinearities", *J. Lightwave Technol.* **8**, pp. 1548-1557 (1990)

13. R. H. Stolen and C, Lin, "Self-phase modulation in silica optical fibers", *Phys. Rev.* **A 4**, pp. 1445-1453 (1978).

14. P. N. Kean, K. Smith and W. Stibbett, "Spectral and Temporal Investigation of SPM and SRS in a Single-Mode Optical Fiber", *IEEE Proc.* **134**, pp. 163-170 (1987).

15. T. Kato, Y. Suetsugu, M. Takagi, E. Sasaoka, M. Nishimira, "Measurement of the the nonlinear refractive index in optical fiber by the cross-phase-modulation method with depolarized pump light", *Opt. Lett.* **20**, p. 988 (1995).

16. C. Lin, W. A.Reed, A.O. Pearson and H. Shang, "Phase matching in the minimum-chromatic-dispersion region of single-mode fibers for stimulated four-photon mixing", *Opt. Lett.* **6**, pp. 493 – 495 (1981).

17. R. H. Stolen and J. E. Bjorkolem, "Parametric amplification and frequency conversion in optical fibers", *IEEE J. Quantum Electron.* **QE-18**, pp. 1062-1072 (1982).

18. R. H. Stolen, Nonlinear properties of optical fibers, in *Optical Fiber Telecommunications,* edited by S. E. Miller and A. G. Chynoweth (Academic Press, San Diego, Calif. 1979) pp. 125-150.

19. A. Yariv, *Optical Electronics in Modern Communications* (Oxford University Press, New York, 1997), pp. 693-702.

20. G. P. Agrawal, *Nonlinear Fiber Optics – Optics and Photonics* (Academic Press, New York, 2001), 3rd edition.

21. B. Crosignani, and P. D. Porto, "Influence of guiding structures on spontaneous and stimulated emission: Raman scattering in optical fibers", *Phys. Rev.* **A 21**, pp. 504-598 (1980).

22. R. H. Stolen and A. M. Johnson, "The effect of pulse walk-off on stimulated Raman Scattering in fibers," *IEEE J. Quantum Electron.* **QE-22**, pp. 2154-2160 (1986).

23. R. H. Stolen and W. J. Tomlinson, "Effect of the Raman part of the nonlinear refractive index on propagation of ultrashort optical pulses in fibers", *J. Opt. Soc. Am.* **B 9**, pp. 565-573 (1992).

24. W. Kaiser and M. Maiser, "Stimulated Rayleigh, Brillouin and Raman Spectroscopy," in *Laser Handbook*, **2**, edited by F. T. Arrechi and E. O. Schulz-Dubois, (Amsterdam: North-Holland, 1972) pp. 1078-1150.

25. P. Narum, M. D. Skeldon and R. w. Boyd, "Effect of laser mode structure on stimulated Brillouin scattering", *IEEE J. Quantum Electron.* **QE-22**, pp. 2161-2167 (1986).

26. Y. Aoki and E. Tajima, "Dependence of stimulated Brillouin scattering thresholds in single-mode fibers on the number of longitudinal modes of the pump laser", in *Conf. Lasers and Electro-optics* (Baltimore, MD), 1987, paper Tu HH5.

27. E. Lichtman, and A. A. Friesem, "Stimulated Brillouin scattering excited by multimode laser in single mode optical fibers", *Opt. Com.* **64,** p. 544 (1987).

28. Y. Aoki, E. Tajima and I. Mito, "Input power limits of single-mode optical fibers due to stimulated Brillouin scattering in optical communication systems", *J. Lightwave Technol.* **6**, p. 710 (1988).

29. G. P. Agrawal and N. K. Dutta, *Semiconductor Lasers,* (Van Nostrand Reinhold, New York, 1993).

30. A. M. Johnson and C. V. Shank, "Pulse compression in single-single mode fibers – picoseconds to femtoseconds", in *The Supercontinuum Laser Source,* edited by R. R. Alfano, (Springer-Verlag, New York, 1989) pp. 399-449.

31. W. J. Tomlinson, R. H. Stolen, C. V. Shank, " Compression of optical pulses chirped by self-phase modulation in fibers", J. Opt. Soc. Am. **B 1,** p. 139 (1984).

32. B. J. Eggleton, G. Lenz, Richart. E. Slusher, N. M. Litchinitser, "Compression of Optical Pulses Spectrally Broadened by Self-Phase Modulation with a Fiber Bragg Grating in Transmission", *Applied Optics-LP,* **37**, pp. 7055-7061 (1998).

33. J. A. R. Williams , I. Bennion , and L. Zhang , "Compression of optical pulse using self-phase modulation and linearly chirped Bragg-gratings in fibers", *IEEE Photonics Technol. Lett.* **7,** pp. 491- 493 (1996).

34. D. S. Peter , W. Hodel , and H. P. Weber , "Compression of pulses spectrally broadened by self-phase modulation using a fiber grating: a theoretical study of the compression efficiency" , Opt. Commun. **112**, pp. 59-66 (1994).

35. M. N akazawa, Hirokazu Kubota, Kenji Kurokawa, Eiichi Yamada, "Femtosecond optical soliton transmission over long distances using adiabatic trapping and soliton standardization", J. *Opt. Soc. Am.* **B 8**, p. 1811 (1991).

36. I. Morita , M. Suzuki , N. Edagawa , S. Yamamoto , and S. Akiba, "Single-channel 40 Gbit/s, 5000 km straight-line transmission experiment using periodic dispersion compensation", *Electron. Lett.* **33,** pp. 698-699 (1997).

37. M. Suzuki , I. Morita , N. Edagawa , S. Yamamoto , and S. Akiba , 20 Gbit/s-based soliton WDM transmission over transoceanic distances using periodic compensation of dispersion and its slope , *Electron. Lett.* **33**, pp. 691- 692 (1997).

38. L. F. Mollenauer, P. V. Mamyshev, and M. J. Neubelt, Demonstration of soliton WDM transmission at up to 810 Gbit/s , error-free over transoceanic distances, in *Optical Fiber Communication Conference , 2 of 1996 OSA Technical Digest Series* (Optical Society of America, Washington, D.C., 1996), paper PD 22.

39. N. Edagawa, I. Morita, M. Suzuki, S. Yamamoto, K. Tanaka, and S. Akiba, "Long distance soliton WDM transmission using a dispersion-flattened fiber", in *Optical Fiber Communication Conference, 6 of 1997 OSA Technical Digest Series* (Optical Society of America, Washington, D.C.1997), paper PD 19.

40. S. G. Evangelides , B. M. Nyman , G. T. Harvey , L. F. Mollenauer , P. V. Mamyshev , M. L. Saylors , S. K. Korotky , U. Koren , T. A. Strasser , J. J. Veselka , J. D. Evankow , A. Lucero , J. Nagel , J. Suhoff , J. Zyskind , P. C. Corbett , M. A. Mills , and G. A. Ferguson , Soliton WDM transmission with and without guiding filters , *IEEE Photonics Technol. Lett.* **8**, pp. 1409-1411 (1996).

41. M. Karasek, M. Menif, "Channel addition/removal response in Raman fiber amplifiers: modeling and experimentation", *J. Lightwave Technol.*, **20**, pp. 1680-1687 (2002).

42. N. Takachio, H. Suzuki, "Application of Raman-distributed amplification to WDM transmission systems using 1.55-μm dispersion-shifted fibers", *J. Lightwave Technol.* **19**, pp. 60-69 (2001).

43. E. M. Dianov, "Advances in Raman fibers", *J. Lightwave Technology*, 20, pp. 1457 -1462 (2002).

44. E. *Desurvire, A. Imamoglu, H. Shaw,* "Low-threshold synchronously pumped all-fiber ring Raman laser", *J. Lightwave Technol.*, **5**, p. 89-96 (1987).

45. T. N. *Nielsen, P. B. Hansen, A. J. Stentz, V. M. Aquari, J. R. Pedrazzani, A. A. Abramov, R. P. Espindola,* "8×10 Gb/s 1.3-μm unrepeatered transmission over a distance of 141 km with Raman post- and pre-amplifiers" *IEEE Photonics Technol. Lett.* **10**, pp. 1492-1494 (1998).

46. P. B. Hansen, G. Jacobovitz-Veselka, L. Gruner-Nielsen, A. J. Stentz, "Raman amplification for loss compensation in dispersion compensating fibre modules" *Electron. Lett.* **34,** pp. 1136-1137 (1998).

47. H. Masuda, S. Kawai, K. Suzuki, K. Aida, "Ultra wide 75-nm 3-dB gain-band optical amplification with erbium-doped fluoride fiber amplifiers and distributed Raman amplifiers" *IEEE Photonics Technol. Lett.* **10**, pp. 516-518 (1998).

48. P. B. Hansen, L. Eskildsen, S. G. Grubb, A. M. Vengsarkar, S. K. Korotky, T. A. Strasser, E. J. Alphonsus, J. J. Veselka, D. J. DiGiovanni, D. W. Peckham, D. Truxal, "442 km repeaterless transmission in a 10 Gbit/s system experiment", *Electron. Lett.* **32**, pp. 1018-1019 (1996).

49. P. B. Hansen, L. Eskilden, S. G. Grubb, A.M. Vengsarkar, S. K. Korotky, T. A. Strasser, J. E. J Alphonsus, J. J. Veselka, D. J. DiGiovanni, D. W. Peckham, E. C. Beck, D. Truxal, W. Y. Cheung, S. G. Kosinski, D. Gasper, P. F. Wysocki, V. L. da Silva, J. R. Simpson, "529 km unrepeatered transmission at 2.488 GBit/s using dispersion compensation, forward error correction, and remote post- and pre-amplifiers pumped by diode-pumped Raman lasers" *Electron. Lett.* **31,** pp. 1460 –1461 (1995).

50. R. H. Stolen and E. P. Ippen, "Raman gain in glass optical waveguides", *Appl. Phys. Lett.*, **22,** pp. 276-279 (1972).

51. E. P. Ippen and R. H. Stolen, "Stimulated Brillouin scattering in optical fibers", *Appl. Phys. Lett.*, **21**, pp. 539-541 (1972).

52. K. S. Kim, W. A. Reed, R. H. Stolen and K. W. Quoi, "Measurement of the nonlinear refractive index of silica core and dispersion shifted fibers", *Opt. Lett.* **19**, pp. 257- 259 (1994).

53. Y. Namihira, A. Miyata and N. Tanahashi, "Nonlinear coefficient measurements for dispersion shifted fibres using self-phase modulation method at 1.55 μm", *Electron. Lett.* **30,** pp. 262-264 (1994).

54. M. Monerie and Y. Durtestse, "Direct interferometric measurement of nonlinear refractive index of optical fibers by cross-phase modulation", *Electron Lett.* **23**, pp. 961-963 (1987).

55. A. Wada, T. O. Tsun aned R. Yamauchi, "Measurement of nonlinear index coefficient of optical fibers through the cross-phase modulation using delayed self-heterodyne technique", *Proceedings of ECOC '92, Berlin, Germany*, p. 42, (1992).

56. R. H. Stolen, W. A. Reed, K. S. Kim, and K. W. Quoi, "Measurement of optical nonlinearity of transmission fibers", *Technical Digest – Smyposium on optical fiber measurements, 1992 (NIST, Special publication.839),* pp. 71-75 (1992).

57. A. Boskovic, S. V. Chenikov, J. R. Taylor, L. Gruner-Nielson and O. A. Levring, Direct measurement of n_2 in various types of telecommunication fiber at 1.55 μm, *Opt. Lett.*, **21**, pp. 1966-1968 (1996).

58. S. Smolors, F. Wise and N. F. Borrelli, "Measurement of the nonlinear response of optical fiber material by use of spectrally resolved two-beam coupling", *Opt. Lett.* **24**, pp. 1103-1105 (1999).

59. S. V. Chernikov and J. R. Taylor, "Measurement of normalization factor of n_2 for random polarization in optical fibers", *Opt. Lett.* **21**, pp. 1103-1105 (1996).

60. J. W. Arkwright, P. Elango, G. R. Atkins, T. Whitbread, and M. J. Digonnet, "Experimental and theoretical analysis of resonant nonlinearity in ytterbium-doped fiber", *J. Lightwave Technol.* **16**, pp. 798-805 (1998).

61. R. H. Kim, B. H. Lee, Y. Chung, U. G. Pack, and W. T. Han, "Resonant optical nonlinearity measurement of Yb^{3+}/Al^{3+} codoped optical fibers by use of long-period fiber grating pair", *Opt. Lett.* **27**, pp. 580-582 (2002).

62. R. H. Stolen, W. A. Reed, K. S. Kim and G. T Harvey, Measurement of the nonlinear refractive index of long dispersion-shifted fibers by self-phase modulation at 1.55 μm, *J. Lightwave Technol.* **16**, pp. 1006-1012 (1998).

63. R. Trebino, C.C. Hayden, A. M. Johnson, W. M. Simpson and A. M. Levine, "Chirp and self-phase modulation in induced-grating autocorrelation measurements of ultrashort pulses", *Opt. Lett.* **15**, pp. 1079-1081 (1990).

64. A. M. Levine E. Ozizmir, R. Trebino, C. C. Hayden, A. M. Johnson and K. L. Tokuda, "Induced grating autocorrelation of ultrashort pulses in slowly responding medium", *J. Opt. Soc. Am.* **B 11**, pp. 1609-1618 (1994).

65. A. M. Johnson, A. M. Glass, W. M. Simpson, and D. H. Olson, "Infrared Picosecond pulse diagnostics using photorefractive beam coupling, in *Conference on Lasers and Electro-Optics 11 of 1989 OSA Technical Digest Series* (Optical Society of America, Washington DC, 1989) p. 226.

66. H. Garcia, A. M. Johnson, F. A. Oguama, and Sudhir Trivedi, "A new approach to the measurement of the nonlinear refractive index of short (<25 m) lengths of silica and erbium-doped fibers," *Accepted for publication in Optics Letters.*

67. H. Garcia, A. M. Johnson, and Sudhir Trivedi, "Photorefractive beam coupling – A new approach to the measurement of the nonlinear refractive index of semiconductor films, *Phys. Stat. Sol.* (b) **220**, pp. 47-51 (2000).

68. F. A. Oguama, H. Garcia, A. M. Johnson and S. Trivedi, "Photorefractive Beam Coupling Measurement of the Nonlinear Refractive Index (n_2) of Erbium-Doped Fibers as a Function of Germania Content", A paper presented at the 84th Annual Meeting/Conference of the Optical Society of America held at Providence, RI, Oct. 22nd – 26th, (2000).

69. F. A. Oguama, H. Garcia, A. M. Johnson and S. Trivedi, "Photorefractive Beam Coupling Measurement of the Nonlinear Refractive Index (n_2) of Erbium-Doped Fibers as a Function of Germania and Aluminum Content", in: *Conf. Lasers and Electro-optics – CLEO'2001 Technical Digest,* Baltimore MD, pp. 303-304 (2001).

70. F. A. Oguama, A. Tchouassi and A. M. Johnson, "Effect of High Germania c Content and Stimulated Raman Scattering on n_2 Measurements in Erbium-Doped Single Mode Fibers", Optical Society of America (OSA) annual meeting, October, 2002 (Orlando Florida).

71. F. A. Oguama, A. Tchouassi and A. M. Johnson, "Influence of Stimulated Raman Scattering and High GeO_2 Doping on the Induced Grating Autocorrelation Measurements in Er-Al-Ge Doped Single Mode Fibers", 2003 Annual Conference of the National society of Black Physicists-NSBP, Feb. 12-15, Atlanta, GA, (2003).

72. D. H. Austin, Picosecond nonlinear optics, *in Ultrashort light pulses – Topics in applied Physics* **8**, edited by S. L. Shapiro, (Spring-Verlag, 1977), pp. 123-194.

73. R. H. Stolen, J. P. Gordon, W. J. Tomlinson, H. A. Haus, "Raman response function of silica-core fibers", *J. Opt. Soc. Am.* **B 6,** pp. 1159-1166 (1989).

7.4. Y. R. Shen, *Principles of nonlinear optics* (Wiley, New York, 1984).

75. R. H. Stolen,H. W. K. Tom, Self-orgnized phase-matched harmonic generation in optica fibers.*Opt. Lett.* **12**, p. 585 (987).

76. J. M. Gabriagues,H. Fevrier, "Analysis of frequency-doubling processes in optical fibers using Raman spectroscopy", *Opt. Lett.* **12,** p. 720 (1987).

77. F. Matera, S. Wabnitz, Nonlinear polarization evolution and instability in a twisted birefringent fiber, *Opt. Lett.*, **11**, p. 467 (1986).

78. B. Nikolaus, D. Grischkowsky,A. C. Balant, Optical pulse reshaping based on the nonlinear birefringence of single-mode optical fibers, *Opt. Lett.* **8**, p. 189 (1983).

79. M. R. Spiegel, Mathematical Handbook – Schaum's outline series in mathematics (McGraw-Hill Book Company, New York, 1978) pp. 11-20.

80. P. W. Milloni and J. H. Eberly, Lasers (Wiley, New York, 1988).

81 .F. Shimizu, Frequency broadening in liquids by a short light pulses. *Phys. Rev. Lett.* **19,** pp. 1097-1100 (1967).

82. R. R. Alfano and S. L. Shapiro, Observation of self-phase modulation and small-scale filaments in crystal and glasses, *Phys. Rev. Lett.* **24**, pp. 592-594 (1970).

83. E. P. Ippen, C. V. Shank and T. K. Gustafson, Self-phase modulation of picosecond pulses in optical fibers, *Appl. Phys. Lett.* **24**, p. 190 (1974).

84. Y. R. Shen and G. Z. Yang, "Theory of Self-Phase Modulation and Spectral Broadening"in The Supercontinuum Laser Source, R. R. Alfano ed., (Springer-Verlag, Berlin 1989) pp. 1-32.

85. A. C. Cheung, D. M Rank, R. Y. Chiao, and C. H. Townes, 'Phase modulation of Q-switched laser beams in small-scale filaments", *Phys. Rev. Lett.* **20**, p. 786. (1968).

86. T. K. Gustafson, J. P. Taran, H. A. Haus, J. R. Lifsitz and P. L. Kelley, Self-phase modulation, self steepening, and spectral development of light in small-scale trapped filaments, *Phys. Rev.* **177,** p. 306 (1969).

87. N. G. R. Broderick, D. Taverner, D, J. Richardson and Morten Ibsen, Cross-phase modulation effects in nonlinear fiber Bragg gratings, *J. Opt. Soc. Am* **B 17**, p. 345 (2000).

88. R. R. Alfano, P. L. Baldeck,P. P. Ho, G. P. Agrawal, Cross-phase modulation and induced focusing due to optical nonlinearities in optical fibers and bulk materials, *J. Opt. Soc. Am.* **B 6,** p. 824 (1989).

89. C.C. Yang,Alex J. S. Wang, "Cross-polarization cross-phase modulation of femtosecond pulses in erbium-doped fiber amplifiers". *J. Opt. Soc. Am.* **B 9,** p. 682 (1992).

90. T. Mirtchev, Off-resonant self- and cross-phase-modulation-induced modulation instabilities in single-mode rare-earth-doped fiber amplifiers *J. Opt. Soc. Am.* **B 15,** p. 171 (1998).

91. B. E. Saleh and M. C. Teich, *Fundamentals of Photonics* (John Wiley and Sons, Inc.New York, 1991).

92. J. Jahanpanah, "Measurement of spectral lines produced by four-wave mixing in 30 km dispersion-shifted single-mode optical fiber", *J. Appl. Phys.* **92**, p. 5642 (2002).

93. N. Shibata, R. P. Braun and R. G. Waarts, Phase-mismatch dependence of efficiency of wave generation through four-wave mixing in single mode optical fiber. IEEE J. Quantum Electron. **QE 23,** pp. 1205-1210 (1987).

94. R. Schulz,H. Harde, "Pulse generation in birefringent optical fibers by four-wave mixing and Raman scattering", J. Opt. Soc. Am. **B 12,** p. 1279 (1995).

95. R. H. Stolen, E. Ippen and A. R. Tynes, *Appl. Phys. Lett.* **20,** p. 62 (1972).

96. C. Lin, L. G. Cohen, R. H. Stolen, G. W. Tasker, and W. G. French, "Near-infrared sources in the 1-1.3 μm region by efficient stimulated Raman emission in glass fibers, Opt. Comm. **20**, p.426 (1977).

97. T. Nakashi, S. Seikai, and M. Nakazawa, "Dependence of Raman gain on relative index difference for GeO_2-doped dingle-mode fibers", *Optics Lett.* **10**, pp. 420-422 (1985).

98. N. Shibata, M. Horigudhi and T. Edahiro, "Raman spectra of binary high-silica glasses and fibers containing GeO_2, P_2O_5 and B_2O_3", *J. Non-crystalline solids,* **45**, pp. 115-126 (1981).

99. R. G. Smith, "Optical power handling capacity of low loss optical fibers as determined by stimulated Raman and Brillouin scattering" Appl. Opt. **11**, pp. pp. 2489-2494 (1972).

100. R. H. Stolen, "Nonlinearity in fiber transmission", *Proc. IEEE*, **60**, p.1232, (1980).

101. D. Heiman, D. S. Hamilton, and R. W. Hellwarth, Brillouin scattering measurements in optical glasses, *Phys. Rev.* **B 19**, p. 6583, (1979).

102. E. N. Tsoy, C. M. de Sterke, F. Kh. Abdullaev, "Influence of two-photon absorption on modulational instability", *J. Opt. Soc. Am.* **B, 18**, pp. 1144-1149 (2001).

103. T. Mizunami and Keiji Takagi, "Wavelength dependence of two-photon absorption properties of silica optical fibers", *Opt. Lett.* **19**, pp. 463-465 (1994).

104. A. Ghatak and K. Thyagarajan "Fiber optics in communications: a perspective". In Trends in fiber optics and optical communications, edited by A.K. Ghatak, B. Culshaw, V. Nagarajan and B. D. Khurana (Viva Books Private Limited, New Delhi, 1995) pp. 1-16.

105. A. Ghatak and K. Thyagarajan, *Introduction to fiber optics* (Cambridge University Press, UK, 1998).

106. T. Kimura, "Single mode systems and components for longer wavelengths", *IEEE Trans. Circuits and Systems,* **CAS-26**, p. 987, (1979).

107. K. S. Kim, W. A. Reed, R. H. Stolen and K. W. Quoi, "Measurement of the nonlinear refractive index of silica core and dispersion shifted fibers", *Opt. Lett.* **19**, pp. 257-259 (1994).

108. M. Artiglia, R. Caponi, F. Cisterninno, C. Naddeo, and D. Roccato, " A new method for the measurement of the nonlinear refractive index of optical fiber", *Opt. Fiber Technol.* **2**, pp. 75-79 (1996).

109. A. Fellegara, A. Melloni, and M. Martinelli, "Measurement of the frequency response induced by electrostriction in optical fibers", *Opt. Lett.* **21**, pp. 1615-1617 (1997).

110. L. Prigent and J. P. Hamaide, "Measurement of fiber nonlinear Kerr coefficient by four-wave mixing", *IEEE Photon. Techn. Lett.* **5**, pp. 1092-1095 (1993).

111. M. Artiglia, E. Ciaramella and B. Sordo, "Using Modulation Instability to determine Kerr coefficient in optical fibers", *Electron. Lett.* **31**, pp. 1012-1013 (1995).

112. E. L. Buckland and R. W. Boyd, "Electrostriction contribution to the intensity-dependent refractive index of optical fibers", *Opt. Lett.* **21,** pp. 1117-1119 (1996).

113. I. Kang, T. Krauss, and F. Wise, "Sensitive measurement of nonlinear refraction and two photon absorption by spectrally resolved two-beam coupling", *Opt. Lett.* **22,** pp. 1077-1079, (1997).

114. B. H. Lee, J. Nishii, "Bending sensitivity of in-series long-period fiber gratings", *Opt. Lett.* **23**, pp. 1624-1626 (1998).

115. J. W. Arkwright, P. Elango, G. R. Atkins, T. Whitbread and G. R. Akins, " Nonlinear phase changes at 1310 nm and 1545 nm observed far from resonance in Diode pumped Ytterbium Doped Fiber", *IEEE Photon. Techn. Lett.* **8**, pp. 408-410 (1996).

116. S.G. Evangelides,., Jr., L. F. Mollenauer, J. P.Gordon, N. S. Bergano, "Polarization multiplexing with solitons", *J. Lightwave Technol.* **10**, pp. 28- 35 (1992).

117. P. K. A. Wai, C. R. Menyuk, H. H. Chen, "Stability of solitons in randomly varying birefringent fibers" *Opt. Lett.*, **16**, pp. 1231- 1233 (1991).

118. H. Coic, M. L. Roblin, F. Gires, R. Grousson, "Degenerate four wave mixing in picosecond pulses: study of the temporal shape of the diffracted signal as a function of the material response time", *J. Opt. Soc. Am.* **B 11,** p.2232 (1994); M. Samoc, A. Samoc, B. Luther-Davies, Z. Bao, Luping Yu, B. Hsieh, U. Scherf, "Femtosecond Z-scan and degenerate four-wave mixing measurements of real and imaginary parts of the third-order nonlinearity of soluble conjugated polymers" *J. Opt. Soc. Am.* **B 15,** pp. 817-825, (1998).

119. R. W. Boyd, *Nonlinear Optics* (Academic Press, New York 1992) pp. 399-427.

120. M. B. Klein, "Physics of Photorefractive Effect in $BaTiO_3$", in *Electro-optics and Photorefractive Materials,* **18,** P. Guitred ed. (Springer-Verlag, New York 1986) pp. 266-282.

121. A. M. Glass, A. M. Johnson, D. H. Olson, W. Simpson and A. A. Ballman, "Four wave mixing in semi-insulating InP and GaAs using the photorefractive effect", *Appl. Phys. Lett.* **44**, pp. 948-950 (1984).

122. A. Partovi, J. Millerd, E. M. Garmire, M. Ziari, W. H. Steier, S. B. Trivedi and M. B. Klein, Photorefractivity at 1.5 μm, *Appl. Phys. Lett.* **57**, pp. 846-848 (1990).

123. F. Jin, J. B. Khurgin, Suhdir Trivedi, Chen-Chia Wang, and Esam Gad, "Displacement measurement and surface profiling using semi-insulating photorefractive semiconductors and linearly frequency-ramped lasers", *Appl. Phys. Lett.* **75**, p. 1374 (1999).

124. C. Wang, Richard A. Linke, David D. Nolte, M. R. Melloch, and Sudhir Trivedi, "Signal strength enhancement and bandwidth tuning in moving space charge field photodetectors using alternating bias field", *Appl. Phys. Lett.* **72**, p. 100 (1998).

125. C. Wang, R. A. Linke, D. D. Nolte, M. R. Melloch, and Sudhir Trivedi, "Enhanced detection bandwidth for optical doppler frequency measurements using moving space charge field effects in GaAs multiple quantum wells", *Appl. Phys. Lett.* **70**, p. 2034 (1997).

126. M. Ziari, W. H. Steier, P. M. Ranon, Sudhir Trivedi, and M. B. Klein, "Photorefractivity in vanadium-doped ZnTe", *Appl. Phys. Lett.* **60**, p. 1052 (1992).

127. N. V. Kukhtarev , V. B. Markov , S. G. Odulov , M. S. Soskin , and V. L. Vinetskii , "Holographic storage in electrooptic crystal. I. Steady state", Ferroelectrics **22** , pp. 949-960 (1979); V. Kukhtarev , V. B. Markov , S. G. Odulov , M. S. Soskin , and V. L. Vinetskii , "Holographic storage in electrooptic crystal. II. Beam coupling-light amplification", Ferroelectrics **22** , 961-964 (1979); N. V. Kukhtarev , "Kinetics of hologram recording and erasure in electro-optic crystals", Sov. Tech. Phys. Lett. **22,** pp. 438- 440 (1977).

128. R. N. Schwartz, C. C. Wang, S. Trivedi, G. V. Jagannathanm F. Davidson, P. R. Boydm U. Lee, "Spectroscopy and Photorefractive Characterization of cadmium telluride crystals codoped with vanadium and manganese", *Phys. Rev.* **B 55**, pp. 378-381 (1997).

129. A. L. Smirl, K. Bohnert, G. C. Valley, R. A. Mullen, T. F. Bogges, "Formation, decay, and erasure of photorefractive gratings written in barium titanate by picosecond laser pulses", *J. Opt. Soc. Am.* **B 6**, pp. 606-615 (1989).

130. G. C. Valley, J. Dubard, A. L. Smith, and A. M. Glass, Picosecond photorefractive response of GaAs, InP:Fe, CdTe:V", *Opt. Lett.* **14**, pp. 961-963 (1989).

131. Quantronix model 416 laser, Technical Manual (Quantronix Corporation, New York).

132. E. P. Ippen and C. V. Shank, "Techniques for measurement" in *Topics in Applied Physics **18**, Ultrashort Light Pulses*, Edited by S. L. Shapiro (Springer-Verlag, New York, 1976) pp. 83-122.

133. E. Desurvire, *Erbium-doped fiber amplifiers - principles and applications,* (John Wiley and Sons, Inc. New York, 1994).

134. P. C. Becker, N. A. Olson and J. R. Simpson, *Erbium-Doped Fiber Amplifiers – Fundamentals and Technology* (Academic Press, New York, 1999) pp. 13-35.

135. W. L. Barnes, R. I. Laming, E. J. tarbox, and P. R. Morkel, "Absorption and emission cross-section of Erbium-doped silica fibers", IEEE J. Quantum Electron. **27**, pp. 1004-1010 (1991).

136. X. Zhu and W. Sibbett, "Propagation characteristics of femtosecond pulses in erbium-doped monomode optical fibers", IEEE J. Quantum Electron, **27**, pp. 101-113 (1991).

137. B. A. Betts, T. T. Tjugiarto, Y. L. Xue and P. L. Chu, "Nonlinear Refractive index in erbium-doped optical fiber: Theory and Experiment", *IEEE J. Quantum Electron.* **27,** pp. 908-913 (1991).

138. M. Idan (JDS Uniphase Inc.) Private communication.

139. T. Geisler, K. A. Shore, M. P. Soerensen, P. L. Christiansen, J. Mork, J. Mark, Nonlinear fiber external cavity mode locking of erbium-doped fiber lasers", *J. Opt. Soc. Am. B* **10**, p. 166, (1993).

140. E. Desurvire, "*Basic physics of erbium-doped fiber amplifiers*", in Guided wave nonlinear optics, eds. D. B. Ostrowsky and R. Reinisch (Kluwer academic pubs. Dordrecht, 1992) p. 553.

141. J. Chen, X. Zhu, W. Sibbett, "Rate-equation studies of erbium-doped fiber lasers with common pump and laser energy bands", *J. Opt. Soc. Am B* **9**, p. 1876 (1992).

142. A. Gloag, N. Langford, K. McCallion, W. Johnstone, "Continuously tunable single-frequency erbium ring fiber laser", *J. Opt. Soc. Am. B* **13**, p. 921 (1996).

143. B. Calvas, P. Urquhart, "Erbium-doped fiber amplifiers: theory of upconversion-pumped operation with a signal wavelength of 850 nm", *J. Opt. Soc. Am. B* **10**, p. 666 (1993).

144. S. Jarabo, I. J. Sola, J. Saez-Landete, "Spectral hole burning induced by reflected amplified spontaneous emission in erbium-doped silica optical fiber pumped at 980 nm", *J. Opt. Soc. Am. B* **20**, p. 1204 (2003).

145. Y. L. Xue, R. A. Betts, P. L. Chu and T. Tjugarto, "Nonlinear refractive index in erbium-doped optical fiber:, in Proc. ACOFT, IREE Sydney, pp. 117-120 (1990).

146. P. L. Chu and W. Wu, "Optical switching in twin-core erbium-doped fibers", *Opt. Lett.* **17**, pp. 255-257 (1992).

147 S. C. Fleming and T. J. Whitley, "Measurement of pump-induced refractive index change in erbium-doped fiber amplifier", *Electron. Lett.* **27**, pp. 1959-1961 (1991).

148. R. H. Pantell, " A model of nonlinear all-optical switching in doped fibers", *J. Lightwave Technol.* **12,** pp. 149-156 (1994).

149. B. R. Bennett, R. A. Soref and J. A. Del Alamo, "Carrier-induced change in refractive index of InP, GaAs and InGaAsP", *IEEE J. Quantum Electron.* **26,** pp. 113-122 (1990).

150. S. B. Poole, "Fabrication of Al_2O_3 co-doped optical fibers by a solution doping technique", in *Proceedings of the 14th European Conference on Optical Fiber Communications*, **Part 1,** pp. 433-436 (1988).

151. R. Billington, "Effective area of optical fibers – definition and measurement Techniques", *Technical Report, the National Physical Laboratory*, Serco Group Plc. (2003).

152. W. Reed, Measurement of Effective area of single mode fibers – Private communication.

153. M. Artiglia, G. Coppa, P. Di Vita, M. Potenza, and A. Sharma, " Mode-field diameter measurements in single mode optical fibers", *J. Lightwave Technol.* 7, p. 1131 (1989).

154. Y. Namihira, A. aamiyata and N. Tanahashi, "Relationship between nonlinear effective area and the mode-field diameter for dispersion shifted fibers" *Electron. Lett.* **30,** pp. 262-263 (1994).

155. EXFO Inc. "Fast and accurate fiber characterization performed in a single set-up" (NR-9200/NR – 9200HR Optical Fiber analyzer)-Technical note – 004.

156. Bell Labs: "*Technical information on the advantages of True wave Rs fiber*", http:/www.bell-labs.com/news/1998/june//11/2.html (website visited July 2003).

157. J. Bromage, OFS Laboratories, *Private communication.*

158. D. J. Dougherty, F. X. Kartner, H. A. Haus, and E. P. Ippen, " Measurement of Raman gain spectrum of optical fibers*", Opt. Lett.* **20**, pp. 31-33 (1995).

159. D. Mahberefteh, D. L. Butler, and J. Goldhar, B. Rosenberg and G. L. Burdge, "Technique for measurement of the Raman gain coefficient in optical fibers",*Opt. Lett.* **21,** pp. 2026-2028 (1996).

160. N. R. Newbury, "Raman gain:pump-wavelength dependence in single mode fiber", *Opt. Lett.* **27**, pp. 1232-1234 (2002).

161. N. Newbury, "Full wavelength dependence of Raman gain in optical fibers: Measurement using a single pump laser.", OFC 2003, Atlanta, Georgia, Paper WB5 (2003).

162. K. J. Cordina and Christopher R. S Flunger, "Changes in Raman gain coefficient with pump wavelength in modern transmission fibers, in *Conference on Optical Amplifiers and their Applications (OAA 2003), Paper OMC3,* Vancouver, Canada (2003).

163. J. Bromage, K. Rottwitt, and M. E. Lines, "A method to predict the Raman gain spectra of germanosilicate fbers with arbitrary index profile", *IEEE Photonics Techn. Lett.* **14**, pp. 24-26 (2002).

164. Fiber provided to Dr. A. M. Johnson by Dr. R. H. Stolen when both were at AT&T Bell Labs.

165. Fiber provided by Dr. Jake Bromade of OFS laboratory, Holmdel, New Jersey

166. F. M. Mitschke and L. F. Mollenauer, "Discovery of the soliton self-frequency shift" *Opt. Lett.* **11**, pp. 659-661 (1986).

167. I. Torres, A. N. Starodmov, Yu. O. Barmenkov, L. A. Zenteno, and P. Gavrilovic "Raman effect based modulators for high power fiber lasers", *Appl. Phys. Lett.* **72**, pp. 401-403 (1998).

168. F. L. Galeener, J. C. Mikkelsen, Jr., R. H. Geils, and W. J. Mosby, "The relative Raman cross sections of vitreous SiO_2, GeO_2, B_2O_3, and P_2O_5", *Appl. Phys. Lett.* **32**, 34-36 (1978); M. Hass, Raman spectra of vitreous silica, germania and sodium silicate glasses", *J. Phys. Chem. Solids*, **31,** pp. 415-422 (1970).

169. J. Manassah and O. Cockings, " Time domain characterization of a Raman pulse in the presence of a pump", *Appl. Opt.* **26,** pp. 3749-3752 (1987)

170. M. Cronin-Golomb, B. Fischer, J. O. White and A. Yariv, Theory and applications of four-wave mixing in photorefractive media *IEEE J. Quantum Electron.* ***QE 20,*** pp. 12-30 (1984).

171 J. Eichler, P. Gunter and D.W. Pohl, "Laser-induced dynamic gratings",(Springer-Verlag, Berlin, Germany, 1986) pp. 119-122.

172 . A. M. Weiner, J. P. Heritage, and R. H. Stolen, "Self-phase modulation and optical compression influenced by stimulated Raman scattering in fibers", *J. Opt. Soc. Am.* **B 5**, pp. 364-372 (1988).

173. P. V. Mamyshev, S. V. Chernikov , "Ultrashort-pulse propagation in optical fibers", Optics Lett.,**15**, p. 1076, (1990).

174. K, J. Blow and D. Wood, "Theoretical description of transient stimulated Raman scattering in optical fibers", *IEEE J. Quantum Electron.* **25**, pp. 2665 -2673 (1989).

175. G. Genty M. Lehtonen and H. Ludvigen, "Spectral modulation due to pulse reshaping in photonic crystal fibers" ", in: *Conf. Lasers and Electro-optics – CLEO'2002 Technical Digest,* Baltimore MD, p. 286 (2002).

176. R. Chubeddu, R. Polloni, C. A. Sacchi and O. Svelto, "Self-Phase modulation and rocking of molecules in trapped filaments of light with picosecond pulses", *Phys. Rev. A* **2**, pp. 1955-1963, (1970).

177. F. Shimizu, Frequency broadening in liquids by a short light pulses. *Phys. Rev. Lett.* **19**, pp. 1097-1100 (1967).

178. C. H. Lin and T. K. Gustafson, *IEEE J. Quantum Electron,* **QE-8,** p. 429 (1972).

179. N. G. R. Broderick, T. M. Monro, P. J. Bennett, and D. J. Richardson, "Nonlinearity in holey optical fibers: measurements and future opportunities", *Opt. Lett.* **24,** pp. 1395-1397 (1999).

180. R. Stegeman, L. Jankovic, H. Kim, C. Rivero, G. Stegeman, K. Richardson, Y. Guo, A. Schulte and T. Cadinal, "Tellurite glasses with peak absolute Raman gain coefficients up to 30 times that of fused silica" *Opt. Lett.* **28,** pp. 1126-1128 (2003).

181. Y. Y. Huang and A. Sarkar, "Relationship between composition, density and refractive index for germaina silica glasses", *Journal of Non-crystalline Solids* **27**, pp. 29-37 (1978).

182. P. D. Maker, R. W. Terhune, and C. M. Savage, "Intensity-Dependent Changes in the Refractive Index of Liquids", *Phys. Rev. Lett.* **12**, pp. 507–509 (1964).

183. R. R. Alfano and S. L. Shapiro, "Direct Distortion of Electronic Clouds of Rare-Gas Atoms in Intense Electric Fields";Phys. *Rev. Lett.* **24**, pp. 1217–1220 (1970).

184. D. Close, C. Giuliano, R. Hellwarth, L. Hess, F. McClung, W. Wagner, " The self-focusing of light of different polarizations", IEEE J. Quantum. Electron. QE 2, p. 553 (1966).

185. C. Bosshard, "Third-order nonlinear optics of polar materials" in *Nonlinear Optical Effects and Materials,* edited by P. Gunter (Springer-Verlag, Berlin Heidelberg, 2000) p. 43.

186. D. H. Auston, A. M. Glass, and A. A. Ballman, "Optical rectificaion by impurities in polar crystals", *Phys. Rev. Lett.* **28**, pp. 897-900 (1972).